Institute for Clinical and Experimental Surgery
Saarland University, Homburg/Saar
(Director: Prof. Dr. med. M. W. Laschke, Ph.D.)

Failed fracture healing in aged mice - model development, pathophysiology and therapeutic approaches

Dissertation with the aim of achieving the doctoral degree
Doktor der Medizin und der Naturwissenschaften (MD-PhD)
at the Medical Faculty of Saarland University

2024

by Dr. med. Michael Maria Maximilian Menger
born on March 25th 1992 in Homburg, Germany

Tag der Promotion: 02.07.2025

Dekan: Univ.-Prof. Dr. med. dent. M. Hannig

Berichterstatter: Univ.-Prof. Dr. med. Matthias Werner Laschke, PhD
PD Dr. med. Matthias Brockmeyer
Univ.-Prof. Dr. med. Ingo Marzi

To my family

Table of contents

1. Summary

Despite increasing insights in the molecular and cellular basis of bone regeneration, delayed healing and non-union formation still represent a major burden for trauma and orthopedic surgery. Segmental defects, infections, severe soft tissue damage and insufficient mechanical stability are associated with a risk of fracture healing failure. However, in a substantial number of cases the reason for non-union formation remains elusive and, thus, effective treatment approaches are often lacking.

Moreover, the health care system is confronted with a steadily increasing aged population. These geriatric patients demonstrate a plethora of age-related pathologies, including osteoporosis and an impaired capacity for bone healing. The latter makes the treatment of fracture healing failure in these aged patients all the more challenging.

Parathyroid hormone (PTH) is secreted by the parathyroid glands and a key regulator of calcium homeostasis. Moreover, it represents a clinically approved, osteoanabolic drug with pro-osteogenic capacities. However, its effects on non-union formation in aged patients have not yet been investigated.

For the analysis of the pathophysiology of failed fracture healing and the evaluation of promising treatment approaches, preclinical animal models are needed. Notably, fracture healing models in mice have gained increasing interest in recent years due to the wide range of available antibodies and genetically modified knockout-mice. In the past, a non-union model involving a segmental defect, stripping of the periosteum and stabilization with a pin-clip device has been introduced. However, this approach does not mimic a trauma-induced fracture and subsequent healing failure. Therefore, a model with a transverse femoral fracture, additional periosteal cauterization and K-wire stabilization may be more suitable.

In the first study of this thesis, we compared these two approaches for generating a reliable non-union model in mice. The two models were applied in CD-1 mice and the callus tissue was analyzed by means of biomechanical, radiological, histological as well as immunohistochemical analyses at 2, 5 and 10 weeks after surgery. In addition, growth factor expression was analyzed by Western blotting at 2 weeks after surgery. Notably, the results demonstrated after 10 weeks a reliable non-union formation of 100 % in the model with the segmental defect and the pin-clip stabilization (pin-clip model). In the model using a transverse fracture with periosteal cauterization and K-wire fixation (K-wire model), however, after 10 weeks only 10 out of 12 mice showed fracture healing failure. This was associated with an increased expression of pro-osteogenic growth factors and osteoclast activity as well as

enhanced bone formation and bending stiffness of the mice femora. However, the callus tissue of animals in the K-wire group demonstrated a lower number of cluster of differentiation (CD)31-positive endothelial cells, indicating a reduced angiogenic capacity after periosteal cauterization. Hence, these findings suggest that the pin-clip model is more suitable for the investigation of non-union formation in mice. The K-wire model with periosteal cauterization, on the other hand, may be applied particularly in preclinical studies investigating the effects of damaged periosteum and a subsequent impaired angiogenic capacity on fracture healing.

In the second study of this thesis, the pin-clip model was established in 18-20 months old CD-1 mice. Additionally, the cellular and biochemical basis of non-unions were characterized and compared with non-unions of young adult animals (3-4 months). For this purpose, the callus tissue of young adult and aged mice was analyzed by biomechanics, X-ray, micro-computed tomography (µCT), histomorphometry as well as immunohistochemistry at 2 and 10 weeks after surgery. Additionally, Western blot analysis was performed at 2 weeks after surgery. All animals in both study groups demonstrated a reliable atrophic non-union formation with rounded bone ends and abundant fibrous tissue within the callus at 10 weeks after surgery. Notably, the segmental defects of aged mice demonstrated a lower expression of bone formation markers as well as a reduced bone formation and vascularization when compared to young adult animals. This was associated with a decreased number of osteoclasts within the callus tissue and an elevated osteoprotegerin (OPG)/receptor activator of NF-κB ligand (RANKL) ratio, indicating a reduction of osteoclast activity. The number of macrophages within the callus of aged mice, on other hand, was significantly increased, revealing an enhanced inflammatory response. The study validates for the first time the application of the pin-clip model in aged mice. In addition, it shows that non-unions of geriatric compared to young adult animals demonstrate distinct differences in bone formation, callus remodeling, growth factor expression as well as vascularization and inflammation.

In the third study of this thesis, the effects of systemic PTH treatment on bone regeneration were evaluated using the pin-clip non-union model in aged mice. For this purpose, the animals received a daily dose of 200 µg/kg body weight PTH subcutaneously. The animals of the control group received saline, respectively. The callus tissue of femora was analyzed at 2 and 10 weeks after surgery by X-ray, biomechanics, µCT, histology and immunohistochemistry as well as at 2 weeks after surgery by Western blotting. The data demonstrated a markedly improved bone formation and increased bending stiffness in PTH-treated aged mice when compared to control animals, most likely mediated by an enhanced expression of cyclooxygenase (COX)-2 and phosphoinositide 3-kinase (PI3K) in PTH-treated mice. These findings were associated with a higher number of tartrate-resistant acid phosphatase (TRAP)-

positive osteoclasts and CD31-positive endothelial cells within the callus tissue. In contrast, the number of myeloperoxidase (MPO)-positive granulocytes and CD68-positive macrophages was significantly decreased, indicating a significantly attenuated inflammatory response. In summary, systemic PTH treatment markedly improves bone regeneration in aged mice. Since, PTH is already a clinically approved drug, it represents a promising candidate for the treatment of non-union formation in geriatric patients. Future prospective clinical trials have to evaluate the effectiveness of PTH treatment in cases of delayed healing and fracture healing failure in aged patients and screen for potential side effects. Thereby, this therapeutic approach can be successfully translated into a clinical setting, and may, thus, help to overcome non-union formation in the aged population.

Taken together, the present thesis demonstrates that the K-wire non-union model is inferior for investigating fracture healing failure. This is due to a higher rate of osseous bridging 10 weeks after surgery when compared to the pin-clip model. Moreover, the experiments of the present thesis could establish the more reliable pin-clip model in aged mice. Thereby, the analysis of non-union callus tissue revealed distinct differences in bone formation, callus remodeling, growth factor expression as well as vascularization and inflammation between young adult and aged animals. Finally, the present thesis reveals some promising pro-osteogenic effects of PTH in overcoming non-union formation in the aged. Thus, this hormone is a promising candidate for the translation into the clinical practice.

2. Zusammenfassung

Eine verzögerte Frakturheilung sowie Pseudarthrosen sind nach wie vor trotz zunehmender Erkenntnisse über die molekularen und zellulären Grundlagen der Knochenregeneration schwerwiegende Komplikationen in der Traumatologie und Orthopädie. Große Substanzdefekte, Infektionen, schwere Weichteilschäden sowie unzureichende mechanische Stabilität bergen ein hohes Risiko für eine ausbleibende Frakturheilung. In einer beträchtlichen Anzahl von Fällen bleibt der Grund für die Bildung einer Pseudarthrose allerdings unklar und dementsprechend fehlt es oft an wirksamen Behandlungsansätzen.

Gleichzeitig ist das Gesundheitssystem mit einem stetig wachsenden Anteil älterer Patienten konfrontiert. Diese geriatrischen Patienten weisen eine Vielzahl altersbedingter Pathologien, wie Osteoporose, und eine beeinträchtigte Knochenregeneration auf. Dies macht die Behandlung älterer Patienten noch anspruchsvoller.

Parathormon (PTH) wird von den Nebenschilddrüsen ausgeschüttet und ist ein wichtiger Regulator der Kalziumhomöostase. Darüber hinaus wird das Hormon bereits zur Behandlung der Osteoporose eingesetzt und besitzt zudem pro-osteogene Eigenschaften. Die Anwendung in der Behandlung von Pseudarthrosen bei geriatrischen Patienten wurde allerdings noch nicht untersucht.

Für die Analyse der Pathophysiologie der Pseudarthrosenbildung und die Erprobung neuer Behandlungsstrategien sind präklinische Tiermodelle unverzichtbar. Dabei stehen Mausmodelle in den letzten Jahren aufgrund einer großen Bandbreite an zur Verfügung stehenden Antikörpern und genetisch veränderten Knockout-Tieren immer mehr im Fokus. In der Literatur wurde bereits ein Pseudarthrose-Modell in der Maus beschrieben, das einen segmentalen Defekt am Femur mit Pin-Clip Stabilisierung und periostalem Stripping verwendet. Dieses Modell hat allerdings den Nachteil, dass es nicht die Situation der ausbleibenden Knochenheilung nach einer traumatisch bedingten Fraktur widerspiegelt. Dafür wäre eine transversale Femurfraktur mit K-Draht Stabilisierung und zusätzlicher Kauterisation des Periosts möglicherweise besser geeignet.

In der ersten Studie der vorliegenden Arbeit wurden die zwei Ansätze für ein Pseudarthrose-Modell in der Maus miteinander verglichen, um zu ermitteln, welcher der beiden valider ist. Die Modelle wurden bei CD-1-Mäusen angewandt, und das Kallusgewebe mittels biomechanischer, radiologischer, histologischer und immunhistologischer Analysen 2, 5 und 10 Wochen nach dem Eingriff untersucht. Zudem wurde die Expression von Wachstumsfaktoren mittels Western blot 2 Wochen nach dem Eingriff analysiert. Die

Ergebnisse zeigten, dass im Modell des segmentalen Defektes und Pin-Clip-Stabilisierung (Pin-Clip-Modell) nach 10 Wochen eine zuverlässige Pseudarthrosenbildung von 100 % erreicht wird. In dem Modell mit transversaler Fraktur, Kauterisieren des Periostes und K-Draht-Fixierung (K-Draht-Modell) zeigten nach 10 Wochen nur 10 von 12 Mäusen eine ausbleibende Frakturheilung. Dies war mit einer erhöhten Expression von pro-osteogenen Wachstumsfaktoren und einer vermehrten Osteoklastenaktivität sowie mit einer gesteigerten Knochenneubildung und Biegesteifigkeit der Femora verbunden. Das Kallusgewebe der Tiere in der K-Draht-Gruppe wies allerdings eine verringerte Anzahl *cluster of differentiation* (CD)31-positiver Mikrogefäße auf, was auf eine eingeschränkte angiogene Kapazität nach dem Kauterisieren des Periostes hindeutet. Diese Ergebnisse belegen, dass das Pin-Clip-Modell für die Untersuchung von Pseudarthrosen in Mäusen besser geeignet ist. Das K-Draht-Modell mit kauterisiertem Periost kann dagegen in präklinischen Studien eingesetzt werden, welche die Auswirkungen von beschädigtem Periost und einer daraus resultierenden beeinträchtigten angiogenen Kapazität auf die Frakturheilung untersuchen.

In der zweiten Studie der vorliegenden Arbeit wurde das Pin-Clip-Modell bei 18-20 Monate alten CD-1-Mäusen etabliert. Darüber hinaus wurden die zellulären und biochemischen Eigenschaften der Pseudarthrosen charakterisiert und mit Pseudarthrosen von jungen erwachsenen Tieren (3-4 Monate) verglichen. Dazu wurde das Kallusgewebe 2 und 10 Wochen nach der Operation mittels Biomechanik, Röntgen, mikro-Computertomographie (µCT), Histomorphometrie und Immunhistochemie analysiert. Weiterhin erfolgten nach 2 Wochen Western blot Untersuchungen. Alle Versuchstiere in beiden Studiengruppen wiesen eine zuverlässige atrophische Pseudarthrosenbildung mit abgerundeten Knochenenden und reichlich fibrösem Gewebe innerhalb des Kallus 10 Wochen nach der Operation auf. Insbesondere zeigten die segmentalen Defekte älterer Mäuse eine geringere Expression von pro-osteogenen Wachstumsfakten sowie eine reduzierte Knochenneubildung und Vaskularisierung im Vergleich zu jungen erwachsenen Tieren. Dies ging mit einer geringeren Anzahl von Osteoklasten im Kallusgewebe und einem erhöhten Verhältnis von Osteoprotegerin (OPG)/*receptor activator of NF-κB ligand* (RANKL) einher, was auf eine geringere Osteoklastenaktivität hindeutet. Die Anzahl der Makrophagen im Kallusgewebe alter Tiere war dagegen deutlich erhöht. Dies deutet auf eine verstärkte Entzündungsreaktion hin. Die Studie bestätigte somit die Validität und Reliabilität des Pin-Clip-Modells bei älteren Mäusen und zeigte zudem, dass atrophe Pseudarthrosen geriatrischer und junger erwachsener Tiere deutliche Unterschiede bei der Knochenbildung, dem Umbau des Kallusgewebes, der Expression von Wachstumsfaktoren sowie der Vaskularisierung und der Entzündungsreaktion aufweisen.

In der dritten Studie der vorliegenden Arbeit wurden die Auswirkungen einer systemischen PTH-Behandlung auf die Knochenregeneration in der alten Maus mit Hilfe des Pin-Clip-Modelles untersucht. Dazu wurde den Tieren täglich eine Dosis von 200 µg/kg Körpergewicht PTH subkutan appliziert. Die Kontrollgruppe erhielt jeweils eine entsprechende Menge an Kochsalzlösung. Das Kallusgewebe der Femora wurde 2 und 10 Wochen nach dem Eingriff durch biomechanische, radiologische, histologische und immunhistochemische Analysen sowie nach 2 Wochen zusätzlich mittels Western blot untersucht. Die Analysen zeigten eine deutlich verbesserte Knochenbildung und erhöhte Biegesteifigkeit bei PTH-behandelten älteren Mäusen im Vergleich zu Kontrolltieren, was wahrscheinlich auf eine verstärkte Expression der Cyclooxygenase (COX)-2 und Phosphoinositid-3-Kinase (PI3K) zurückzuführen ist. Weiterhin zeigte sich eine höhere Anzahl *tartrate-resistant acid phosphatase* (TRAP)-positiver Osteoklasten und CD31-positiver Mikrogefäße im Kallusgewebe der PTH-Gruppe. Im Gegensatz dazu war die Zahl der Myeloperoxidase (MPO)-positiven Granulozyten und CD68-positiven Makrophagen im Kallusgewebe der PTH-behandelten Mäuse deutlich verringert, was auf eine abgeschwächte Entzündungsreaktion hindeutet. Es kann festgehalten werden, dass eine systemische PTH-Behandlung die Knochenregeneration bei alten Mäusen substanziell verbessern kann. Da PTH bereits ein klinisch zugelassenes Präparat ist, stellt es einen vielversprechenden Kandidaten zur Behandlung von Pseudarthrosen bei geriatrischen Patienten dar. Künftige prospektive klinische Studien müssen nun die Wirksamkeit der PTH-Behandlung bei verzögerter und fehlgeschlagener Frakturheilung in älteren Patienten bewerten und auf mögliche Nebenwirkungen untersuchen. Auf diese Weise kann dieser therapeutische Ansatz erfolgreich in die klinische Praxis umgesetzt werden, und dazu beitragen, die Behandlung von Pseudarthrosen in der älteren Bevölkerung zu verbessern.

Zusammenfassend zeigt die vorliegende Arbeit, dass in der Maus das K-Draht-Modell für die Untersuchung von Pseudarthrosen dem Pin-Clip-Modell unterlegen ist, da es eine höhere Rate an knöcherner Überbrückung 10 Wochen nach der Operation aufweist. Darüber hinaus konnte die vorliegende Arbeit das zuverlässigere Pin-Clip-Modell in alten Mäusen etablieren. Dabei zeigte die Analyse der Pseudarthrose deutliche Unterschiede in der Knochenbildung, Kallusumbau, Wachstumsfaktoren-Expression sowie der Vaskularisierung und Entzündung zwischen jungen erwachsenen und alten Tieren. Schließlich konnte in der vorliegenden Arbeit vielversprechende pro-osteogene Effekte von PTH bei der Behandlung von Pseudarthrose in der alten Maus nachgewiesen werden. Somit ist dieses Hormon ein vielversprechender Ansatz für die Einführung in die klinische Praxis.

3. Introduction

The skeleton of an adult human consists of 213 bones, excluding the sesamoids [Clarke, 2008]. Bone serves a plethora of functions within the human body, including (i) structural support, (ii) protection of vital internal organs, (iii) locomotion by providing levers for the musculature, (iv) maintenance of mineral homeostasis and acid-base balance, (v) reservoir for growth factors and cytokines as well as (vi) hematopoiesis within the bone marrow space [Taichman, 2005; Clarke, 2008]. Notably, bone is constantly undergoing a remodeling process, adapting to changing biomechanical forces and replacing old and damaged bone, with novel mechanical durable bone tissue [Clarke, 2008].

Long bones are anatomically composed of a hollow shaft, the diaphysis, a cone-shaped metaphysis below the growth plates and a rounded epiphysis above the growth plates. Noteworthy, the diaphysis consists mainly of cortical bone, whereas the metaphysis and epiphysis mostly consist of trabecular bone tissue surrounded by a thin cortical shell [Clarke, 2008]. Overall, the human skeleton contains 80 % cortical and 20 % trabecular bone. The dense and solid cortical bone tissue surrounds the marrow space. Trabecular bone, on the other hand, consists of trabecular plates and rods forming a honeycomb-like network [Clarke, 2008]. Of note, the microstructure between these 2 types of bone tissue differs significantly. Cortical bone is made out of osteons with a longitudinal cylindric shape running parallel to the long bones' axis, called the Haversian system. These osteons are formed with concentric lamellae surrounding a Haversian canal, which contains blood vessels, lymphatics and nerves. The trabecular bone, in contrast, is arranged in semicircular shapes called packets, which forms the trabecular architecture [Clarke, 2008; Buck and Dumanian, 2012]. Cortical as well as trabecular bone are formed in a lamellar pattern, in which collagen fibrils are organized in tightly packed sheets. Lamellar bone is biomechanically durable and strong. Woven bone, on the other hand, is characterized by disorganized and more irregular patterns of collagen fibrils, hence exhibiting an inferior biomechanical durability and strength. The embryonic skeleton is formed out of woven bone tissue. In the adult skeleton this woven bone tissue only occurs in growth plates and in early stages of fracture repair [Buck and Dumanian, 2012].

The outer cortical bone surface is covered by the periosteum, which consists of fibrous tissue and contains vital blood vessels, nerve fibers and a reservoir for osteoblasts as well as osteoclasts. The inner surface of cortical and trabecular bone, on the other hand, is covered by the endosteum, which has direct contact to the bone marrow space and blood vessel canals [Clarke, 2008].

3.1 Bone regeneration

Bone possess an extraordinary capacity of regeneration to fully restore its anatomical and biomechanical properties [Dimitriou et al., 2011]. After injury of the skeleton, two different modes of healing can be distinguished: (i) Direct or primary healing only occurs with a rigid fracture fixation and without any gap formation. Only when these two requirements are achieved direct bone healing can occur by direct transition of mesenchymal cells to bone-forming osteoblasts (intramembranous ossification) [Bahney et al., 2019]. Notably, this type of bone healing is often the primary goal after open fracture reduction and internal fixation. (ii) Indirect or secondary healing occurs in consequence of unstable or semi-rigid fracture fixation. In this case, the fracture heals by formation of a large callus with cartilaginous intermediate and subsequent bone formation (endochondral ossification) [Bahney et al., 2019]. This type of healing occurs in unstabilized fractures or internal fixations with weight bearing, such as intramedullary nailing [Marsell and Einhorn, 2011].

Bone regeneration is a highly complex and well-orchestrated process, which involves the temporal and spatial interaction of a plethora of cell lines and growth factors [Schlundt et al., 2018]. After trauma to the skeleton, a hematoma is formed due to disruption of the vascular network [Schell et al., 2017]. Inflammatory cells, such as granulocytes and macrophages are among the first cells to arrive at the fracture site. Macrophages stimulate the infiltration of mesenchymal stem cells (MSCs) by pro-inflammatory cytokines, such as interleukin (IL)-1β and tumor necrosis factor (TNF)-α. These cells infiltrate the callus tissue by sprouting capillaries from both the endosteum and bone marrow [Loi et al., 2016; Menger et al., 2022b].

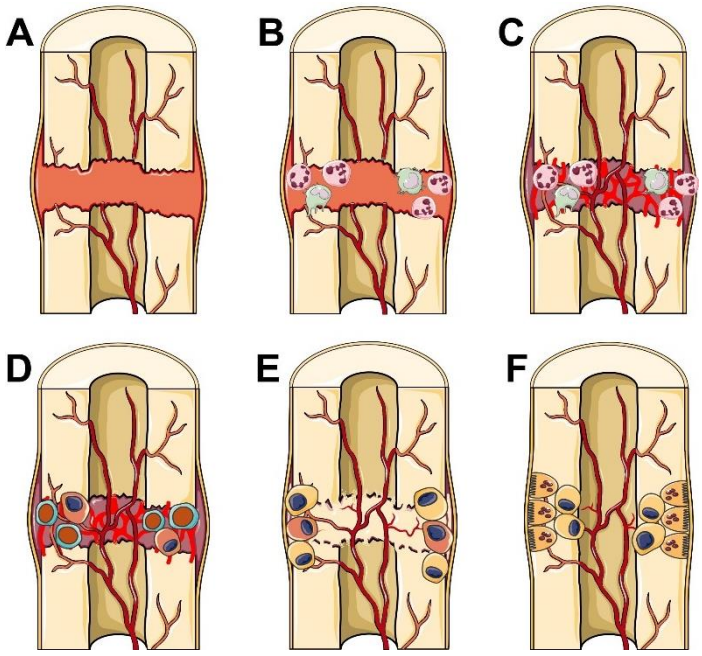

Figure 1. *A hematoma fills the fracture site after injury (A), in which inflammatory cells, such as granulocytes and macrophages, are the first to arrive (B). The sprouting of newly formed microvessels within the callus tissue is induced (C). MSCs invade the fracture site and a soft callus tissue is formed, consisting of chondrocytes and fibrous tissue (D). Subsequently, the cartilaginous tissue is replaced by osteoblasts forming novel bone tissue (E). Finally, a remodeling cascade is induced, in which novel bone tissue is remodeled to mature lamellar bone (F). The figure was created using pictures from Servier Medical Art, provided by Servier, licensed under a Creative Commons Attribution 4.0 unported license (https://creativecommons.org/licenses/by/4.0/).*

Afterwards, fibrocartilage tissue fills the fracture site and forms a soft callus, resulting in the primary stabilization of the fracture. Subsequently, the cartilaginous tissue matures and

hypertrophies. A hard callus tissue is formed by novel woven bone, replacing the hypertrophic cartilaginous cells. Finally, a remodeling cascade is induced, in which osteoclasts remove excessive bone tissue leading to the development of mature lamellar bone [Schlundt et al., 2018] (Figure 1).

3.2 Failure of bone healing

Despite the high regeneration potential of bone tissue, up to 10 % of all fractures result in delayed healing or non-union formation [Einhorn and Gerstenfeld, 2015]. Notably, there is no unified definition for the diagnosis of non-union. The U.S. Federal Drug Administration defines non-unions as 'failure to achieve union by 9 months since the injury, and for which there has been no signs of healing for 3 months' [Andrzejowski and Giannoudis, 2019]. However, other authors define non-union in long bones by the absence of radiological signs of fracture healing after a period of 6 months [Fayaz et al., 2011]. Obviously, the diagnosis of non-union formation and the subsequent decision for a specific therapy should always include both, the radiological as well as the clinical examination of the patient [Hak et al., 2014]. Failed fracture healing represents a major complication in trauma and orthopedic surgery, resulting in loss of function of the affected limb, increased and prolonged pain as well as extensive revision surgeries and an extended hospitalization for the patient. Additionally, the emerging costs pose a considerable financial burden on the health care system [Victoria et al., 2009; Schlundt et al., 2018].

Fracture healing failure can be discriminated between atrophic and hypertrophic non-union formation. Atrophic non-unions are characterized by sparse callus formation, sclerosis of the intramedullary canal, rounded fracture ends and mostly fibrous tissue filling the fracture gap [Garcia et al., 2013]. In contrast, hypertrophic non-unions demonstrate significant callus formation and endochondral bone formation at the fracture ends. Notably, in humans the term "pseudarthrosis" is defined as non-union formation accompanied by false joint formation and development of a synovial membrane [Heppenstall et al., 1987]. Hypertrophic non-unions are usually the result of an insufficient mechanical stability at the fracture site. Accordingly, in these cases successful bone regeneration can be achieved by stable osteosynthesis [Garcia et al., 2013].

Large segmental bone defects, severe soft tissue injuries, mechanical instability as well as systemic comorbidities bear a high risk for the development of atrophic non-union formation [Gustilo et al., 1987; Schmidmaier et al., 2009; Menger et al., 2022b]. However, despite the rapidly increasing knowledge about the molecular and cellular mechanisms of fracture repair, the cause for bone healing failure remains unclear in a substantial amount of cases [Garcia et

al., 2012]. Therefore, effective treatment strategies are often lacking. In general, atrophic non-unions are thought to be the result of an avascular and avital environment at the fracture site. Preclinical studies could demonstrate that the interruption of angiogenesis leads to the failure of bone healing. In fact, blockade of an adequate vascularization by non-steroidal anti-inflammatory drugs (NSAIDs), fumagillin and TNP-470 disturbed the process of bone regeneration resulting in atrophic non-unions [Fang et al., 2005; Murnaghan et al., 2006; Fassbender et al., 2011]. However, there is increasing evidence that this view is oversimplified. In fact, a variety of reports revealed by histological analyses that the callus tissue of non-unions indeed contains a considerable amount of blood vessels [Santavirta et al., 1992; Brownlow et al., 2002; Reed et al., 2003]. Furthermore, Garcia et al. [Garcia et al., 2012] could demonstrate by the analysis of growth factor expression in unions and non-unions that the intrinsic angiogenic response within atrophic non-unions is sufficient for a considerable vascularization during the development of non-union formation. A possible explanation for this observation may be a compensatory upregulation of vascular endothelial growth factor (VEGF) during non-union formation, caused by hypoxic conditions at the fracture site. Accordingly, the vascular structures observed by histological analysis may be non-functional vascular structures without blood perfusion and, thus, do not provide a sufficient oxygen supply.

Additional analyses of the subpopulations and biological function of progenitor cells in non-union patients revealed a decreased pool of bone marrow-derived MSCs as well as altered serum levels of related growth factors, such as leptin, stem cell factor (SCF) and insulin-like growth factor (IGF)-1. Since MSCs transform into osteoprogenitor cells during fracture, this pool defect may substantially contribute to the pathogenesis of non-union formation [Mathieu et al., 2013]. In a recent meta-analysis, Saul et al. [2023] illustrated further potential mechanisms resulting in failure of fracture healing, which include comorbidities and risk factors, such as diabetes, obesity, open factures, immune dysregulation and smoking [Saul et al., 2023]. Taken together, the pathophysiology of non-unions appears to be manifold and highly complex. The “diamond concept” by Andrzejowski et al. [2019] provides a summary of 6 hallmarks for successful bone regeneration, including (i) a functional vascular network, (ii) a sufficient pool of osteogenic cells, (iii) mechanical stability, (iv) consideration of host factors and the availability of (v) an osteoconductive matrix as well as (vi) osteoinductive mediators at the fracture site. Future research should consider all these factors during the development of novel treatment approaches.

Due to a steadily growing older population, the treatment of geriatric patients represents another great challenge for trauma and orthopedic surgery [Rollmann et al., 2019]. In the year 2020, 53.5 million people in the United States (US) were older than 65 years, representing 16

% of the overall population [Saul and Khosla, 2022]. Aging has significant effects on metabolism, resulting in deteriorating effects on the skeletal system, including diseases, such as osteoporosis and osteoarthritis. In addition, the process of aging also affects bone regeneration [Clark et al., 2017]. Aged individuals demonstrate a reduced differentiation and proliferation of stem cells, an impaired chondrogenesis and ossification as well as an alteration of the cellular composition within the periosteum [Bergman et al., 1996; Gruber et al., 2006; Lu et al., 2008]. Moreover, aging is associated with a dysfunction of the bone vascular system and a decreased vascular perfusion of the skeleton, which may result in a delay of angiogenesis and vascularization during fracture repair [Prisby et al., 2007; Clark et al., 2017]. This view is supported by a delayed expression of the pro-angiogenic factors VEGF and hypoxia inducible factor (HIF)-1α as well as a lower surface density of blood vessels within the callus tissue of aged mice compared to young animals [Lu et al., 2008]. Additionally, aged individuals demonstrate a prolonged and overshooting inflammatory response, which may negatively affect fracture healing. An adequate inflammatory status at the beginning of bone repair is of pivotal importance for stimulating the migration of stem cells to the fracture site [Kon et al., 2001]. The resolution of the inflammatory state, however, is also critical for successful bone regeneration. In fact, chronically elevated activity of pro-inflammatory cytokines, such as nuclear factor kappa-light-chain-enhancer (NF-kappaB) of activated B cells, impairs the function of MSCs for osteogenic differentiation [Lin et al., 2017]. There is evidence that these detrimental effects of aging on bone regeneration also increase the risk for delayed healing and non-union formation in geriatric patients [Robinson et al., 2004; Gruber et al., 2006; Parker et al., 2007]. Accordingly, novel treatment strategies are necessary to overcome this problem.

3.3 Parathyroid hormone

Parathyroid hormone (PTH) is a key regulator of calcium homeostasis and secreted by the parathyroid glands [Wojda and Donahue, 2018]. Human PTH (hPTH) (1-84) and its equally effective recombinant peptide teriparatide (PTH 1-34) increase the calcium serum level by the absorption of calcium within the kidney and the intestine as well as by stimulating osteoclast-dependent bone resorption and calcium release [McSheehy and Chambers, 1986; Milstrey et al., 2017]. Notably, the stimulation of osteoclast proliferation and differentiation by PTH is mediated by osteoblasts, since osteoclasts are lacking the corresponding PTH-receptor [McSheehy and Chambers, 1986]. Moreover, PTH has been approved as drug with osteoanabolic properties in clinical practice and is well established in the treatment of osteoporosis [Milstrey et al., 2017; Wojda and Donahue, 2018]. Clinical studies demonstrated that PTH treatment reduces the risk of fragility fractures of the os ilium of post-menopausal woman and improves trabecular bone architecture [Neer et al., 2001; Jiang et al., 2003].

Furthermore, PTH enhances the bone mineral density (BMD) in the lumbar spine in male and female patients [Dempster et al., 2001; Black et al., 2003]. In addition, there is increasing evidence that PTH stimulates the process of bone regeneration and fracture repair. Andreassen et al. [1999] showed that systemic treatment with PTH increases callus formation and mechanical strength of tibia fractures in rats. Furthermore, PTH accelerated bone regeneration in femoral osteotomies by replacing woven with mature lamellar bone [Komatsubara et al., 2005] and enhanced novel bone formation in rat calvaria bone defects [Andreassen and Cacciafesta, 2004]. The exact molecular mechanisms on how PTH stimulates bone regeneration are not completely understood. PTH mediates its anabolic action through the G protein coupled receptor, type 1 PTH receptor (PTHR1) [Jilka, 2007], but also by induction of MSC differentiation into the osteoblast lineage by stimulating the signaling of bone morphogenetic protein (BMP) [Yu et al., 2012]. Moreover, PTH may facilitate bone regeneration by directly increasing the proliferation of endothelial cells and, thus, the vascularization at the fracture site. This hypothesis is supported not only by the fact that endothelial cells directly respond to PTH [Brandi and Collin-Osdoby, 2006], but also by the capacity of PTH for stimulating the migration of angiogenic cluster of differentiation (CD)45^+/$CD34^+$ progenitor cells during myocardial infarction, and, thereby, improving neovascularization and cell survival [Zaruba et al., 2008]. Taken together, the pro-angiogenic and pro-osteogenic activities of PTH indicate that this compound may be a promising candidate to overcome non-union formation, particularly in aged patients.

3.4 Animal models of non-union formation

To gain further knowledge about the molecular and cellular mechanisms of non-union formation, animal models are of increasing interest in preclinical trauma research [Histing et al., 2011a]. These animal models allow the investigation of novel treatment approaches, before applying them in a clinical setting. In the past, large animals like dogs [Clark and Hayes, 1963; Olerud and Danckwardt-Lilliestrom, 1968], rabbits [Veneroni et al., 1962; Lettin, 1965] and sheep [Nunamaker and Perren, 1979; Perren and Rahn, 1980] were preferred to analyze bone healing in preclinical research. In recent years, however, models in mice and rats have moved into the spotlight. Compared to large animals, rodents offer some distinct advantages. Due to their small size, housing is less expensive and more feasible for keeping numerous animals in a limited space. Furthermore, breeding cycles are significantly shorter, and, thus, a sufficient number of animals is provided within a short period of time. In addition, mice are genetically well-defined and a wide range of monoclonal antibodies for immunohistochemical and biochemical analyses are available, thereby, allowing a molecular in-depth analysis of fracture healing and non-union formation. Genetically modified knockout-mice enable the investigation of distinct pathways and their role in the process of bone regeneration [Histing et al., 2011a].

Moreover, surgical interventions and subsequent investigations can be performed by one investigator, whereas large animals, such as sheep, require more personal [Garcia et al., 2013].

Garcia et al. [2008] developed an atrophic non-union model in mice by creating a 1.8 mm critical-sized defect within the femoral shaft. The defect was stabilized by a pin-clip device providing both axial and rotational stability. Additional periosteal stripping was performed along the longitudinal axis 2 mm distal and proximal to the defect. The radiological and histomorphometric analysis demonstrated rounded bone ends as well as abundant fibrous tissue within the bone defect 10 weeks after surgery, indicating atrophic non-union formation. Notably, the large segmental defect of the described non-union model has the advantage of resembling the resection of established non-unions in clinical practice. Furthermore, the model is especially suited for the implantation of bone substitutes and scaffolds used in tissue engineering applications [Menger et al., 2021]. However, the critical-sized defect does not completely mimic the pathophysiology of fractures induced by trauma. A different approach for a rodent non-union model by a simple transverse femoral fracture with additional periosteal injury may overcome this problem. The highly vascularized periosteum is crucial for successful bone regeneration, as it provides the cortical blood supply [Squier et al., 1990] and serves as a reservoir for osteoprogenitor cells [Arnsdorf et al., 2009]. A variety of studies demonstrated the importance of a preserved periosteum at the fracture site, making it a crucial requirement for successful bone repair [Whiteside and Lesker, 1978; Park et al., 1999; Landry et al., 2000]. Hence, a periosteal injury may compromise the process of angiogenesis and osteogenesis, resulting in non-union formation. Kokubu et al. [2003] introduced such a model in rats by stabilizing a transverse femoral fracture with a K-wire and subsequent periosteal injury by cauterization [Kokubu et al., 2003]. However, this model has not yet been established in mice. Both approaches, segmental defect as well as transverse facture with periosteal injury, represent promising approaches for the analysis of non-union formation in preclinical research. The validity and reliability of these two models in mice, however, have yet to be compared.

3.5 Study protocols for the thesis

In the first study of this thesis, the non-union model of Garcia et al. [2008] and a modified version of the model of Kokubu et al. [2003] were compared for their ability to achieve non-union formation in CD-1 mice [Menger et al., 2022a]. For this purpose, a 1.8 mm sized segmental defect was induced in the femoral shaft and stabilized by a pin-clip device for axial and rotational stability in the first study group. Moreover, the periosteum was stripped 2 mm proximal and distal of the defect along the longitudinal axis. In the second study group, a 0.6 mm K-wire (Depuy Synthes, Umkirch, Germany) was implanted into the medullary cavity

through the intercondylar notch of the right femur in a retrograde fashion. Subsequently, the femur was fractured by a 3-point bending device [Histing et al., 2011b] and the periosteum was cauterized circumferentially with a distance of 2 mm on each side of the fracture by a lateral approach. The callus tissue of the femora was analyzed at 2, 5 and 10 weeks after surgery by X-ray, biomechanics, micro-computed tomography (µCT), histology, immunohistochemistry as well as at 2 weeks after surgery by Western blotting. The process of bone remodeling was assessed by tartrate-resistant acid phosphatase (TRAP)-staining for identifying osteoclasts within the callus. Furthermore, angiogenesis and cell proliferation were analyzed by staining of CD31-positive endothelial cells and proliferating cell nuclear antigen (PCNA)-positive cells. Finally, the pro-osteogenic growth factors BMP-2 and BMP-4 as well as markers of bone remodeling, such as receptor activator of NF-κB ligand (RANKL) and osteoprotegerin (OPG) were analyzed.

The segmental defect model by Garcia et al. [2008] showed a superior validity and reliability for non-union formation in mice and was, therefore, established in aged CD-1 mice in the **second study** of this thesis. Moreover, non-union formation in young adult and aged mice was characterized by immunohistochemical and biochemical methods [Menger et al., 2022c]. For this purpose, segmental defects with subsequent pin-clip stabilization were generated in young adult CD-1 mice (3-4 months) and geriatric CD-1 mice (18-20 months), respectively. Notably, the age of 18 months and older was chosen according to previous reports demonstrating age-related physiological dysfunction and tumor development in 16 months old male and 18 months old female CD-1 mice [Homburger et al., 1975]. The callus tissue of non-unions in young adult and aged mice was analyzed by X-ray, biomechanics, µCT, histology and immunohistochemistry at 2 and 10 weeks after surgery as well as by Western blotting at 2 weeks after surgery. Callus composition and remodeling were assessed by Safranin-O and TRAP-staining. Additionally, angiogenesis and inflammation were analyzed by immunohistochemical staining of CD31-positive endothelial cells as well as of myeloperoxidase (MPO)-positive granulocytes and CD68-positive macrophages. Finally, the expression of a plethora of pro-osteogenic and pro-angiogenic growth factors within the callus tissue was assessed to identify different expression patterns in non-union formation between young adult and aged mice.

Finally, to overcome non-union formation in the aged, the effects of systemic PTH treatment on bone regeneration was evaluated **in the third study** of this thesis [Menger et al., 2023b]. For this purpose, segmental femoral defects with subsequent pin-clip stabilization were generated in 18-20 months old CD-1 mice, according to Garcia et al. [2008]. The animals were treated daily with a subcutaneous injection of 200 µg/kg body weight PTH 1–34 (Bachem AG,

Budendorf, Switzerland) dissolved in 100 µL saline (PTH group). Animals of the control group received an equal amount of saline (control group) subcutaneously. The healing process was investigated by X-ray, biomechanical, µCT, histological as well as immunohistochemical analyses at 2 and 10 weeks after surgery. Additional Western blot analyses were performed at 2 weeks after surgery. Callus composition, bone remodeling, angiogenesis and inflammation were assessed as described in the second study by Safranin-O and TRAP-staining, immunohistochemical analysis of CD31-positive endothelial cells as well as of MPO-positive granulocytes and CD68-positive macrophages. Furthermore, the impact of systemic PTH treatment on protein expression such as VEGF, cyclooxygenase (COX)-2 and phosphoinositide 3-kinase (PI3K) within the callus tissue was investigated.

4. Aim of the study

The original articles of the present thesis compare the validity and reliability of 2 different non-union models in mice, describe an atrophic non-union model in aged animals and evaluate the effects of PTH treatment on bone regeneration in aged mice.

In the first study published in ***Bone***, two non-union models with damaged periosteum in mice were compared for their validity and reliability. The following questions were addressed:

- What non-union model in mice is the most valid: A model using a segmental defect and pin-clip fixation with periosteal stripping or a model using K-wire stabilization of a trauma-induced fracture and periosteal cauterization?
- Do the femora with K-wire stabilization show an increased biomechanical stiffness when compared to the femora with segmental defect and pin-clip fixation?
- Does the callus tissue of the K-wire group demonstrate an increased bone remodeling when compared to the callus tissue of the pin-clip group?
- Does the callus tissue of the K-wire group demonstrate a higher number of microvessels when compared to the callus tissue of the pin-clip group?
- Does the callus tissue of the K-wire group demonstrate a higher cell proliferation when compared to the callus tissue of the pin-clip group?
- Does the callus tissue of the K-wire group demonstrate a higher expression of pro-angiogenic and pro-osteogenic growth factors when compared to the callus tissue of the pin-clip group?

In the second study published in ***The Journals of Gerontology Series A: Biological Sciences***, the above mentioned non-union model with segmental defect and pin-clip stabilization was established in aged mice. In addition, cellular and biochemical differences in non-union formation between young adult and aged mice were analyzed. The following questions were addressed:

- Is the pin-clip non-union model also valid in aged mice?
- Do the non-unions of aged mice demonstrate a lower bending stiffness when compared to non-unions of young adult animals?
- Do the non-unions of aged mice demonstrate a decreased bone formation and remodeling when compared to non-unions of young adult animals?
- Do the non-unions of aged mice demonstrate a decreased angiogenesis when compared to non-unions of young adult animals?

- Do the non-unions of aged mice demonstrate an increased inflammatory response when compared to non-unions of young adult animals?
- Do the non-unions of aged mice demonstrate a lower expression of pro-angiogenic and pro-osteogenic growth factors when compared to non-unions of young adult animals?

In the third study, published in the ***Journal of Translational Medicine***, the pro-angiogenic and pro-osteogenic effects of PTH on bone regeneration were assessed in an atrophic non-union model in aged mice. The goal of this study was to overcome non-union formation in aged mice. The following questions were addressed:

- Does PTH treatment stimulate bone regeneration in aged mice?
- Does PTH treatment increase bone remodeling in aged mice?
- Does PTH treatment improve the biomechanical stiffness of femora of aged mice?
- Does PTH treatment increase angiogenesis within the callus tissue of aged mice?
- Does PTH treatment reduce the inflammatory response within the callus tissue of aged mice?
- Does PTH treatment increase the expression of pro-angiogenic and pro-osteogenic growth factors within the callus tissue of aged mice?

5. Original articles

Bone 162 (2022) 116475

Contents lists available at ScienceDirect

Bone

journal homepage: www.elsevier.com/locate/bone

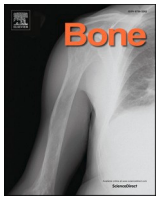

Full Length Article

Comparison of two non-union models with damaged periosteum in mice: Segmental defect and pin-clip fixation versus transverse fracture and K-wire stabilization

Maximilian M. Menger [a,b,*], David Bauer [b], Michelle Bleimehl [b], Claudia Scheuer [b], Sabrina Ehnert [c], Michael D. Menger [b], Tina Histing [a], Matthias W. Laschke [b]

[a] Department of Trauma and Reconstructive Surgery, Eberhard Karls University Tuebingen, BG Trauma Center Tuebingen, 72076 Tuebingen, Germany
[b] Institute for Clinical and Experimental Surgery, Saarland University, 66421 Homburg/Saar, Germany
[c] Department of Trauma and Reconstructive Surgery, BG Trauma Center Tuebingen, Siegfried Weller Institute for Trauma Research, Eberhard Karls University Tuebingen, 72076 Tuebingen, Germany

ARTICLE INFO

Keywords:
Non-union
Periosteum
Segmental defect
Bone regeneration
Angiogenesis
Fracture healing
Mice
Murine model
K-wire
Periosteal cauterization

ABSTRACT

Despite growing knowledge about the mechanisms of fracture healing, non-union formation still represents a major complication in trauma and orthopedic surgery. Non-union models in mice gain increasing interest, because they allow investigating the molecular and cellular mechanisms of failed fracture healing. These models often use segmental defects to achieve non-union formation. Alternatively, failed fracture healing can be induced by transverse fractures with additional periosteal injury. The present study systematically compared the reliability of these two approaches to serve as non-union model. A 0.6 mm K-wire was inserted into the femora of CD-1 mice in a retrograde fashion and a closed transverse femoral fracture was created. Subsequently, the fracture site was exposed and the periosteum was cauterized. This approach was compared with a well-established non-union model involving the pin-clip fixation of a 1.8 mm segmental defect. The callus tissue was analyzed by means of radiography, biomechanics, histology and Western blotting. At 10 weeks after surgery 10 out of 12 femora (83.3 %) of the K-wire group showed a non-union formation. The pin-clip model resulted in 100 % non-union formation. The K-wire group showed increased bone formation, osteoclast activity and bending stiffness when compared to the group with pin-clip fixation. This was associated with a higher expression of bone formation markers. However, the number of CD31-positive microvessels was reduced in the K-wire group, indicating an impaired angiogenic capacity after periosteal cauterization. These findings suggest that the pin-clip model is more reliable for the study of non-union formation in mice. The K-wire model including periosteal injury by cauterization however, may be particularly applied in preclinical studies which explore the effects of damaged periosteum and reduced angiogenic capacity to trauma-induced fractures.

1. Introduction

Fracture healing is a complex process, which is characterized by the temporal and spatial interaction of multiple cell types and growth factors [1]. Despite the extraordinary capacity of bone to regenerate, 10 % of all fractures still result in delayed healing or non-union formation [2]. The treatment of non-unions is often difficult and highly challenging [3]. A variety of strategies have been developed to treat non-union formation, but there is no consensus on the ideal management [4]. Failed fracture healing does not only result in increased pain, loss of mobility and prolonged rehabilitation rates for the patients, but also imposes a considerable economic burden on the health care system [5].

To gain further insights in the molecular and cellular mechanisms of non-union formation, appropriate animal models are required. Ideally, these models should be reliable and should mimic the clinical pathophysiology in humans in order to develop novel treatment strategies. In recent years, particularly mouse models have gained increasing interest in trauma research due to their cost effectiveness and the opportunity to generate genetically modified strains [6].

In 2008, Garcia et al. [7] introduced such a non-union model in mice

* Corresponding author at: Department of Trauma and Reconstructive Surgery, Eberhard Karls University Tuebingen, BG Trauma Center Tuebingen, 72076 Tuebingen, Germany.
E-mail address: maximilian.menger@uks.eu (M.M. Menger).

https://doi.org/10.1016/j.bone.2022.116475
Received 26 March 2022; Received in revised form 8 June 2022; Accepted 17 June 2022
Available online 23 June 2022

by creating a critically sized femoral osteotomy. This model provides axial and rotational stability due to the application of a pin-clip fixation technique. Another approach for a non-union model in mice represents the creation of a simple transverse femoral fracture with additional periosteal injury. The periosteum is a highly vascularized tissue providing the cortical blood supply [8] and serving as a reservoir for osteoprogenitor cells [9]. In fact, multiple experimental studies on fracture healing have highlighted the importance of preserving the periosteum at the fracture site [10–12]. Hence, the periosteum represents a major prerequisite for successful bone regeneration. A periosteal injury induced by thermal cauterization may thus result in an avascular and biologically inert environment leading to compromised fracture healing and non-union formation [13]. In 2003, Kokubu et al. [14] established such a non-union model in rats by stabilizing femoral fractures with K-wire fixation and subsequent periosteal cauterization of the fracture zone. However, this non-union model has yet not been introduced in mice.

Both approaches may be promising for the investigation of non-union formation in preclinical research. However, so far there is no study, which directly compared the validity and reliability of these two models in mice. For this purpose, we herein analyzed the course of non-healing within the callus tissue of these two non-union models by means of radiography, biomechanics, histology and Western blotting.

2. Materials and methods

2.1. Animals

In this study, 62 male and female CD-1 mice with a mean body weight of 30–40 g and an age of 12–16 weeks were used. The animals were bred at the Institute for Clinical and Experimental Surgery, Saarland University, Germany, and housed at a regular light and dark cycle with free access to tap water and standard pellet food (Altromin, Lage, Germany).

All experiments were performed according to the German legislation on the protection of animals and the National Institutes of Health (NIH) Guide for the Care and Use of Laboratory Animals (Institute of Laboratory Animal Resources, National Research Council, Washington DC, USA). The experiments were approved by the local governmental animal protection committee.

2.2. Surgical procedure

All the surgeries of the present study were performed by the same person to guarantee highly standardized conditions. Mice were anesthetized by an intraperitoneal (i.p.) injection of ketamine (75 mg/kg body weight, Ursotamin®, Serumwerke Bernburg, Bernburg, Germany) and xylazine (15 mg/kg body weight, Rompun®, Bayer, Leverkusen, Germany). The non-union model using periosteal cauterization was performed as follows. Under aseptic conditions, a ~4 mm medial parapatellar incision was made at the right knee and the patella was dislocated laterally. A 0.6 mm K-wire (Depuy Synthes, Umkirch, Germany) was inserted through the intracondylar notch into the medullary cavity with a motor-driven drill. The K-wire was advanced through the great trochanter and out of the skin. Then, a ~4 mm incision was performed in the skin around the K-wire and the wire was cut in proximity to the proximal femur. In addition, the distal end of the K-wire was cut close to the femoral condyles. Afterwards, the femur was fractured by a 3-point bending device as described previously [15]. Subsequently, the fracture site was exposed by a lateral approach and the periosteum was cauterized circumferentially within a distance of 2 mm on each side of the fracture. The periosteum was only cauterized once to avoid thermal necrosis of the bone. Moreover, care was taken to protect all soft tissue except the periosteum during the procedure. The wounds were irrigated with saline solution and closed using 5-0 synthetic sutures. Adequate reduction of the fracture and position of the implant were confirmed by radiography (MX-20, Faxitron X-ray Corporation, Wheelin, IL, USA). Of note, a comminuted or incomplete fracture was observed in none of the animals.

The pin-clip model using a segmental defect was performed as described previously [7]. Under aseptic conditions, a ~4 mm medial parapatellar incision was created at the right knee and the patella was dislocated laterally. After drilling a hole (diameter of 0.5 mm) into the intracondylar notch, a distally flattened pressfit 24 Gauge needle (diameter of 0.55 mm) was implanted intramedullary and the wound was closed. The pin was flattened at the distal end to avoid secondary dislocation. After insertion of the pin, the diaphysis of the femur was exposed by a lateral approach. Subsequently, a custom-made clip of 6 mm length was implanted ventrodorsally into the femur and lateral of the already implanted pin. A gap size of 1.8 mm was created by means of a spherical trephine under permanent saline solution cooling. Moreover, the periosteum was stripped 2 mm proximally and distally of the gap along the longitudinal axis of the femoral bone. The implant position was confirmed by radiography (MX-20, Faxitron X-ray Corporation, Wheelin, IL, USA). All procedures were done under an operating microscope, guaranteeing a high level of precision. For analgesia the mice received tramadol-hydrochloride (Grünenthal, Aachen, Germany) in the drinking water (1 mg/mL) starting on the day prior to surgery until three days after surgery. At 2 weeks (n = 8 each group), 5 weeks (n = 8 each group) and 10 weeks (n = 12 each group) the animals were sacrificed by an overdose of anesthetics and the femora were excised for further radiological and histological analysis. Moreover, additional animals were sacrificed accordingly at 2 weeks (n = 3 each group) for Western blot analysis.

2.3. X-ray analysis

At 2, 5 and 10 weeks after surgery the animals were anesthetized again and ventrodorsal radiographs of the fractured and osteotomized femora were performed. Fracture healing was analyzed according to the Goldberg score with stage 0 indicating radiological non-union, stage 1 indicating possible union and stage 2 indicating radiological union [16].

2.4. Biomechanical analysis

After removal of the soft tissue and the implants, the bending stiffness of the femora was measured by a 3-point-bending device using a non-destructive approach. This allowed a subsequent use of the specimens for micro computed tomography (μCT) as well as histological and immunohistochemical investigations and, thus, a reduction of the number of laboratory animals needed. Due to the different stages of healing, the loads, which had to be applied varied markedly between the individual animals. Loading was stopped individually in every case when the actual load-displacement curve deviated >1 % from linearity. Bending stiffness (N/mm) was calculated from the linear elastic part of the load-displacement diagram [17].

2.5. μCT analysis

The specimens were scanned (Skyscan 1172; Bruker, Billerica, MA, USA) at a spatial resolution of 6.5 μm with a standardized setup (tube voltage: 50 kV; current: 200 μA; intervals: 0.4°; exposure time: 3500 ms; filter: 0.5 mm aluminum). Images were stored in three-dimensional arrays. To express gray values as mineral content (bone mineral density (BMD)), calcium hydroxyapatite (CaHA) phantom rods with known BMD values (0.250 g and 0.750 g CaHA/cm^3) were employed for calibration. The region of interest (ROI) defining the novel bone was contoured manually excluding any original cortical bone. The thresholding allowed distinguishing soft tissue from bone tissue and the differentiation between lowly and highly mineralized bone (CTAnalyser; Bruker, Billerica, MA, USA). The thresholds to distinguish between poorly and highly mineralized bone were based upon visual inspection of the

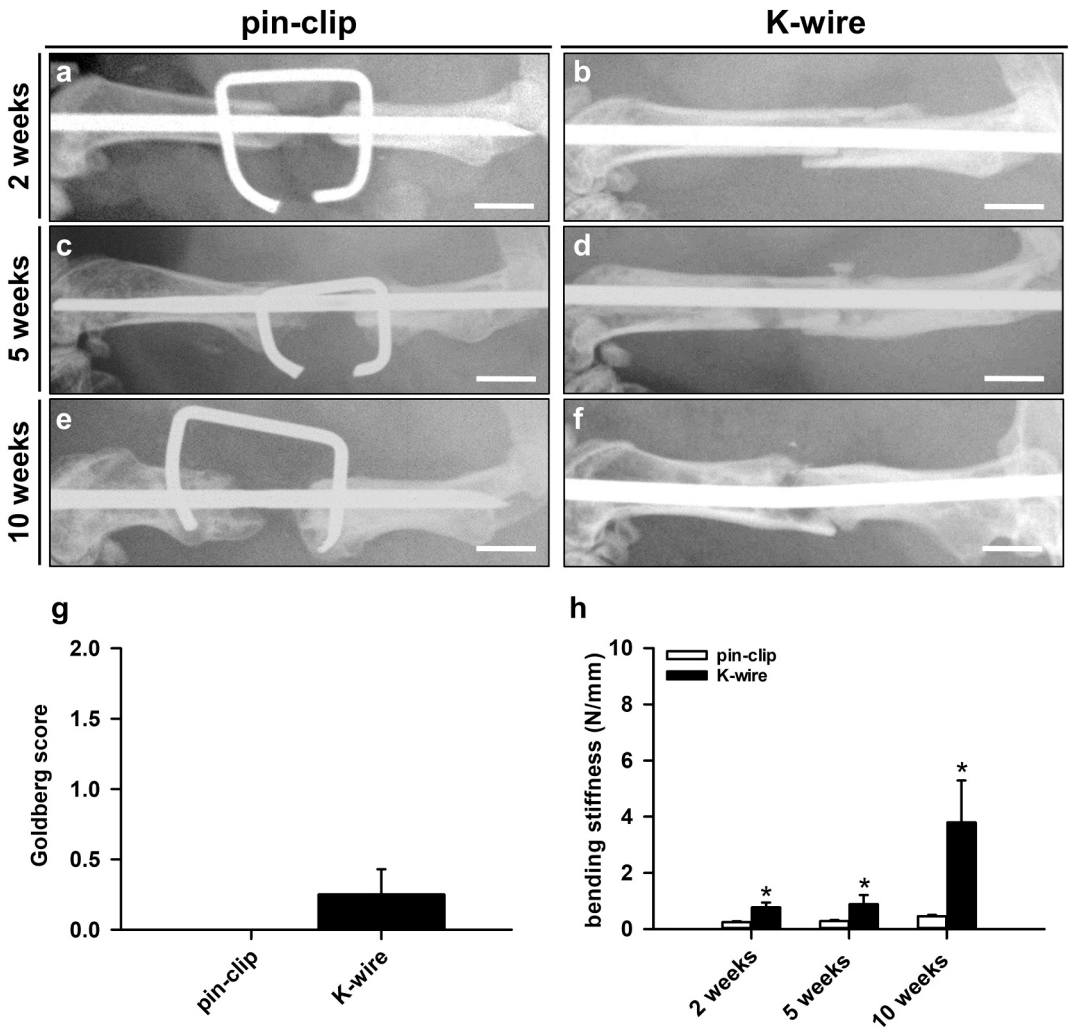

Fig. 1. (a–f) Representative X-rays of femora of the pin-clip group (a, c, e) and K-wire group (b, d, f) at 2 (a, b), 5 (c, d) and 10 weeks (e, f) after surgery. Scale bars: 2 mm. (g) Goldberg score of the callus tissue of animals of in the pin-clip group (n = 12) and the K-wire group (n = 12) at 10 weeks after surgery, as assessed by X-ray analysis. (h) Bending stiffness (N/mm) in the pin-clip group (white bars, n = 8 at 2 and 5 weeks after surgery, n = 12 at 10 weeks after surgery) and the K-wire group (black bars, n = 8 at 2 and 5 weeks after surgery, n = 12 at 10 weeks after surgery) at 2, 5 and 10 weeks after surgery, as assessed by biomechanical analysis. Mean ± SEM; *$p < 0.05$ vs. pin-clip.

images, qualitative comparison with histological sections and other studies investigating bone repair and callus tissue by μCT [18–20]. A BMD with >0.642 g/cm^3, resulting in gray values of 98–255, was defined as highly mineralized bone. Poorly mineralized bone was assumed to have a BMD value between 0.410 g/cm^3 and 0.642 g/cm^3, resulting in gray values of 68–97.

The following parameters were calculated from the callus region of interest for each specimen: poorly mineralized bone volume (mm^3), highly mineralized bone volume (mm^3), bone volume fraction of tissue volume (BV/TV, %), bone surface density (1/mm^3), trabecular thickness (mm), trabecular separation (mm) and trabecular number (1/mm).

2.6. Histomorphometric analysis

After biomechanical testing and μCT analyses, bones were fixed in paraformaldehyde for 24 h. Subsequently, the specimens were embedded in a 30 % sucrose solution for another 24 h and then freezed at −80 °C. Longitudinal sections through the femoral axis with a thickness of 4 μm were cut by the Kawamotos film method for histomorphometric analyses and stained with Safranin-O. At a magnification of 12.5× (BX60 Microscope; Olympus, Shinjuku, Japan; Zeiss Axio Cam and Axio Vision 3.1, Zeiss) structural indices were calculated according to the recommendations of Gerstenfeld et al. [21]. The following histomorphometric parameters of the bone defects were evaluated at 2, 5 and 10 weeks after surgery: (i) bone callus area; (ii) cartilaginous callus area and (iii) fibrous callus area. Pre-existing cortical bone of the proximal and distal fragment was excluded. Each area was marked and calculated using the ImageJ analysis system (NIH, Bethesda, USA).

Moreover, tartrate-resistant acid phosphatase (TRAP) activity was analyzed to determine the number of osteoclasts in the callus at 2, 5 and 10 weeks after fracture. For this purpose, additional longitudinal sections through the femoral axis with a thickness of 4 μm were cut and incubated in a mixture of 5 mg naphthol AS-MX phosphate and 11 mg fast red TR salt in 10 mL 0.2 M sodium acetate buffer (pH 5.0) for 1 h at 37 °C. Sections were counterstained with methyl green and covered with glycerine gelatine. TRAP-positive multinucleated cells (three or more nuclei per cell) were counted. For this purpose, one high-power field (HPF, 400× magnification) was placed in a standardized manner in the central region of the callus, while three additional HPFs were placed on each site of the periosteal callus. Thus, a total of 7 HPFs were analyzed from each specimen. The data on histomorphological osteoclast analyses are given as numbers of osteoclasts per HPF.

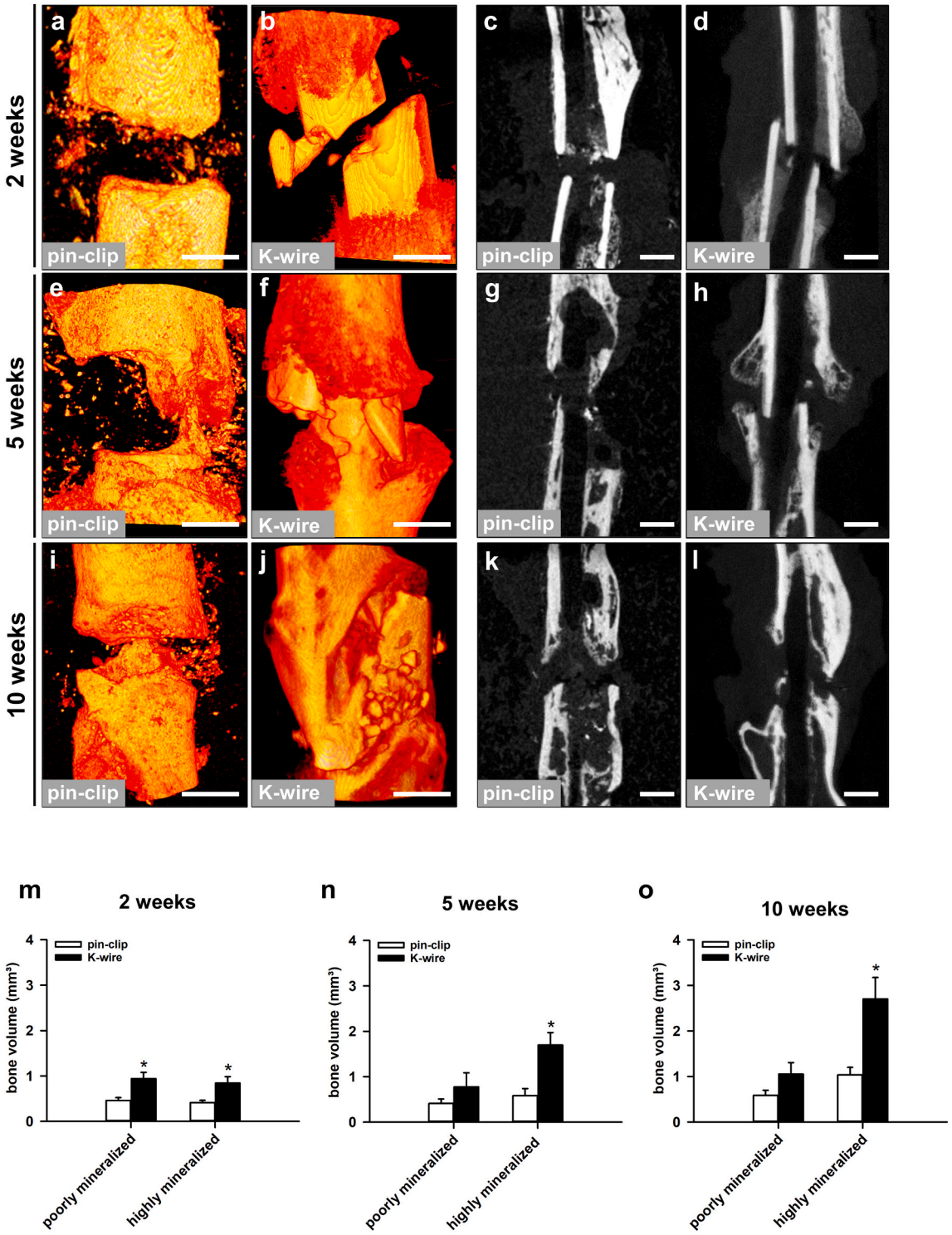

Fig. 2. (a–l) Representative μCT-3D reconstructions (a, b, e, f, i, j) and transversal μCT images (c, d, g, h, k, l) of femora of the pin-clip group and K-wire group at 2 (a–d), 5 (e–h) and 10 weeks (i–l) after surgery. Scale bars: 1 mm. (m–o) Poorly and highly mineralized bone volume (mm^3) of the callus tissue of animals of the pin-clip group (white bars, n = 8 at 2 and 5 weeks after surgery, n = 12 at 10 weeks after surgery) and the K-wire group (black bars, n = 8 at 2 and 5 weeks after surgery, n = 12 at 10 weeks after surgery) at 2 (m), 5 (n) and 10 (o) weeks after surgery, as assessed by μCT analysis. Mean ± SEM; *$p < 0.05$ vs. pin-clip.

2.7. Immunohistochemical analysis

In order to analyze the vascularization within the callus tissue at 2, 5 and 10 weeks after surgery, longitudinal sections with a thickness of 4 μm were cut. For the immunohistochemical detection of microvessels, sections were stained with a monoclonal rat anti-mouse antibody against the endothelial cell marker CD31 (1:100; Abcam, Cambridge, UK). A goat anti-rat IgG-Alexa555 antibody served as secondary antibody (1:100; Life Technologies, Eugene, USA). Cell nuclei were stained with Hoechst 33342 (2 μg/mL, Sigma-Aldrich, Taufkirchen, Germany). Moreover, for the detection of proliferating cells, sections were stained with a monoclonal mouse-anti mouse antibody against the proliferation marker proliferating cell nuclear antigen (PCNA) (1:100, Agilant Dako, Santa Clara, USA). A goat anti-mouse peroxidase antibody served as

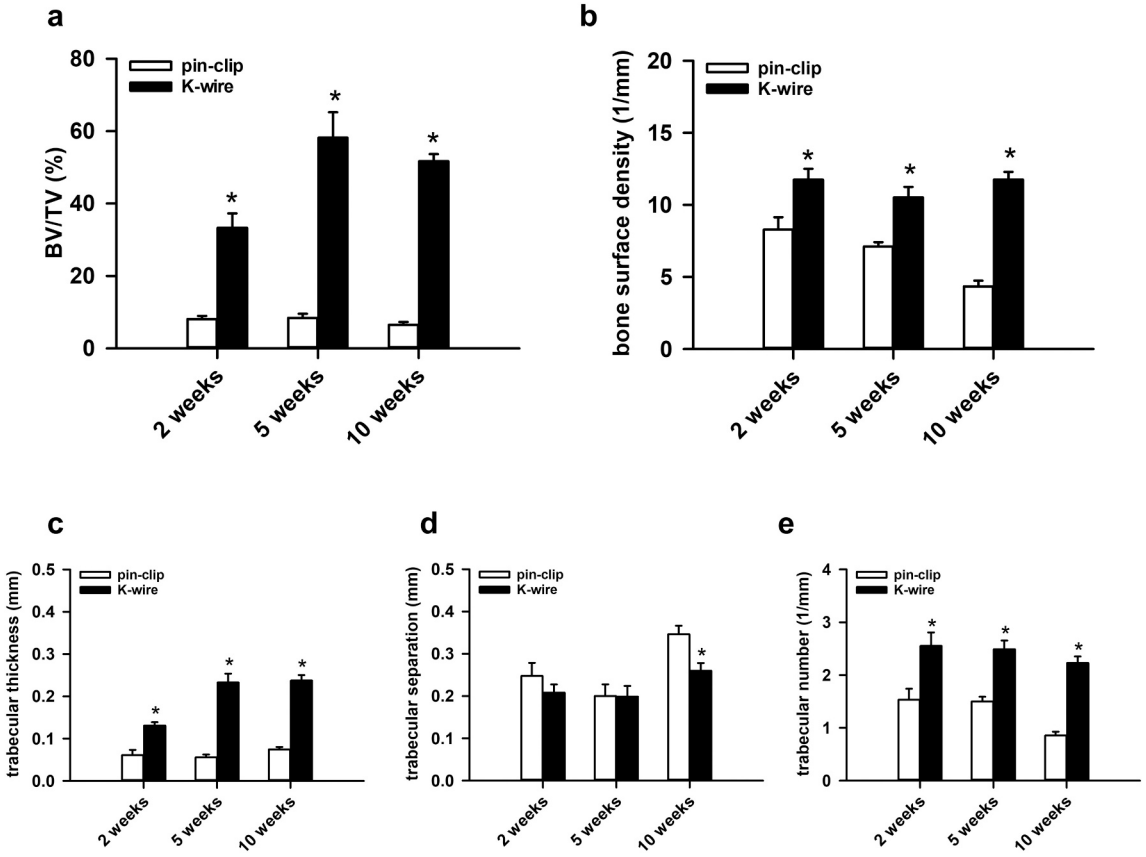

Fig. 3. (a–e) BV/TV (%) (a), bone surface density (1/mm) (b), trabecular thickness (mm) (c), trabecular separation (mm) (d) and trabecular number (1/mm) (e) of the callus tissue of animals of the pin-clip group (white bars, n = 8 at 2 and 5 weeks after surgery, n = 12 at 10 weeks after surgery) and the K-wire group (black bars, n = 8 at 2 and 5 weeks after surgery, n = 12 at 10 weeks after surgery) at 2, 5 and 10 weeks after surgery, as assessed by μCT analysis. Mean ± SEM; *$p < 0.05$ vs. pin-clip.

secondary antibody. CD31-positive microvessels and PCNA-positive cells were counted. For this purpose, one HPF was placed in a standardized manner in the central region of the callus, while three additional HPFs were placed on each site of the periosteal callus. Thus, a total of 7 HPFs were analyzed on each specimen. The data on immunohistochemical microvessel analyses and PCNA-positive cells are given as number of microvessels per HPF and number of PCNA-positive cells per HPF respectively.

2.8. Western blot analysis

Protein expression within the callus tissue was determined by Western blot analysis, including the expression of bone morphogenetic protein-2 (BMP-2) and -4 (BMP-4), PCNA, cysteine-rich protein (CYR) 61, receptor activator of NF-κB ligand (RANKL) and osteoprotegerin (OPG). The callus tissue was frozen and stored at −80 °C until required. Analyses were performed from callus tissue at 2 weeks after fracture healing (n = 3 each group). After saving the whole protein fraction, analysis was performed using the following antibodies: goat anti-mouse BMP-2/BMP-4 (1:300, R&D Systems, Minneapolis, USA), mouse anti-mouse PCNA (1:500, Proteintech Germany GmbH, Planegg-Martinsried, Germany), sheep anti-mouse CYR 61 (1:300, R&D Systems), rabbit anti-mouse RANKL (1:300, Abcam, Cambridge, UK) and rabbit anti-mouse OPG (1:300, Biozol Diagnostica, Eching, Germany). Primary antibodies were followed by corresponding horseradish peroxidase-conjugated secondary antibodies (1:1000, R&D Systems). Protein expression was visualized by means of luminol-enhanced chemiluminescence after exposure of the membrane to the Intas ECL Chemocam Imager (Intas Science Imaging Instrument GmbH, Göttingen, Germany) and normalized to β-actin signals (1:1000, mouse anti-mouse β-actin, Santa Cruz Biotechnology, Heidelberg, Germany) to correct for unequal loading.

2.9. Statistical analysis

All data are given as means ± SEM. After testing the data for normal distribution (Kolmogorov-Smirnov test) and equal variance (*F*-test), comparisons between the two groups were performed by the Student's *t*-test. For non-parametrical data, a Mann-Whitney *U* test was used. All statistics were performed using the SigmaPlot 13.0 software (Jandel Corporation, San Rafael, CA, USA). A *p*-value of <0.05 was considered to indicate significant differences.

3. Results

3.1. X-ray analysis

The radiographic analyses revealed a complete lack of osseous bridging in the pin-clip group throughout the 10-weeks observation period (Fig. 1a, c, e). X-rays showed a reliable non-union formation in all animals with a large persisting gap between the adjoining rounded bone fragments (Fig. 1e). In the K-wire group, X-rays demonstrated a persisting fracture gap without osseous bridging in most cases (Fig. 1b, d, f). Notably, at 2 and 5 weeks after surgery no sign of bony union was observed in the K-wire group (Fig. 1b, d). At 10 weeks after surgery the radiographic analyses revealed a complete non-union formation in 10 out of 12 (83.3 %) animals in the K-wire group, whereas 2 out 12 (16.7 %) animals exhibited radiographic signs of bony bridging. Accordingly,

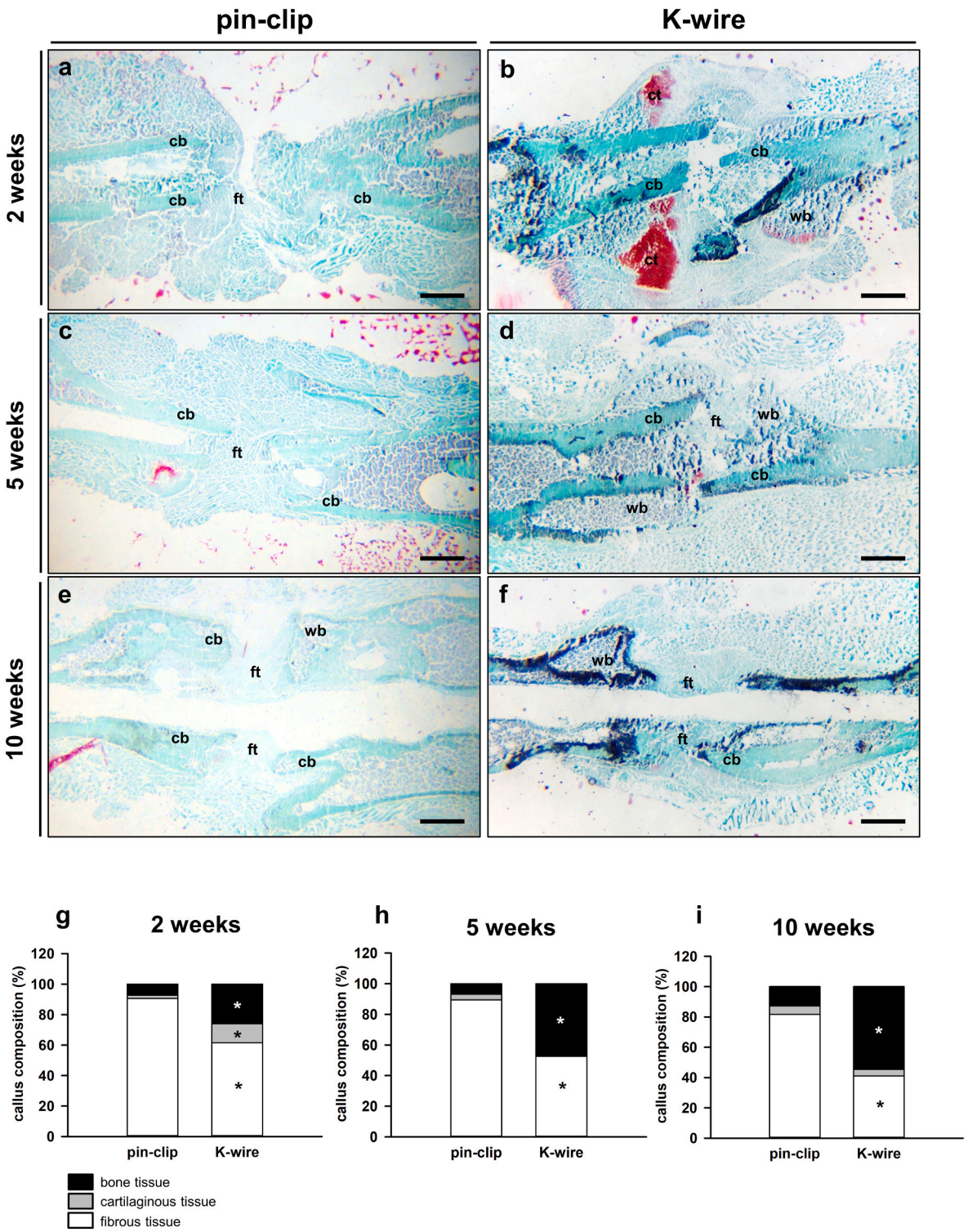

Fig. 4. (a–f) Representative histological images of Safranin-O-stained femora in the pin-clip group (a, c, e) and K-wire group (b, d, f) at 2 (a, b), 5 (c, d) and 10 weeks (e, f) after surgery. Fibrous tissue (ft), cartilaginous tissue (ct), woven bone (wb) and cortical bone (cb) are indicated. Scale bars: 1 mm. (g–i) Callus composition (%), including fibrous tissue (white), cartilaginous tissue (gray) and osseous tissue (black), of the callus tissue of animals of the pin-clip group (n = 8 at 2 and 5 weeks after surgery, n = 12 at 10 weeks after surgery) and the K-wire group (n = 8 at 2 and 5 weeks after surgery, n = 12 at 10 weeks after surgery) at 2 (g), 5 (h) and 10 (i) weeks after surgery, as assessed by histomorphometric analyses. Mean ± SEM; *$p < 0.05$ vs. pin-clip.

the analysis showed a slightly higher Goldberg score at 10 weeks after surgery in animals of the K-wire group when compared to the pin-clip group (Fig. 1g). However, this difference did not prove to be statistically significant ($p > 0.05$).

3.2. Biomechanical analysis

The biomechanical analysis demonstrated a significantly higher bending stiffness in the K-wire group at 2, 5 and 10 weeks after surgery when compared to animals, which underwent pin-clip stabilization

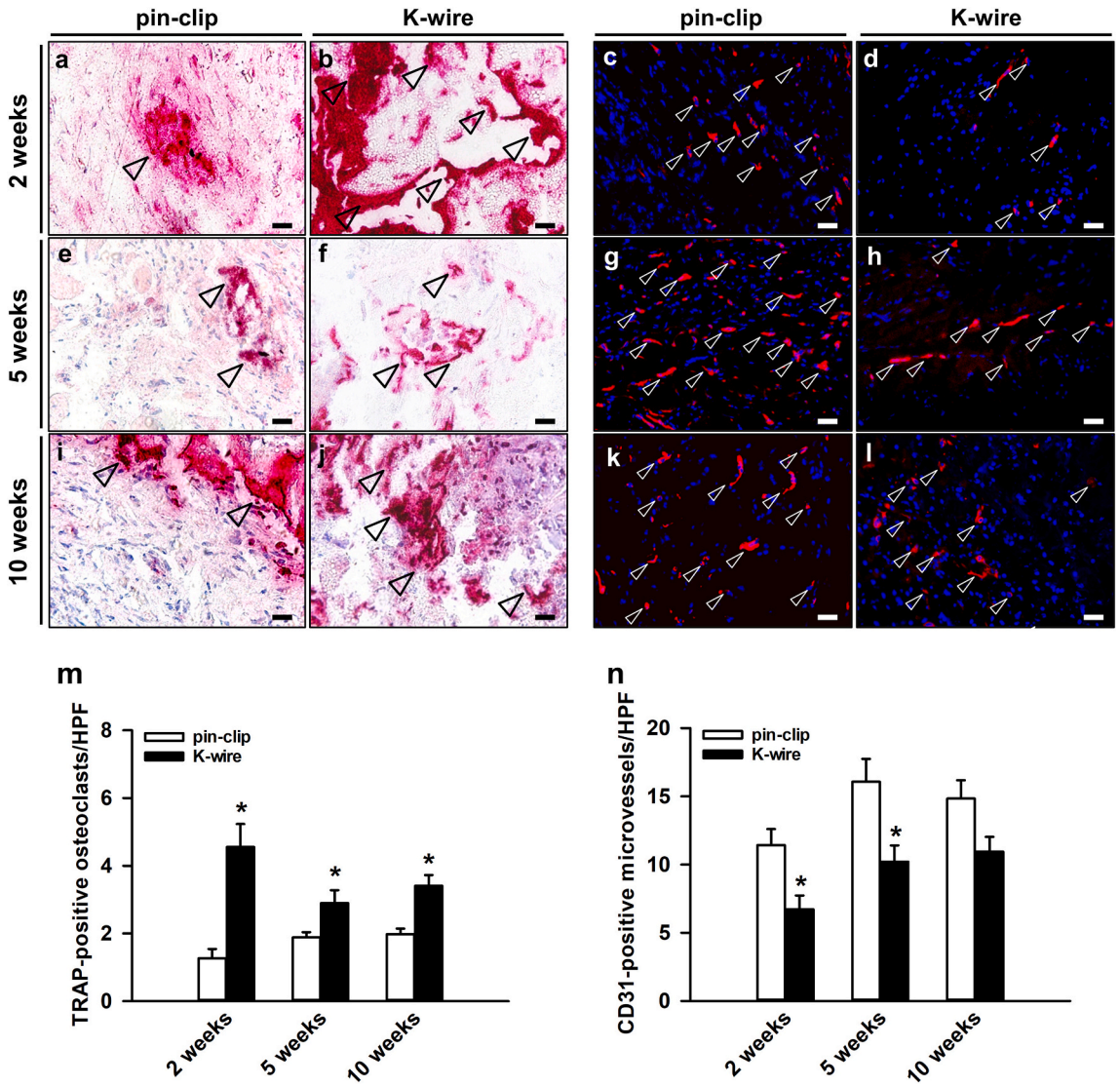

Fig. 5. (a–l) Representative histological and immunohistochemical images of TRAP-positive osteoclasts (a, b, e, f, i, j, arrowheads) and CD31-positive microvessels (c, d, g, h, k, l, arrowheads) in the callus tissue of animals of the pin-clip group (a, c, e, g, i, k) and the K-wire group (b, d, f, h, j, l) at 2 (a–d), 5 (e–h) and 10 weeks (i–l) after surgery. Scale bars: 25 μm. (m, n) TRAP-positive osteoclasts/HPF (m) and CD31-positive microvessels/HPF (n) within the callus tissue of animals of the pin-clip group (white bars, n = 8 at 2 and 5 weeks after surgery, n = 12 at 10 weeks after surgery) and the K-wire group (black bars, n = 8 at 2 and 5 weeks after surgery, n = 12 at 10 weeks after surgery) at 2, 5 and 10 weeks after surgery, as assessed by histological and immunohistochemical analysis. Mean ± SEM; *$p < 0.05$ vs. pin-clip.

(Fig. 1h). In the pin-clip group, the bending stiffness remained <1 N/mm confirming a complete failure of bone healing. In the K-wire group, the bending stiffness of the fractured femora increased only to ~3.8 N/mm at 10 weeks after surgery, also indicating comprised bone healing (Fig. 1h).

3.3. μCT analysis

In line with the radiographic analysis, the μCT analysis revealed a reliable non-union formation with no signs of osseous bridging in all animals of the pin-clip group throughout the 10-weeks observation period (Fig. 2a, c, e, g, i, k). In the K-wire group, we observed periosteal callus formation at 2 (Fig. 2b, d) and 5 weeks (Fig. 2f, h) after surgery. However, this still resulted in compromised fracture healing, as indicated by a lack of osseous bridging in 10 out of 12 animals at 10 weeks after surgery (Fig. 2j, l). The μCT analysis demonstrated a significantly enhanced amount of both poorly and highly mineralized bone volume at 2 weeks after surgery within the callus tissue of animals of the K-wire group when compared to the pin-clip group (Fig. 2m). At 5 and 10 weeks after surgery only the amount of highly mineralized bone volume was still significantly enhanced in the K-wire group when compared to the pin-clip group (Fig. 2n, o).

Of note, at 5 and 10 weeks after surgery the amount of poorly mineralized bone volume showed no significant differences between the two study groups (Fig. 2n, o).

Further analyses revealed a significantly higher BV/TV and bone surface density during the entire observation period in animals with periosteal cauterization and K-wire stabilization when compared to mice undergoing periosteal stripping and gap formation with pin-clip fixation. (Fig. 3a, b). The evaluation of the trabecular architecture demonstrated a greater trabecular thickness in the K-wire group throughout the entire observation period (Fig. 3c). The analysis further showed a reduced trabecular separation at 10 weeks after surgery and an elevated trabecular number at 2, 5 and 10 weeks after surgery in the K-wire group when compared to the pin-clip group (Fig. 3d, e).

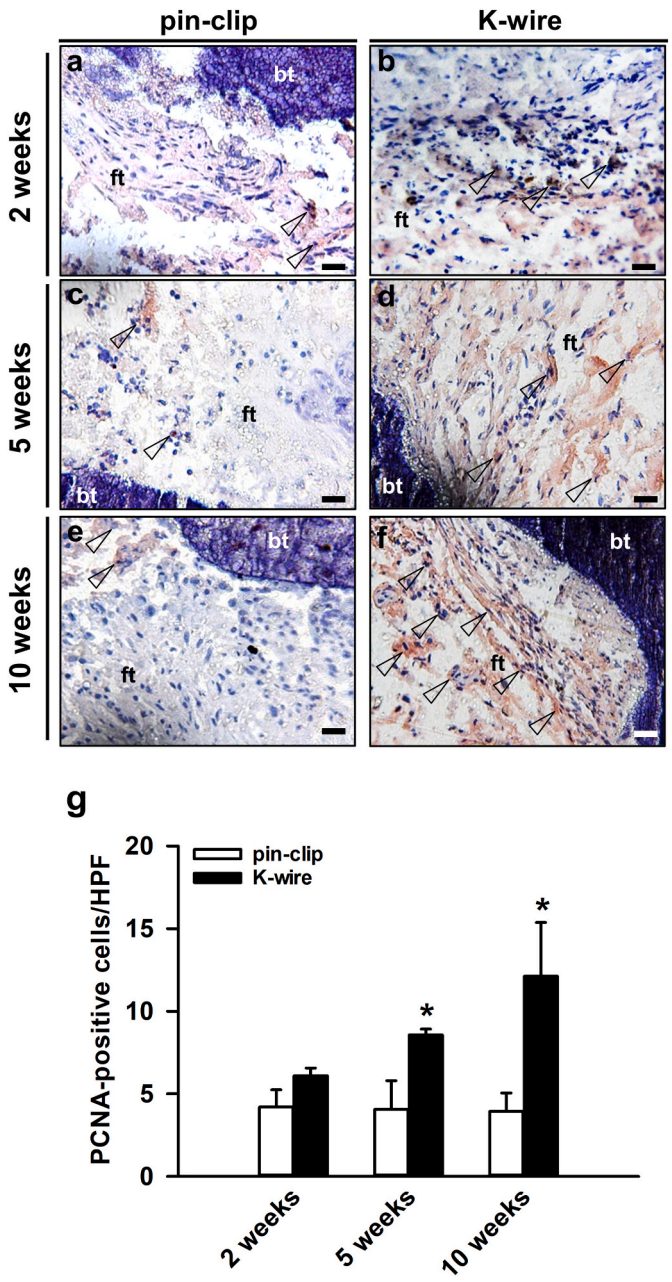

Fig. 6. (a–f) Representative immunohistochemical images of PCNA-positive cells (a, b, c, d, e, f, arrowheads) in the callus tissue of animals of the pin-clip group (a, c, e,) and the K-wire group (b, d, f) at 2 (a, b), 5 (c, d) and 10 weeks (e, f) after surgery. Fibrous tissue (ft) and bone tissue (bt) are indicated. Scale bars: 25 μm. (g) PCNA-positive cells/HPF within the callus tissue of animals of the pin-clip group (white bars, n = 8 at 2 and 5 weeks after surgery, n = 12 at 10 weeks after surgery) and the K-wire group (black bars, n = 8 at 2 and 5 weeks after surgery, n = 12 at 10 weeks after surgery) at 2, 5 and 10 weeks after surgery, as assessed by immunohistochemical analysis. Mean ± SEM; *$p <$ 0.05 vs. pin-clip.

3.4. Histomorphometric and immunohistochemical analysis

According to our radiological analysis, the histomorphometry showed a complete lack of osseous bridging in the pin-clip group with abundant fibrous tissue between the two bone fragments throughout the entire observation period (Fig. 4a, c, e). Interestingly, in the K-wire group we found signs of endochondral fracture healing at 2 weeks after surgery (Fig. 4b) and an increasing amount of bone tissue within the callus at 5 and 10 weeks after surgery (Fig. 4d, f). However, even at 10 weeks after surgery the fracture gap was filled with fibrous tissue, indicating incomplete and impaired bone healing (Fig. 4f). Quantitative histomorphometric analyses revealed a significantly higher fraction of cartilaginous tissue at 2 weeks after surgery in animals of the K-wire group when compared to animals in the pin-clip group (Fig. 4g), whereas at 5 and 10 weeks after surgery the amount of cartilaginous tissue did not significantly differ between the two study groups (Fig. 4h, i). The amount of bone tissue was markedly greater in animas of the K-wire group throughout the entire observation period, whereas the amount of fibrous tissue was smaller when compared to animals of the pin-clip group (Fig. 4g, h, i).

In addition, we analyzed the number of TRAP-positive osteoclasts within the callus tissue. Of interest, in the K-wire group the number of osteoclasts was significantly higher at 2, 5 and 10 weeks after surgery when compared to the pin-clip group (Fig. 5a, b, e, f, i, j, m). Further examination of the vascularization within the callus tissue demonstrated an increase in microvessel density from 2 to 5 weeks after surgery in both study groups (Fig. 5c, d, g, h, k, l, n). Moreover, we found a significantly lower number of CD31-positive microvessels in the K-wire group when compared to the pin-clip group at 2 and 5 weeks after surgery (Fig. 5c, d, g, h, n). The analysis of cell proliferation demonstrated a slightly increased number of PCNA-positive cells at 2 weeks after surgery in the K-wire group (Fig. 6a, b, g), and a significantly higher number of PCNA-positive cells at 5 and 10 weeks after surgery in the K-wire group when compared to the pin-clip group (Fig. 6c, d, e, f, g).

3.5. Western blot analysis

Western blot analyses of the callus tissue at 2 weeks after surgery revealed an over 3-fold higher expression of BMP-2 in the K-wire group when compared to animals undergoing pin-clip stabilization (Fig. 7a, b). Moreover, the expression of BMP-4 was significantly higher in animals of the K-wire group (Fig. 7a, c). The expression of the proliferation marker PCNA and the pro-angiogenic factor CYR61 was also higher in animals of the K-wire group when compared to that of the pin-clip group. However, this difference did not prove to be statistically significant (Fig. 7d, e, f). In addition, the expression of OPG, an inhibitor of osteoclastogenesis, was significantly higher in the K-wire group (Fig. 7g, h). RANKL, a stimulator of osteoclastogenesis, was almost not detectable within the callus tissue of animals of the pin-clip group, whereas animals of the K-wire group showed a considerable RANKL expression (Fig. 7g, i).

4. Discussion

Lack of union still represents a major burden in trauma and orthopedic surgery. To gain novel insights to the molecular and cellular mechanisms of failed fracture healing, murine animal models are of increasing interest in preclinical research. However, mice are a species on the lower physiological scale and, thus, exhibit a great potential for bone regeneration [22]. This makes the development of reliable non-union models in this species challenging. To identify the most reliable approach for the study of non-union formation in mice, we established for the first time a non-union model in mice, which uses a transverse femoral fracture and K-wire stabilization, and compared its validity and reliability with the model of Garcia et al. [7].

The majority of preclinical studies use segmental defects to investigate long bone non-union formation [23,24]. For instance, Garcia et al. [7] introduced a large femoral gap to generate reliable non-union formation in mice. In the present study, we detected a non-union rate of 100 % in this model with typical characteristics of atrophic non-union formation, including lack of fracture bridging, absent bone tissue formation and rounded bone ends. Large segmental defects have the advantage of mimicking the resection of established non-union in clinical practice and allow the study of mechanisms of atrophic non-union formation. However, the disadvantage of this approach is that the

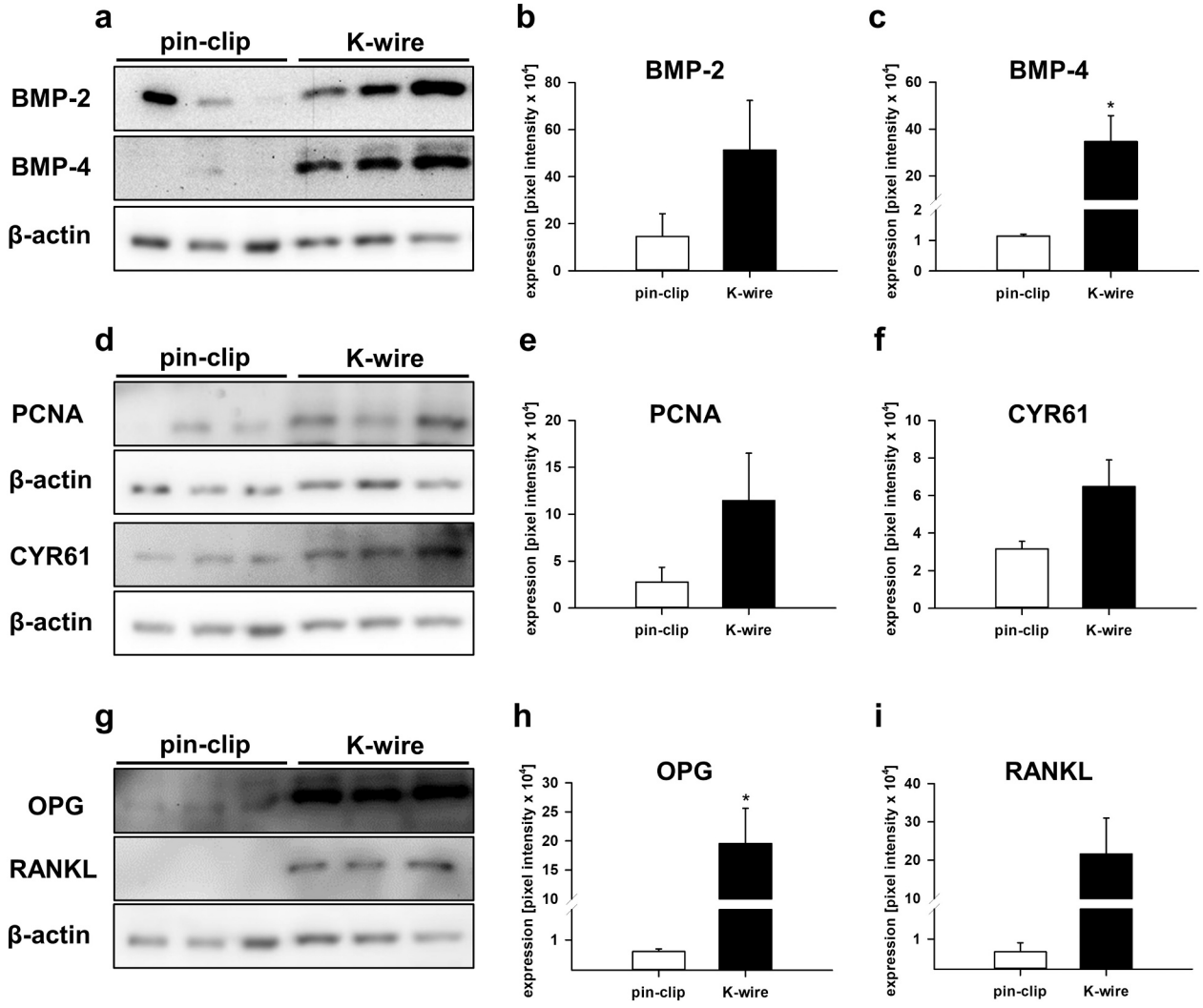

Fig. 7. (a) Representative Western blots of BMP-2, BMP-4 and β-actin expression within the callus tissue of animals of the pin-clip group and the K-wire group at 2 weeks after surgery. (b, c) Expression of BMP-2 (pixel intensity × 10^4) (b) and BMP-4 (pixel intensity × 10^4) (c) within the callus tissue of animals of the pin-clip group (white bars, n = 3) and the K-wire group (black bars, n = 3) at 2 weeks after surgery, as assessed by Western blot analysis. Mean ± SEM; *$p < 0.05$ vs. pin-clip. (d) Representative Western blots of PCNA, CYR61 and β-actin expression within the callus tissue of animals of the pin-clip group and the K-wire group at 2 weeks after surgery. (e, f) Expression of PCNA (pixel intensity × 10^4) (e) and CYR61 (pixel intensity × 10^4) (f) within the callus tissue of animals of the pin-clip group (white bars, n = 3) and the K-wire group (black bars, n = 3) at 2 weeks after surgery, as assessed by Western blot analysis. Mean ± SEM. (g) Representative Western blots of OPG, RANKL and β-actin expression within the callus tissue of animals of the pin-clip group and the K-wire group at 2 weeks after surgery. (h, i) Expression of OPG (pixel intensity × 10^4) (h) and RANKL (pixel intensity × 10^4) (i) within the callus tissue of animals of the pin-clip group (white bars, n = 3) and the K-wire group (black bars, n = 3) at 2 weeks after surgery, as assessed by Western blot analysis. Mean ± SEM; *$p < 0.05$ vs. pin-clip.

pathophysiology does not resemble the injury of trauma-induced fractures. In fact, in clinical practice many non-unions occur without significant bone loss. Interestingly, there is evidence that the integrity of the periosteum is a crucial prerequisite for successful bone regeneration, whereas periosteal disruption at the fracture site may lead to impaired fracture healing [13].

Based on these findings, Kobubu et al. [14] developed a non-union model in rats using a stable closed fracture with additional periosteal cauterization, which was stabilized by a 1.25 mm K-wire. The authors reported a 100 % rate of non-union formation 8 weeks after fracture healing [14]. In the present study, we adapted this model to mice, cauterizing the periosteum circumferentially within a distance of 2 mm on each side of the fracture and stabilizing the femur by a 0.6 mm K-wire. The 0.6-mm diameter of the K-wire allowed the press fit fixation of the fracture without implant dislocation, axial instability or fatigue failure over the entire observation period. Notably, our radiological and histological analyses revealed that 10 out of 12 femora resulted in non-union formation at 10 weeks after surgery. These results indicate that in mice periosteal cauterization is not sufficient to guarantee complete cessation of fracture healing. In rats, on the other hand, the periosteal cauterization leads to a reliable non-union formation [14]. This may be due to a higher bone healing capacity in mice when compared to rats [25]. As a result, the present model may be less reliable for the investigation of non-union formation than the already established segmental defect model by Garcia et al. [7], which resulted in a 100 %-rate of failed fracture healing at 10 weeks after surgery.

Our μCT and histological analyses revealed an increased bone formation in animals of the K-wire group when compared to animals of the pin-clip group. Moreover, our histomorphometric analysis demonstrated a significant fraction of cartilaginous tissue at 2 weeks after surgery in the K-wire group, indicating endochondral ossification. In contrast, in the pin-clip group cartilaginous tissue at 2 weeks after surgery was rarely observed. This finding was associated with a higher expression of the bone formation markers BMP-2, BMP-4 and CYR61 as well as the proliferation marker PCNA in the K-wire group. In general, endochondral fracture healing is characterized by the formation of a soft

callus, which gradually transforms into bone by the resorption of calcified cartilage and the formation of novel bone tissue [26]. This osteogenic phase is characterized by the expression of bone formation markers and cell proliferation, approximately peaking between 2 and 3 weeks after fracture [27]. Hence, the increased expression of bone formation markers associated with endochondral ossification may have resulted in the enhanced bone tissue formation and, thus, the higher bending stiffness in the K-wire group.

We further investigated the number and activity of osteoclasts within the callus tissue. Interestingly, we found a higher number of TRAP-positive osteoclasts and a higher expression of OPG and RANKL within the callus tissue in the K-wire group. It is widely accepted that RANKL acts as potent activator of bone resorption by binding RANK on the osteoclast cell membrane. OPG, on the other hand, is a soluble decoy receptor for RANKL that prevents RANKL-RANK binding, eventually leading to an inhibition of osteoclastogenesis [28,29]. Of note, cartilage resorption and novel bone formation are characterized by a peak in RANKL and OPG expression [30]. Moreover, previous studies have demonstrated that inhibition of RANKL by means of melatonin and pantoprazole delays callus remodeling and leads to an impaired fracture healing in mice [27,31]. Accordingly, successful bone regeneration requires osteoclast-mediated cartilage resorption. Therefore, the elevated expressions of OPG and RANKL within the callus tissue as well as the increased number of osteoclasts probably resulted in an enhanced formation of novel bone tissue in the K-wire group.

Vascularization is thought to be a crucial prerequisite for successful bone regeneration. Newly formed blood vessels allow nutrients and mesenchymal stem cells to invade the fracture site and induce callus formation and remodeling [32]. Furthermore, experimental studies could show that a stimulation of vascularization accelerates fracture healing [33,34], whereas an inhibition of angiogenesis leads to non-union formation [35]. However, the role of vascularization in the pathogenesis of non-unions is still controversially discussed. Several studies demonstrated that non-unions are associated with an avascular and biological inert environment [36,37]. In contrast, others reported a rich vascularization within the callus tissue of non-unions [7,38,39]. The latter view is supported by the present study. In fact, in both study groups we observed a considerable density of CD31-positive microvessels in the callus tissue. However, the number of microvessels was significantly lower in the K-wire group when compared to animals undergoing the pin-clip fixation technique. This is most likely due to the thermal damage of the periosteum induced by the circumferential cauterization. The periosteum plays a vital role in bone regeneration by providing an adequate blood supply to the fracture callus [13]. Apparently, mechanical periosteal stripping, as performed in the pin-clip model, posed less damage to the periosteum when compared to the injury induced by periosteal cauterization. The impaired angiogenesis and vascularization due to periosteal cauterization may lead to ischemic conditions within the callus, suppressing osteogenic differentiation and, on the other hand, inducing fibrogenic proliferation. This process results in the formation of fibrous tissue in place of bone tissue, ultimately leading to failed fracture healing [40,41]. Accordingly, our immunohistochemical staining revealed that proliferating PCNA-positive cells were mainly located within the fibrous tissue of the callus.

Taken together, it may be hypothesized that the compromised fracture healing observed in the K-wire group is due to an impaired angiogenic capacity and vascularization of the callus tissue caused by significant damage to the periosteum. On the other hand, non-union formation in the pin-clip group may be caused by a low expression of pro-osteogenic markers and a reduced osteoclast number and activity, hindering adequate bone formation and callus remodeling. However, future studies are required to clearly delineate the pathophysiology of the failed bone healing in these non-union models.

5. Conclusion

In conclusion, the present study demonstrates that the generation of a large segmental defect and rigid pin-clip stabilization are superior for the reliable induction of non-union formation in mice when compared to the model using periosteal cauterization. Large segmental defects may be particularly suitable for the evaluation of the molecular and cellular mechanisms of atrophic non-union formation. The model with a trauma-induced femoral fracture, K-wire stabilization and additional periosteal damage, on the other hand, may be used in preclinical studies investigating the effects of damaged periosteum and impaired angiogenic capacity on trauma-induced fractures.

CRediT authorship contribution statement

The authors declare no conflicts of interest.

CRediT authorship contribution statement

Maximilian M. Menger: Conceptualization, Methodology, Investigation, Formal analysis, Writing – original draft, Writing – review & editing, Visualization. **David Bauer:** Formal analysis, Visualization. **Michelle Bleimehl:** Formal analysis, Visualization. **Claudia Scheuer:** Formal analysis, Visualization. **Sabrina Ehnert:** Supervision, Writing – review & editing. **Michael D. Menger:** Supervision, Writing – review & editing, Conceptualization. **Tina Histing:** Supervision, Writing – review & editing, Conceptualization. **Matthias W. Laschke:** Supervision, Writing – review & editing, Conceptualization.

Acknowledgements

We are grateful for the excellent technical assistance of Sandra Hans and Julia Parakenings.

References

[1] C. Schlundt, C.H. Bucher, S. Tsitsilonis, H. Schell, G.N. Duda, K. Schmidt-Bleek, Clinical and research approaches to treat non-union fracture, Curr. Osteoporos. Rep. 16 (2) (2018) 155–168. http://www.ncbi.nlm.nih.gov/pubmed/29536393.
[2] T.A. Einhorn, L.C. Gerstenfeld, Fracture healing: mechanisms and interventions, Nat. Rev. Rheumatol. 11 (1) (2015) 45–54. http://www.ncbi.nlm.nih.gov/pubmed/25266456.
[3] P. Megas, Classification of non-union, Injury 36 (Suppl. 4) (2005) S30–S37. https://www.ncbi.nlm.nih.gov/pubmed/16291321.
[4] R.A. Hayda, M.J. Bosse, Moderators' summary: management of segmental bone defects, J. Am. Acad. Orthop. Surg. 14 (10 Spec No.) (2006) S142–S144. http://www.ncbi.nlm.nih.gov/pubmed/17003187.
[5] G. Victoria, B. Petrisor, B. Drew, D. Dick, Bone stimulation for fracture healing: what's all the fuss? Indian J. Orthop. 43 (2) (2009) 117–120. http://www.ncbi.nlm.nih.gov/pubmed/19838359.
[6] T. Histing, P. Garcia, J.H. Holstein, M. Klein, R. Matthys, R. Nuetzi, R. Steck, M. W. Laschke, T. Wehner, R. Bindl, S. Recknagel, E.K. Stuermer, B. Vollmar, B. Wildemann, J. Lienau, B. Willie, A. Peters, A. Ignatius, T. Pohlemann, L. Claes, M.D. Menger, Small animal bone healing models: standards, tips, and pitfalls results of a consensus meeting, Bone 49 (4) (2011) 591–599. https://www.ncbi.nlm.nih.gov/pubmed/21782988.
[7] P. Garcia, J.H. Holstein, S. Maier, H. Schaumloffel, F. Al-Marrawi, M. Hannig, T. Pohlemann, M.D. Menger, Development of a reliable non-union model in mice, J. Surg. Res. 147 (1) (2008) 84–91. http://www.ncbi.nlm.nih.gov/pubmed/18061614.
[8] C.A. Squier, S. Ghoneim, C.R. Kremenak, Ultrastructure of the periosteum from membrane bone, J. Anat. 171 (1990) 233–239. http://www.ncbi.nlm.nih.gov/pubmed/2081707.
[9] E.J. Arnsdorf, L.M. Jones, D.R. Carter, C.R. Jacobs, The periosteum as a cellular source for functional tissue engineering, Tissue Eng. Part A 15 (9) (2009) 2637–2642. http://www.ncbi.nlm.nih.gov/pubmed/19207046.
[10] P.S. Landry, A.A. Marino, K.K. Sadasivan, J.A. Albright, Effect of soft-tissue trauma on the early periosteal response of bone to injury, J. Trauma 48 (3) (2000) 479–483. https://www.ncbi.nlm.nih.gov/pubmed/10744288.
[11] S.H. Park, K. O'Connor, R. Sung, H. McKellop, A. Sarmiento, Comparison of healing process in open osteotomy model and closed fracture model, J. Orthop. Trauma 13 (2) (1999) 114–120. https://www.ncbi.nlm.nih.gov/pubmed/10052786.
[12] L.A. Whiteside, P.A. Lesker, The effects of extraperiosteal and subperiosteal dissection. II. On fracture healing, J. Bone Joint Surg. Am. 60 (1) (1978) 26–30. https://www.ncbi.nlm.nih.gov/pubmed/624757.

[13] M.M. Menger, M.W. Laschke, M. Orth, T. Pohlemann, M.D. Menger, T. Histing, Vascularization strategies in the prevention of non-union formation, Tissue Eng. B Rev. 27 (2) (2020) 107–132. https://www.ncbi.nlm.nih.gov/pubmed/32635857.
[14] T. Kokubu, D.J. Hak, S.J. Hazelwood, A.H. Reddi, Development of an atrophic nonunion model and comparison to a closed healing fracture in rat femur, J. Orthop. Res. 21 (3) (2003) 503–510. https://www.ncbi.nlm.nih.gov/pubmed/12706024.
[15] J.H. Holstein, M.D. Menger, U. Culemann, C. Meier, T. Pohlemann, Development of a locking femur nail for mice, J. Biomech. 40 (1) (2007) 215–219. https://www.ncbi.nlm.nih.gov/pubmed/16376352.
[16] V.M. Goldberg, A. Powell, J.W. Shaffer, J. Zika, G.D. Bos, K.G. Heiple, Bone grafting: role of histocompatibility in transplantation, J. Orthop. Res. 3 (4) (1985) 389–404. http://www.ncbi.nlm.nih.gov/pubmed/3906062.
[17] T. Histing, J.H. Holstein, P. Garcia, R. Matthys, A. Kristen, L. Claes, M.D. Menger, T. Pohlemann, Ex vivo analysis of rotational stiffness of different osteosynthesis techniques in mouse femur fracture, J. Orthop. Res. 27 (9) (2009) 1152–1156. http://www.ncbi.nlm.nih.gov/pubmed/19215028.
[18] P. Bosemark, H. Isaksson, M.M. McDonald, D.G. Little, M. Tagil, Augmentation of autologous bone graft by a combination of bone morphogenic protein and bisphosphonate increased both callus volume and strength, Acta Orthop. 84 (1) (2013) 106–111. http://www.ncbi.nlm.nih.gov/pubmed/23409846.
[19] E.F. Morgan, Z.D. Mason, K.B. Chien, A.J. Pfeiffer, G.L. Barnes, T.A. Einhorn, L. C. Gerstenfeld, Micro-computed tomography assessment of fracture healing: relationships among callus structure, composition, and mechanical function, Bone 44 (2) (2009) 335–344. http://www.ncbi.nlm.nih.gov/pubmed/19013264.
[20] H. Isaksson, I. Grongroft, W. Wilson, C.C. van Donkelaar, B. van Rietbergen, A. Tami, R. Huiskes, K. Ito, Remodeling of fracture callus in mice is consistent with mechanical loading and bone remodeling theory, J. Orthop. Res. 27 (5) (2009) 664–672. http://www.ncbi.nlm.nih.gov/pubmed/18985689.
[21] L.C. Gerstenfeld, T.J. Wronski, J.O. Hollinger, T.A. Einhorn, Application of histomorphometric methods to the study of bone repair, J. Bone Miner. Res. Off. J. Am. Soc. Bone Miner. Res. 20 (10) (2005) 1715–1722. http://www.ncbi.nlm.nih.gov/pubmed/16160729.
[22] C. Colnot, Z. Thompson, T. Miclau, Z. Werb, J.A. Helms, Altered fracture repair in the absence of MMP9, Development 130 (17) (2003) 4123–4133. https://www.ncbi.nlm.nih.gov/pubmed/12874132.
[23] P. Choi, C. Ogilvie, Z. Thompson, T. Miclau, J.A. Helms, Cellular and molecular characterization of a murine non-union model, J. Orthop. Res. 22 (5) (2004) 1100–1107. http://www.ncbi.nlm.nih.gov/pubmed/15304285.
[24] Z.Y. Zhang, S.H. Teoh, M.S. Chong, E.S. Lee, L.G. Tan, C.N. Mattar, N.M. Fisk, M. Choolani, J. Chan, Neo-vascularization and bone formation mediated by fetal mesenchymal stem cell tissue-engineered bone grafts in critical-size femoral defects, Biomaterials 31 (4) (2010) 608–620. http://www.ncbi.nlm.nih.gov/pubmed/19836073.
[25] P. Garcia, T. Histing, J.H. Holstein, M. Klein, M.W. Laschke, R. Matthys, A. Ignatius, B. Wildemann, J. Lienau, A. Peters, B. Willie, G. Duda, L. Claes, T. Pohlemann, M.D. Menger, Rodent animal models of delayed bone healing and non-union formation: a comprehensive review, discussion 12-4, Eur. Cell. Mater. 26 (2013) 1–12, https://www.ncbi.nlm.nih.gov/pubmed/23857280.
[26] R. Marsell, T.A. Einhorn, The role of endogenous bone morphogenetic proteins in normal skeletal repair, Injury 40 (Suppl. 3) (2009) S4–S7. http://www.ncbi.nlm.nih.gov/pubmed/20082790.
[27] T. Histing, D. Stenger, C. Scheuer, W. Metzger, P. Garcia, J.H. Holstein, M. Klein, T. Pohlemann, M.D. Menger, Pantoprazole, a proton pump inhibitor, delays fracture healing in mice, Calcif. Tissue Int. 90 (6) (2012) 507–514. http://www.ncbi.nlm.nih.gov/pubmed/22527206.
[28] D.L. Lacey, E. Timms, H.L. Tan, M.J. Kelley, C.R. Dunstan, T. Burgess, R. Elliott, A. Colombero, G. Elliott, S. Scully, H. Hsu, J. Sullivan, N. Hawkins, E. Davy, C. Capparelli, A. Eli, Y.X. Qian, S. Kaufman, I. Sarosi, V. Shalhoub, G. Senaldi, J. Guo, J. Delaney, W.J. Boyle, Osteoprotegerin ligand is a cytokine that regulates osteoclast differentiation and activation, Cell 93 (2) (1998) 165–176. http://www.ncbi.nlm.nih.gov/pubmed/9568710.
[29] W.S. Simonet, D.L. Lacey, C.R. Dunstan, M. Kelley, M.S. Chang, R. Luthy, H. Q. Nguyen, S. Wooden, L. Bennett, T. Boone, G. Shimamoto, M. DeRose, R. Elliott, A. Colombero, H.L. Tan, G. Trail, J. Sullivan, E. Davy, N. Bucay, L. Renshaw-Gegg, T.M. Hughes, D. Hill, W. Pattison, P. Campbell, S. Sander, G. Van, J. Tarpley, P. Derby, R. Lee, W.J. Boyle, Osteoprotegerin: a novel secreted protein involved in the regulation of bone density, Cell 89 (2) (1997) 309–319. http://www.ncbi.nlm.nih.gov/pubmed/9108485.
[30] L.C. Gerstenfeld, D.J. Sacks, M. Pelis, Z.D. Mason, D.T. Graves, M. Barrero, M. S. Ominsky, P.J. Kostenuik, E.F. Morgan, T.A. Einhorn, Comparison of effects of the bisphosphonate alendronate versus the RANKL inhibitor denosumab on murine fracture healing, J. Bone Miner. Res. 24 (2) (2009) 196–208. http://www.ncbi.nlm.nih.gov/pubmed/19016594.
[31] T. Histing, C. Anton, C. Scheuer, P. Garcia, J.H. Holstein, M. Klein, R. Matthys, T. Pohlemann, M.D. Menger, Melatonin impairs fracture healing by suppressing RANKL-mediated bone remodeling, J. Surg. Res. 173 (1) (2012) 83–90. http://www.ncbi.nlm.nih.gov/pubmed/20888595.
[32] J.M. Kanczler, R.O. Oreffo, Osteogenesis and angiogenesis: the potential for engineering bone, Eur. Cell Mater. 15 (2008) 100–114. http://www.ncbi.nlm.nih.gov/pubmed/18454418.
[33] H. Eckardt, M. Ding, M. Lind, E.S. Hansen, K.S. Christensen, I. Hvid, Recombinant human vascular endothelial growth factor enhances bone healing in an experimental nonunion model, J. Bone Joint Surg. Br. 87 (10) (2005) 1434–1438. http://www.ncbi.nlm.nih.gov/pubmed/16189323.
[34] R. Li, D.J. Stewart, H.P. von Schroeder, E.S. Mackinnon, E.H. Schemitsch, Effect of cell-based VEGF gene therapy on healing of a segmental bone defect, J. Orthop. Res. 27 (1) (2009) 8–14. http://www.ncbi.nlm.nih.gov/pubmed/18634016.
[35] M. Fassbender, C. Strobel, J.S. Rauhe, C. Bergmann, G. Schmidmaier, B. Wildemann, Local inhibition of angiogenesis results in an atrophic non-union in a rat osteotomy model, Eur. Cell. Mater. 22 (2011) 1–11. http://www.ncbi.nlm.nih.gov/pubmed/21732278.
[36] D. Paley, M.A. Catagni, F. Argnani, A. Villa, G.B. Benedetti, R. Cattaneo, Ilizarov treatment of tibial nonunions with bone loss, Clin. Orthop. Relat. Res. (241) (1989) 146–165. http://www.ncbi.nlm.nih.gov/pubmed/2924458.
[37] B.G. Weber, C. Brunner, The treatment of nonunions without electrical stimulation, Clin. Orthop. Relat. Res. (161) (1981) 24–32. http://www.ncbi.nlm.nih.gov/pubmed/7030568.
[38] C.T. Hu, S.C. Offley, Z. Yaseen, R.J. O'Keefe, C.A. Humphrey, Murine model of oligotrophic tibial nonunion, J. Orthop. Trauma 25 (8) (2011) 500–505. http://www.ncbi.nlm.nih.gov/pubmed/21738067.
[39] H.C. Brownlow, A. Reed, A.H. Simpson, The vascularity of atrophic non-unions, Injury 33 (2) (2002) 145–150. http://www.ncbi.nlm.nih.gov/pubmed/11890916.
[40] C. Lu, T. Miclau, D. Hu, R.S. Marcucio, Ischemia leads to delayed union during fracture healing: a mouse model, J. Orthop. Res. 25 (1) (2007) 51–61. https://www.ncbi.nlm.nih.gov/pubmed/17019699.
[41] M.M. Menger, J. Stutz, S. Ehnert, A.K. Nussler, M.F. Rollmann, S.C. Herath, B. J. Braun, T. Pohlemann, M.D. Menger, T. Histing, Development of an ischemic fracture healing model in mice, Acta Orthop. 93 (2022) 466–471. https://www.ncbi.nlm.nih.gov/pubmed/35478260.

THE GERONTOLOGICAL SOCIETY OF AMERICA®

Journals of Gerontology: Biological Sciences
cite as: *J Gerontol A Biol Sci Med Sci*, 2022, Vol. 77, No. 5, 909–917
https://doi.org/10.1093/gerona/glab304
Advance Access publication October 9, 2021

OXFORD

Original Article

Establishment of a Reliable Model to Study the Failure of Fracture Healing in Aged Mice

Maximilian M. Menger, MD,[1,2,*] Matthias W. Laschke, MD, PhD,[1] Claudia Scheuer, PhD,[1] David Bauer,[1] Michelle Bleimehl,[1] Thomas Später, PhD,[1] Mika F. Rollmann, MD,[2] Benedikt J. Braun, MD,[2] Steven C. Herath, MD,[2] Ahsan Raza, PhD,[3] Michael D. Menger, MD,[1] and Tina Histing, MD[1,2]

[1]Institute for Clinical & Experimental Surgery, Saarland University, Homburg, Germany. [2]Department of Trauma and Reconstructive Surgery, BG Trauma Center Tuebingen, Eberhard Karls University Tuebingen, Tuebingen, Germany. [3]Department of Experimental and Clinical Pharmacology and Toxicology, Saarland University, Homburg, Germany.

*Address correspondence to: Maximilian M. Menger, MD, Department of Trauma and Reconstructive Surgery, BG Trauma Center Tuebingen, Eberhard Karls University Tuebingen, 72076 Tuebingen, Germany. E-mail: maximilian.menger@uks.eu

Received: March 25, 2021; Editorial Decision Date: September 27, 2021

Decision Editor: Rozalyn Anderson, PhD, FGSA

Abstract

The failure of fracture healing represents a substantial clinical problem. Moreover, aged patients demonstrate an elevated risk for failed bone healing. However, murine models to study the failure of fracture healing are established only in young adult animals. Therefore, the aim of this study was to develop a reliable model to study failed fracture healing in aged mice. After creation of a 1.8-mm segmental defect and periosteal resection, femora of aged mice (18–20 months) and young adult control mice (3–4 months) were stabilized by pin-clip fixation. Segmental defects were analyzed by means of biomechanics, x-ray, and micro-computed tomography, as well as histomorphometric, immunohistochemical, and Western blot analysis. After 10 weeks, all animals showed a complete lack of osseous bridging, resulting in fracture healing failure. Segmental defects in aged mice revealed a reduced bone formation and vascularization when compared to young adult mice. This was associated with a decreased expression of bone formation markers. In addition, we detected a reduced number of tartrate-resistant acid phosphatase-positive osteoclasts and an elevated osteoprotegerin/receptor activator of NF-κB ligand ratio in aged animals, indicating a reduced osteoclast activity. Moreover, aged animals showed also an enhanced inflammatory response, characterized by an increased infiltration of macrophages within the callus tissue. Taken together, we herein report for the first time a reliable model to study fracture healing failure in aged mice. In the future, the use of this model enables us to study novel therapeutic strategies and molecular mechanics of failed fracture healing during aging.

Keywords: Aging, Fracture healing, Inflammation, Murine, Vascularization

Despite growing knowledge of the mechanisms in fracture healing, delayed unions and nonunions remain a major clinical problem. Nowadays, approximately 10% of all fractures fail to heal or show a delayed healing (1). Failure of bone healing does not only lead to significant pain and loss of function with subsequent reduction of the patient's quality of life, but also imposes a substantial economic burden on society (2).

Considering the fact that the older population steadily increases worldwide, the treatment of geriatric patients has become one of the greatest future challenges for our health care systems. The bone metabolism in older adults is subject to pathophysiological changes, leading to osteoporosis and osteoarthritis (3). These patients suffer from a higher incidence in bone fractures, which is associated with an increased morbidity and mortality due to a reduced healing potential (4–6). Indeed, several clinical reports have confirmed that the older population shows an increased rate of delayed fracture healing and nonunion formation (7–9).

There are multiple factors contributing to the age-related changes in bone repair, including a decreased differentiation and proliferation of stem cells (7,10) as well as a delay in chondrogenesis and osteochondral ossification (11). Nonetheless, the exact pathophysiological mechanisms that result in a decreased healing capacity and nonunion formation in the aged are not fully understood.

To study the pathophysiology of nonunion formation, suitable animal models are required. Nonunion models in mice gain increasing interest, because they particularly allow to study the molecular aspects of fracture healing due to the availability of genetically modified animal strains and a large array of antibodies. Currently, however, nonunion models have been solely established in young adult animals (12–14). To provide a model which enables the analysis of the cellular and molecular processes during nonunion formation in the aged, we herein validate for the first time a reliable nonunion model in aged mice. For this purpose, we analyzed the nonunions in these animals by means of biomechanics, x-rays, micro-computed tomography (µCT), histology, immunohistochemistry as well as Western blot analyses and compared them with nonunions in young adult mice.

Method

Animals

In this study, we used aged CD-1 mice (n = 15) with a mean body weight of 30–40 g and an age of 18–20 months. The age of 18–20 months of the "aged animals" was chosen according to reports of others, demonstrating in CD-1 mice age-associated physiological dysfunctions and tumor development after 16 months in male and 18 months in female animals (15). Young adult CD-1 mice (n = 18) with a mean body weight of 30–40 g and an age of 3–4 months served as controls. The animals were bred at the Institute for Clinical and Experimental Surgery, Saarland University, Homburg, Germany and housed at a regular 12-hour/12-hour light/dark cycle and with free access to tap water and standard pellet food (Altromin, Lage, Germany).

All experiments were performed according to the German legislation on protection of animals and the National Institutes of Health (NIH) Guide for the Care and Use of Laboratory Animals (Institute of Laboratory Animal Resources, National Research Council, Washington, DC). The experiments were approved by the local governmental animal protection committee (permit number: 04/19).

Surgical Procedure

We established a femoral atrophic nonunion model in aged mice that consists of a pin-clip fixation, as described previously in detail in young adult animals (16). Mice were anesthetized by intraperitoneal injection of ketamine (75 mg/kg body weight) and xylazine (25 mg/kg body weight). Under aseptic conditions, an approximately 4-mm medial parapatellar incision was performed at the right knee and the patella was dislocated laterally. After drilling a hole (diameter of 0.50 mm) into the intracondylar notch, a distally flattened 24 gauge needle (diameter of 0.55 mm) was implanted intramedullary. The pin was flattened at the distal end to avoid secondary dislocation. After insertion of the pin, the diaphysis of the femur was exposed by a lateral approach. Subsequently, a custom-made clip of 6 mm length was implanted ventrodorsally, being placed laterally to the already implanted pin. Then, an osteotomy with a gap size of 1.8 mm was created under permanent saline cooling between the 2 brackets of the metallic clip using size-standardized spherical trephines. The gap size was controlled by a custom-made template. The metallic clip inserted before creation of the gap guaranteed that the gap size was maintained. Moreover, the periosteum was stripped 2 mm proximally and distally of the gap along the longitudinal axis of the femoral bone. All procedures were performed under an operating microscope, guaranteeing a high level of precision.

Young adult mice, which served as controls, were sacrificed 2 weeks (n = 7) or 10 weeks (n = 8) after surgery. Aged mice were sacrificed accordingly, 2 weeks (n = 4) or 10 weeks (n = 8) after surgery. The femora of the animals were harvested and used for further biomechanical, µCT, histomorphometric, and immunohistochemical analyses. Additionally, animals were sacrificed 2 weeks after surgery (n = 3 per group) to harvest callus tissue for Western blot analysis. Directly prior to sacrifice, x-rays of the operated femora were taken to exclude secondary dislocation of the metallic implants and to control bone healing.

Radiographic Analysis

At the end of the 2- and 10-week observation period, the animals were anesthetized and a ventrodorsal radiograph of the osteotomized femora was performed. Fracture healing was analyzed according to the classification of the Goldberg score (17) with stage 0 indicating radiological nonunion, stage 1 indicating possible union, and stage 2 indicating radiological union.

Biomechanical Analysis

After removal of the soft tissue and the implants, bending stiffness of the osteotomized femora was measured by a 3-point bending device using a nondestructive approach (18). This allowed the use of the specimens also for µCT, histological, and immunohistochemical analyses and, thus, a reduction of the number of laboratory animals needed.

Micro-computed tomography

The specimens were scanned (Skyscan 1172, Bruker, Billerica, MA) at a spatial resolution of 6.5 µm with a standardized setup (tube voltage: 50 kV; current: 200 µA; intervals: 0.4°; exposure time: 3500 ms; filter: 0.5 mm aluminum). Images were stored in 3-dimensional arrays. To express gray values as mineral content (bone mineral density [BMD]), calcium hydroxyapatite (CaHA) phantom rods with known BMD values (0.250 g and 0.750 g CaHA/cm^3) were employed for calibration. The region of interest (ROI) defining the novel bone was contoured manually excluding any original cortical bone. The thresholding allowed the differentiation between highly and poorly mineralized bone. The thresholds to distinguish between highly and poorly mineralized bone were based upon visual inspection of the images, qualitative comparison with histological sections, and other studies investigating bone repair and callus tissue by µCT (19,20). A BMD with more than 0.642 g/cm^3 resulting in gray values of 98–255 was defined as highly mineralized bone. Poorly mineralized bone was assumed to have a BMD value between 0.410 and 0.642 g/cm^3 resulting in gray values of 68–97.

The following parameters were calculated from the callus ROI for each specimen: poorly mineralized bone volume (BV_{low}), highly mineralized BV (BV_{high}), BV fraction (BV/total volume [TV]), bone surface (BS) density (BS/TV), trabecular thickness, trabecular separation, and trabecular number.

Histology and Histomorphometry

After biomechanical testing and µCT analysis, bones were fixed in paraformaldehyde for 24 hours. Subsequently, the specimens were embedded in a 30% sucrose solution for another 24 hours and then frozen at −80 °C. Longitudinal sections through the femoral axis with a thickness of 4 mm were cut for histomorphometric

analysis and stained with Safranin-O. At a magnification of 12.5× (Olympus BX60 Microscope, Olympus, Shinjuku, Japan; cellSens Dimension 1.11 software, Olympus), structural indices were calculated according to the recommendations of Gerstenfeld et al. (21). The following histomorphometric parameters of the bone defects were evaluated: (i) total callus area, (ii) bone callus area, (iii) cartilaginous callus area, and (iv) fibrous callus area. The total callus area was defined as the entire osseous, cartilaginous, and fibrous callus tissue between the 2 drilling holes of the clip outside of the cortices. Preexisting cortical bone of the proximal and distal fragment, however, was excluded. Each area was marked and calculated using the ImageJ analysis system (NIH, Bethesda, MD).

In addition, tartrate-resistant acid phosphate (TRAP) activity was analyzed in the callus tissue at 2 and 10 weeks after surgery. For this purpose, longitudinal sections of 4 µm were incubated in a mixture of 5 mg naphthol AS-MX phosphate and 11 mg fast red TR salt in 10 mL 0.2 M sodium acetate buffer (pH 5.0) for 1 h at 37 °C. Sections were counterstained with methyl green and covered with glycerin gelatin. TRAP-positive multinucleated cells (≥3 nuclei each cell) were counted at the bone surface within the callus tissue with a 400× magnification in a standardized manner.

Immunohistochemistry

In order to analyze the cellular composition of the callus tissue in atrophic nonunions, longitudinal sections with a thickness of 4 µm were cut. For the immunohistochemical detection of microvessels, sections were stained with a monoclonal rat anti-mouse antibody against the endothelial cell marker CD31 (1:100; Abcam, Cambridge, UK). A goat anti-rat IgG-Alexa555 antibody served as secondary antibody (1:100; Life Technology, Eugene, OR). Cell nuclei were stained with Hoechst 33342 (2 µg/mL; Sigma-Aldrich, Taufkirchen, Germany). To detect the neutrophilic granulocyte marker myeloperoxidase (MPO) and the macrophage marker CD68, sections were stained with a polyclonal rabbit anti-mouse antibody against MPO (1:100; Abcam) and a polyclonal rabbit anti-mouse antibody against CD68 (1:100; Abcam). A goat anti-rabbit IgG-antibody (1:200; Dianova, Hamburg, Germany) served as corresponding secondary antibody.

In the specimens, the number of CD31-positive microvessels, and MPO- and CD68-positive cells was counted with a 400× magnification in a standardized manner (given in number of cells/area examined).

Western Blot

The protein expression within the callus tissue was determined by Western blot analysis, including the expression of bone morphogenetic protein (BMP)-2 and -4, cysteine-rich angiogenic inducer (CYR)61, vascular endothelial growth factor (VEGF), runt-related transcription factor-2 (RUNX2), cyclooxygenase-2 (COX-2), heme oxygenase-1 (HO-1), endothelial nitric oxide synthase (eNOS), phosphorylated eNOS (peNOS), receptor activator of NF-κB ligand (RANKL), and osteoprotegerin (OPG). Furthermore, the RANKL/OPG ratio was determined. Callus tissue was harvested on postoperative day 14 (n = 3 each group) between the bone fragments of the osteotomy, transferred in lysis buffer, and stored at –80 °C. After saving the whole protein fraction, proteins were separated and transferred by standard protocols and probed using the following antibodies: goat anti-mouse BMP-2 and BMP-4 (both 1:25; R&D Systems, Wiesbaden, Germany), sheep anti-mouse CYR61 (1:50; R&D Systems), rabbit anti-mouse VEGF (1:25; Abcam), rabbit anti-mouse RUNX2 (1:20; Abcam), rabbit anti-mouse COX-2 (1:50; Abcam), rabbit anti-mouse HO-1 (1:100; Enzo Life Science, Lörrach, Germany), mouse anti-mouse eNOS (1:50; BD Biosciences, Heidelberg, Germany), rabbit anti-mouse peNOS (1:50; Cell Signaling Technology, Frankfurt, Germany), rabbit anti-mouse RANKL (1:25; Abcam), and rabbit anti-mouse OPG (1:50; Bioss by Antibodies-Online, Aachen, Germany). The appropriate peroxidase-conjugated anti-IgG antibodies served as secondary antibodies (1:1 500; Dako Cytomation, Hamburg, Germany and 1:1 000; R&D Systems). Protein expression was visualized by means of luminol-enhanced chemiluminescence after exposure of the membrane to the Intas ECL Chemocam Imager (Intas Science Imaging Instrument GmbH, Göttingen, Germany). Signals were normalized to β-actin signals (1:1 000; mouse monoclonal β-actin antibody, Santa Cruz Biotechnology, Heidelberg, Germany) to correct for unequal loading.

Statistical Analysis

All data are given as means ± *SD*. After testing the data for normal distribution (Kolmogorov–Smirnov test) and equal variance (F test), comparison between the experimental groups was performed by the unpaired Student's t test. For nonparametrical data, a Mann–Whitney U-test was used. To test for time effects within individual groups, 1-way analysis of variance was applied. All statistics were performed using the SigmaPlot software (version 13.0; Jandel Corporation, San Rafael, CA). A p value of $<.05$ was considered to indicate significant differences.

Results

X-Ray Analysis Confirms Nonunion Formation in Aged Mice

Our results showed a reliable nonunion formation in both study groups 10 weeks after osteotomy. However, the radiological and biomechanical analysis revealed significant differences in callus composition and biomechanical properties between young adult and aged mice. The radiographic analysis at 2 and 10 weeks after osteotomy demonstrated a complete lack of osseous bridging in the femora of young adult and aged mice (Figure 1A–D). The Goldberg score did not differ between the 2 study groups at 2 weeks (p = 1.0) and 10 weeks (p = 1.0) after osteotomy (0.0 ± 0.0 vs 0.0 ± 0.0). The adjoining bone fragments showed rounding towards the osteotomy gap 10 weeks after osteotomy in both study groups (Figure 1B and D), which is a typical sign of nonunion formation. Interestingly, femora of aged mice showed a wider fracture gap (Figure 1D) 10 weeks after surgery when compared to femora of young adult animals (Figure 1B).

Bending Stiffness in Nonunions of Aged Mice Is Significantly Reduced

At 2 weeks after osteotomy, the biomechanical analysis revealed that the bending stiffness did not differ between the 2 groups (p = .225) (Figure 1E). At 10 weeks, bending stiffness in young adult animals was found to be significantly increased by almost 3-fold (p = .001) compared to that at 2 weeks (Figure 1E). In contrast, the increase in bending stiffness in aged animals at 10 weeks compared to 2 weeks did not exceed 50% (p = .200). Accordingly, at 10 weeks after surgery, the bending stiffness of aged mice was only half of that of young adult animals (p = .028) (Figure 1E).

Nonfractured contralateral femora of aged animals exhibited a significantly lower bending stiffness compared to that of young adult

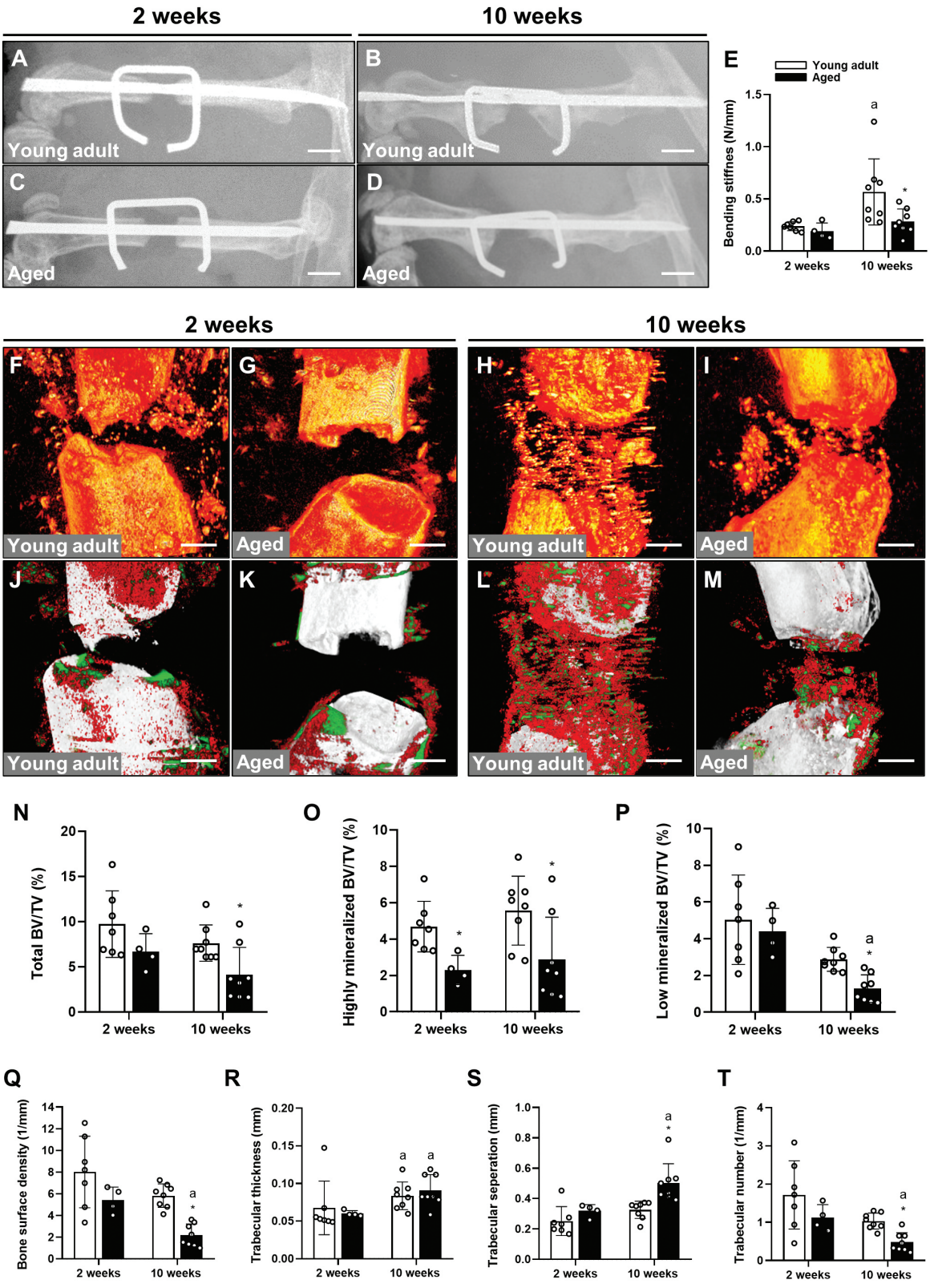

Figure 1. x-Rays of the osteotomized mouse femora with a segmental defect of 1.8 mm at 2 wk (**A** and **C**) and 10 wk (**B** and **D**) after osteotomy in young adult (A and B) and aged (C and D) animals. Note the wider fracture gap at 10 wk after surgery in femora of aged mice. Scale bar: 2 mm. Biomechanical analysis of osteotomized mouse femora at 2 and 10 wk (**E**) after osteotomy in young adult mice (white bars) and aged animals (black bars). µCT images of femora in young adult (**F** and **H**) and aged mice (**G** and **I**) at 2 wk (F and G) and 10 wk (H and I) after osteotomy. µCT images of femora in young adult (**J** and **L**) and aged mice (**K** and **M**) at 2 wk (J and K) and 10 wk (L and M) after osteotomy (white: cortical bone, red: highly mineralized bone volume, green: low-mineralized bone volume). Scale bar: 1 mm. µCT analysis of total (**N**), highly (**O**) and low-mineralized (**P**) BV/TV in young adult (white bars) and aged mice (black bars) 2 and 10 wk after osteotomy. µCT analysis of bone surface density (**Q**), trabecular thickness (**R**), trabecular separation (**S**), and trabecular number (**T**) at 2 and 10 wk after osteotomy in young adult (white bars) and aged mice (black bars). Mean ± *SD*; young adult: $n = 7$ at 2 wk, $n = 8$ at 10 wk; aged: $n = 4$ at 2 wk, $n = 8$ at 10 wk; $^{*}p < .05$ vs young adult; $^{a}p < .05$ vs 2 wk. BV/TV = bone volume/total volume; µCT = micro-computed tomography.

mice at both 2 weeks (59.0 ± 13.2 vs 81.7 ± 9.4 N/mm, $p = .042$) and 10 weeks (61.6 ± 9.3 vs 89.0 ± 8.7 N/mm, $p = .004$) after surgery.

µCT Analysis Shows Lower BV/TV Ratios in the Callus of Nonunions in Aged Mice

µCT analysis was able to quantify differences in bone formation and trabecular architecture between the 2 study groups. At 2 weeks after osteotomy, total BV/TV was slightly but not significantly lower in aged compared to young adult animals ($p = .166$) (Figure 1F, G, and N). At 10 weeks, total BV/TV was found to be reduced by 25% in young adults and even by 40% in aged animals, indicating nonunion formation in both groups (Figure 1H, I, and N). As a consequence, at 10 weeks, aged animals showed a 50% lower total BV/TV when compared to young adult controls ($p = .015$) (Figure 1N).

More detailed analysis revealed that at 2 weeks after surgery, the highly mineralized BV/TV in aged animals was less than half of that of young adult animals ($p = .013$) (Figure 1J, K, and O). At 10 weeks after surgery, the highly mineralized BV/TV was not changed compared to 2 weeks in both aged and young adult animals (Figure 1O). Accordingly, at 10 weeks, the highly mineralized BV/TV was still significantly lower in aged compared to young adult animals ($p = .024$) (Figure 1L, M, and O).

Analysis of the low-mineralized BV/TV at 2 weeks after surgery could not detect significant differences between aged and young adult animals (Figure 1J, K, and P). Of interest, at 10 weeks, the low-mineralized BV/TV was found to be significantly reduced in aged animals by 71% ($p < .001$) but only slightly reduced in young adult controls by 43% ($p = .072$) (Figure 1P). Accordingly, at 10 weeks, the low-mineralized BV/TV of aged animals was less than half compared to that of young adult controls ($p < .001$) (Figure 1L, M, and P).

The 3D reconstruction of femora 10 weeks after osteotomy showed indeed the typical rounding and narrowing towards the osteotomy gap of adjoining bone fragments in both study groups (Figure 1H, I, L, and M).

Additional analysis of bone surface density at 2 weeks after surgery could not detect significant differences between aged and young adult animals (Figure 1Q). At 10 weeks, the bone surface density was found to be significantly reduced in aged animals ($p < .001$) but not in young adult controls ($p = .189$) (Figure 1Q). Accordingly, the bone surface density in aged animals at 10 weeks was lowered to about one-third compared to that of young adult animals ($p < .001$) (Figure 1Q).

The trabecular thickness showed no significant differences between the 2 study groups at both 2 and 10 weeks after surgery. However, it increased by 30%–50% from 2 to 10 weeks in aged animals ($p = .028$) and young adult controls ($p = .029$) (Figure 1R).

The analysis of trabecular separation at 2 weeks after surgery could not detect significant differences between aged and young adult animals (Figure 1S). At 10 weeks, it was found to be increased in aged animals by 70% ($p = .004$) but not in young adult controls ($p = .087$) (Figure 1S). Accordingly, the trabecular separation at 10 weeks was 70% higher in aged compared to young adult animals ($p < .001$) (Figure 1S).

The analysis of the trabecular number at 2 weeks after surgery was slightly but not significantly lower in aged compared to young adult animals (Figure 1T). At 10 weeks, it was found to be reduced in aged animals by ~60% ($p = .004$), and in young adult controls by only ~40% ($p = .094$) (Figure 1T). Accordingly, the trabecular number of aged animals at 10 weeks was less than half of that of young adult animals ($p < .001$) (Figure 1T).

Osseous Callus Tissue Is Reduced in Nonunions of Aged Mice

To gain further insights in the callus composition and cellular mechanisms of nonunions, we performed histomorphometric and immunohistochemical analyses. The histomorphometric analysis confirmed the lack of osseous bridging in both study groups at 2 and 10 weeks after osteotomy with abundant fibrous tissue within the osteotomy gaps (Figure 2A–D). Furthermore, quantitative analysis revealed that the total callus area at 2 weeks did not significantly differ between the 2 study groups (Figure 2E). Until 10 weeks, the total callus area was found to be increased by only one-third in aged animals ($p = .271$), but by 2-fold in young adult animals ($p = .011$) (Figure 2E). This resulted in a 50% lower total callus area at 10 weeks in aged mice when compared to young adult controls ($p = .038$) (Figure 2E).

Further evaluation of the callus composition at 2 weeks after osteotomy showed that in both groups, the callus tissue mostly consisted of fibrous tissue (Figure 2F–H). At 2 weeks after surgery, the fraction of osseous tissue within the callus was less than 5% and did not differ between the 2 groups (Figure 2F). At 10 weeks, there was a 4.3-fold increase of the osseous tissue fraction in aged animals ($p = .097$) and a 6.4-fold increase in young adult controls ($p < .001$) (Figure 2F). Accordingly, the osseous tissue fraction in aged mice at 10 weeks was less than half of that of young adult controls ($p = .004$) (Figure 2F).

The fraction of cartilaginous tissue within the callus at 2 weeks after surgery was ~5% and did not differ between the 2 groups (Figure 2G). At 10 weeks, the cartilaginous tissue fraction was slightly reduced, however, still without significant differences between the 2 groups (Figure 2G).

The fraction of fibrous tissue within the callus at 2 weeks after surgery was ~90% and did not differ between the 2 groups (Figure 2H). At 10 weeks, the fibrous tissue fraction remained almost unchanged in aged animals ($p = .315$) but was found to be reduced by one-third in young adult controls ($p < .001$) (Figure 2H). Accordingly, at 10 weeks, the fraction of fibrous tissue was ~30% higher in aged animals compared to young adult controls ($p < .001$) (Figure 2H).

Moreover, our histochemical analysis showed a 50% reduction in the number of TRAP-positive osteoclasts at 2 weeks after surgery in aged compared to young adult animals ($p = .035$) (Figure 2I and J). Until 10 weeks, this number increased by 73% in aged animals ($p = .048$) and by 33% in young adult controls ($p = .080$) (Figure 2J). Despite this more pronounced increase in aged animals, the number of TRAP-positive osteoclasts at 10 weeks was still one-third lower in aged compared to young adult mice ($p = .016$) (Figure 2J).

Vascularization Is Reduced in Nonunions of Aged Mice

Furthermore, we performed immunohistochemical analysis to gain further insights in vascularization and immunological processes within the callus tissue of nonunions. The analysis of the number of CD31-positive microvessels within the callus tissue at 2 weeks after surgery showed an almost 50% smaller number in aged compared to young adult mice ($p = .046$) (Figure 3A and B). Until 10 weeks, the number of CD31-positive microvessels slightly increased by 41% in aged animals and by 30% in young adult controls (Figure 3B). This resulted in a still substantially lower number of CD31-positive microvessels at 10 weeks in aged compared to young adult mice ($p = .005$) (Figure 3B).

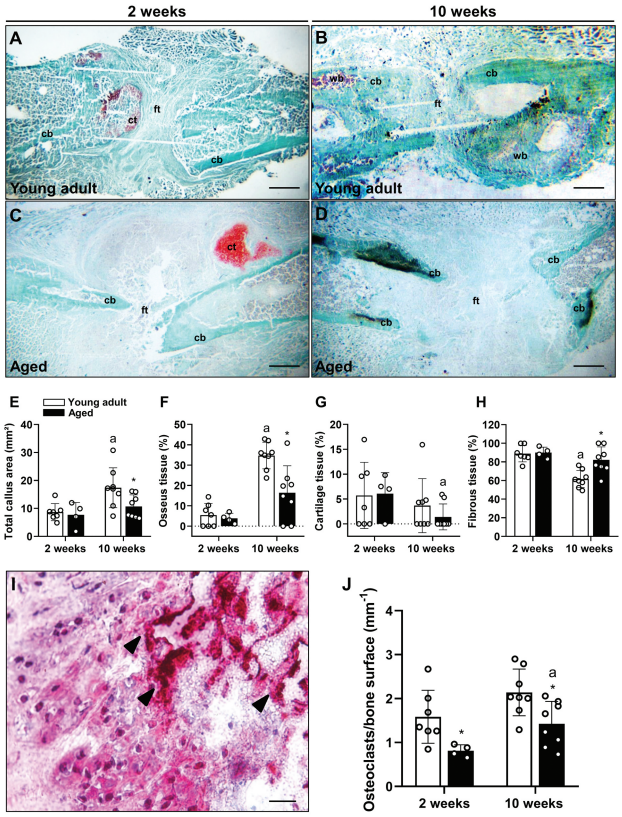

Figure 2. Representative histological images of Safranin-O-stained femora at 2 wk (**A** and **C**) and 10 wk (**B** and **D**) after osteotomy in young adult (A and B) and aged (C and D) animals. Fibrous tissue (ft), cartilage tissue (ct), cortical bone (cb), and woven bone (wb) are indicated. Scale bar: 1 mm. Histomorphometric analysis of the callus tissue including the total callus area (**E**), the fraction of osseous tissue (**F**), cartilaginous tissue (**G**), and fibrous tissue (**H**) at 2 and 10 wk after osteotomy in young adult (white bars) and aged mice (black bars). Representative histological image (**I**) of tartrate-resistant acid phosphate-positive osteoclasts (arrowheads) within the callus tissue of a young adult mouse at 2 wk after osteotomy. Scale bar: 20 µm. Number of osteoclasts/bone surface within the callus tissue at 2 and 10 wk (**J**) after osteotomy in young adult (white bars) and aged (black bars) mice. Mean ± *SD*; young adult: $n = 7$ at 2 wk, $n = 8$ at 10 wk; aged: $n = 4$ at 2 wk, $n = 8$ at 10 wk; $^{*}p < .05$ vs young adult; $^{a}p < .05$ vs 2 wk.

The additional MPO staining demonstrated a slightly higher number of neutrophilic granulocytes in the callus tissue of aged compared to young adult mice at 2 weeks after osteotomy ($p = .196$) (Figure 3C and D). These numbers were found to be reduced until 10 weeks by 76% in the aged animals ($p = .004$) and by 58% in the young adult controls ($p = .397$) (Figure 3D). Intergroup analysis at 10 weeks could not detect any significant difference between the 2 groups (Figure 3D).

The additional analysis of CD68-positive macrophages in the bone defects revealed a significantly higher number in the callus tissue of aged compared to young adult mice at 2 weeks after surgery ($p = .001$) (Figure 3E and F). Until 10 weeks, these numbers were found to be reduced by 43% in the aged animals ($p = .048$) and by 69% in the young adult controls ($p < .001$) (Figure 3F). Accordingly, at 10 weeks, the number of CD68-positive cells was found to be 3.5-fold higher in aged compared to young adult animals ($p = .010$) (Figure 3F).

Proosteogenic Activity Is Reduced in Aged Mice

Western blot analysis provided further information about growth factor and protein expression within the callus tissue of nonunions.

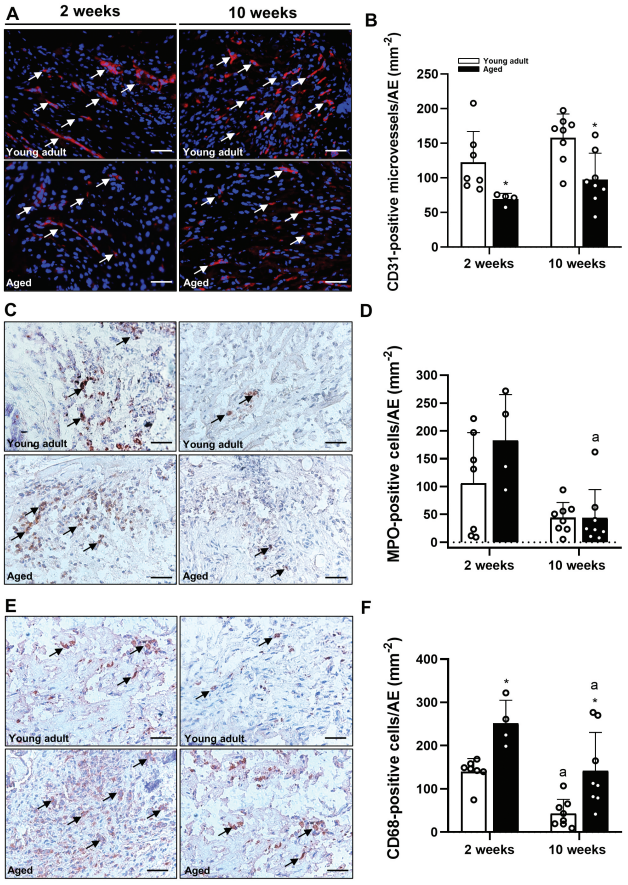

Figure 3. Representative immunohistological images (**A**) of CD31-positive microvessels within the callus tissue of young adult and aged mice at 2 and 10 wk after osteotomy. Scale bar: 50 µm. Number of CD31-positive microvessels/AE (**B**) within the callus tissue at 2 and 10 wk after osteotomy in young adult (white bars) and aged (black bars) mice. Representative immunohistological images (**C**) of MPO-positive cells within the callus tissue of young adult and aged mice at 2 and 10 wk after osteotomy. Scale bar: 50 µm. Number of MPO-positive cells/AE (**D**) within the callus tissue 2 and 10 wk after osteotomy in young adult (white bars) and aged (black bars) mice. Representative immunohistological images (**E**) of CD68-positive cells within the callus tissue of young adult and aged mice 2 and 10 wk after osteotomy. Scale bar: 50 µm. Number of CD68-positive cells/AE (**F**) within the callus tissue 2 and 10 wk after osteotomy in young adult (white bars) and aged (black bars) mice. Mean ± *SD*; young adult: $n = 7$ at 2 wk, $n = 8$ at 10 wk; aged: $n = 4$ at 2 wk, $n = 8$ at 10 wk; $^{*}p < .05$ vs young adult; $^{a}p < .05$ vs 2 wk. AE = area examined; MPO = myeloperoxidase.

Potential differences in expression patterns of proangiogenic and proosteogenic factors may elucidate pathophysiological mechanisms of nonunion formation in aged individuals. The biochemical analysis 2 weeks after osteotomy revealed a reduced expression of BMP-2 ($p = .213$) and BMP-4 ($p = .340$) in the callus tissue of aged mice when compared to young adult animals (Table 1). Moreover, the expression of the angiogenic and osteogenic CYR61 was significantly reduced in these mice ($p = .011$) (Table 1). However, the expression of VEGF did not differ between the 2 study groups ($p = .943$) (Table 1). The expression of RUNX2 ($p = .155$), an essential regulator of osteoblast differentiation, and RANKL ($p = .283$), a stimulator of osteoclastogenesis, was downregulated in aged animals (Table 1). In contrast, OPG, an inhibitor of osteoclastogenesis, was 2-fold higher in aged mice ($p = .466$) (Table 1). This resulted in an increased OPG/RANKL ratio in aged animals ($p = .378$) (Table 1). Additional

Table 1. Expression of BMP-2, BMP-4, CYR61, VEGF, RUNX2, OPG, RANKL, COX-2, HO-1, eNOS, and peNOS within the callus tissue 2 wk after osteotomy in young adult ($n = 3$) and aged mice ($n = 3$)

Protein Expression	Young Adult	Aged	*p* Value
BMP-2 (pixel intensity × 10^4)	8.3 ± 6.9	2.3 ± 1.7	.213
BMP-4 (pixel intensity × 10^4)	8.5 ± 10.9	1.7 ± 0.8	.340
CYR61 (pixel intensity × 10^4)	29.8 ± 4.7	7.7 ± 7.0*	.011
VEGF (pixel intensity × 10^4)	7.9 ± 7.0	7.6 ± 3.3	.943
RUNX2 (pixel intensity × 10^4)	30.2 ± 16.8	12.5 ± 4.6	.155
OPG (pixel intensity × 10^4)	0.5 ± 3.1	1.2 ± 1.4	.466
RANKL (pixel intensity × 10^4)	4.7 ± 3.4	2.2 ± 0.9	.283
OPG/RANKL ratio	0.1 ± 0.1	0.8 ± 1.2	.378
COX-2 (pixel intensity × 10^4)	68.9 ± 30.3	46.1 ± 13.0	.296
HO-1 (pixel intensity × 10^4)	13.1 ± 8.5	7.6 ± 3.9	.400
eNOS (pixel intensity × 10^4)	12.4 ± 6.1	10.2 ± 5.3	.658
peNOS (pixel intensity × 10^4)	5.8 ± 2.5	1.9 ± 0.5	.060
peNOS/eNOS ratio	0.5 ± 0.3	0.3 ± 0.2	.335

Notes: BMP-2 = bone morphogenetic protein; COX-2 = cyclooxygenase-2; CYR61 = cysteine-rich angiogenic inducer 61; eNOS = endothelial nitric oxide synthase; HO-1 = heme oxygenase-1; OPG = osteoprotegerin; peNOS phosphorylated endothelial nitric oxide synthase; RANKL = receptor activator of NF-κB ligand; RUNX2 = runt-related transcription factor-2; VEGF = vascular endothelial growth factor. All data are mean ± *SD*.

*$p < .05$ vs young adult.

protein biochemical analysis showed a downregulated expression of COX-2 ($p = .296$), HO-1 ($p = .400$), and peNOS ($p = .060$) in aged mice (Table 1). Interestingly, the expression of eNOS did not notably differ between the 2 study groups ($p = .658$), leading to a markedly lower peNOS/eNOS ratio in aged animals ($p = .335$) (Table 1).

Discussion

The present study had the purpose to establish a reliable nonunion model in aged mice and to compare the biological response in such a model with that in the corresponding nonunion model in young adult mice. This response was studied by radiological, biomechanical, histological, and biochemical analyses. Our results show a reliable atrophic nonunion formation in all aged animals 10 weeks after surgery. Interestingly, nonunions of aged mice exhibited a reduced BV and vascularization as well as an increased inflammation when compared to those of young adult animals. This was associated with a reduced bone formation, as indicated by a lower expression of the proosteogenic proteins BMP-2, BMP-4, and CYR61 and a decreased bone remodeling, as indicated by a reduced number of osteoclasts and an increased OPG/RANKL ratio.

There is a considerable number of experimental models available in order to provoke nonunions, including interposition of foreign materials (22), unstable osteosynthesis (23), and periosteal resection (24). However, despite a growing older population, these models are only established in young adult animals, which hinders the investigation of age-associated changes in bone healing and nonunion formation. Therefore, the establishment and characterization of a reliable nonunion model in aged mice is of high clinical interest.

Previous studies demonstrated an elevated risk for nonunion formation in older patients (9,25). In line with this finding, our data show a decreased bending stiffness and bone formation in critical-sized bone defects of aged mice. This was associated with an impaired trabecular architecture, as indicated by an increased trabecular separation and a decreased trabecular number when compared to controls. Hence, our results also confirm several other studies reporting an inferior bone healing capacity in aged animals. For instance, Clark et al. (26) demonstrated in an unstable tibia fracture model a reduced BV in old mice (24 months) when compared to young animals (3 months). Moreover, Lu et al. (11) showed a delayed fracture healing in aged mice (18 months) due to a delay in cell differentiation, a protracted period of endochondral ossification and impaired bone remodeling. Interestingly, we herein found a decreased expression of the bone formation markers BMP-2, BMP-4, and CYR61 in osteotomized femora of aged mice. Additionally, COX-2, which has been shown to play a critical role in endochondral ossification (27), was slightly reduced in these animals. After fracture and development of a soft callus, this temporary structure undergoes a process of remodeling, involving the resorption of calcified cartilage and the formation of new bone tissue (28). This osteogenic phase is characterized by the expression of bone formation markers peaking between 2 and 3 weeks. Thus, the reduction in bone formation and bending stiffness observed in aged mice may be caused by the reduction of the bone formation markers.

We further investigated the number and activity of osteoclasts in the segmental defects of the mouse femora. Of note, we found a significantly decreased number of TRAP-positive osteoclasts within the callus tissue of aged mice. It is widely accepted that RANKL is a potent promotor of osteoclastogenesis by binding to its receptor RANK on bone marrow macrophages (29). OPG, a decoy receptor, can bind to RANKL and, thus, prevent its binding and activation with RANK (30). Therefore, the increased OPG/RANKL ratio in aged animals indicates a reduced osteoclast differentiation and activity. On the other hand, RUNX2 is an essential protein for the stimulation of osteoblastogenesis, as it serves as a regulator in many signaling pathways of osteoblast differentiation (31). The reduced RUNX2 expression in bone defects of aged mice may thus additionally result in an impaired differentiation and activity of osteoblasts. Cartilage and bone resorption by osteoclasts and the formation of new bone tissue by osteoblasts are the key components of callus remodeling (32). Therefore, the reduction in the number and activity of osteoclasts and an impaired osteoblast differentiation in aged animals indicate an overall reduced bone turnover. This may be the cause for the reduced formation of new bone tissue and for the delay in bone remodeling.

An adequate vascularization is recognized as a major prerequisite for successful bone healing. The stimulation of the endosteal circulation allows mesenchymal stem cells to invade the fracture site by newly formed capillaries and to induce the remodeling process (33). Furthermore, it has been shown that the stimulation of vascularization can accelerate fracture healing (34,35), whereas an inhibition of vascularization leads to nonunion formation (36,37). Nevertheless, the vascularization of nonunions is controversially discussed throughout the literature. Some studies consider nonunion formation as the result of an avascular and biologically inert environment (38,39). Others, however, demonstrated that the callus tissue of nonunions contains a rich vasculature (40,41). The latter observation is supported by our findings. In fact, we detected a considerable number of CD31-positive microvessels within the bone defects of young adult and aged animals. The density of blood vessels even increased from 2 to 10 weeks after osteotomy. Nonetheless, bone defects of aged animals contained a significantly lower number of microvessels when compared to those of young adult mice. This may be explained by the fact that impaired fracture healing in the older population is associated with an age-related dysfunction in the bone vascular system and its capacity to regenerate (3). The enzyme eNOS is expressed in endothelial cells and produces NO, the most important vasodilatory molecule synthesized by the endothelium (42). Reduced production and

bioavailability of NO result in an impaired endothelium-dependent vasodilatation (43). Moreover, it has been reported that eNOS is directly involved in the process of fracture repair (44). Of interest, the expression of eNOS within the callus tissue did not significantly differ between the 2 study groups in the present study. However, we found a reduced expression of the activated phosphorylated isoform, peNOS, in aged animals, leading to a lower peNOS/eNOS ratio. This indicates an impaired activation of eNOS and might, thus, compromise the vascular function within the callus tissue in bone defects of aged mice. For these reasons, the decrease of vascularization and the age-related dysfunction of the vascular system may further contribute to the reduced bone formation in aged animals.

The inflammatory phase is an essential part of fracture healing, as mesenchymal stem cells are directed to the fracture site (45). The perturbation of the inflammatory phase of fracture repair, however, can have detrimental effects on the outcome of the healing process (46). This is evident in older patients, who exhibit higher levels of circulating proinflammatory cytokines leading to a chronically increased inflammatory status, also referred to as "inflamm-aging" (47). Macrophages are inflammatory cells, which are crucially involved in bone healing. They release proinflammatory cytokines, such as interleukin 1 (IL-1), IL-6, and tumor necrosis factor-α, and promote the inflammatory response (48). Interestingly, we found an increased number of macrophages in the bone defects of aged mice. Moreover, the expression of the protein HO-1 was reduced in aged animals. HO-1 plays a major role in the defense against oxidative stress (49). Furthermore, there is an accumulating evidence that HO-1 also downregulates inflammatory processes in a variety of tissues (50). Of note, HO-1 is thought to exert its anti-inflammatory effects by enhancing adipose macrophage polarization towards the M2 phenotype (51). Thus, the reduced HO-1 expression in aged animals may be associated with a proinflammatory M1 macrophage dominance. It might be speculated that the elevated number of macrophages as well as the imbalance in M1/M2 macrophage polarization contribute to the chronic increased inflammatory status in aged animals and, thus, hamper the process of bone healing. Accordingly, Clark et al. (26) could demonstrate that the inhibition of macrophage recruitment by macrophage-colony stimulating factor (M-CSF)1R resulted in an improved fracture healing in aged mice. Therefore, targeting inflammatory cells might be a promising approach to prevent nonunion formation in the older population.

Taken together, we established for the first time a reliable murine model, which consistently results in atrophic nonunion formation in aged mice. Future studies using this model will be helpful to gain better insights into the mechanisms of nonunion formation in aged individuals. There are numerous current and emerging strategies to overcome nonunion formation, such as the implantation of bone substitutes or tissue engineering constructs as well as biophysical applications and pharmacological treatment. These treatment strategies can now be compared and evaluated in the present model. Moreover, the use of genetically modified mouse strains in combination with the herein established model represents a promising option to further elucidate the molecular basis of nonunion formation in the aged.

Funding

None declared.

Conflict of Interest

None declared.

Acknowledgments

We are grateful for the excellent technical assistance of Caroline Bickelmann, Sandra Hans, and Julia Parakenings from the Institute for Clinical & Experimental Surgery, Saarland University.

References

1. Einhorn TA, Gerstenfeld LC. Fracture healing: mechanisms and interventions. *Nat Rev Rheumatol*. 2015;11(1):45–54. doi:10.1038/nrrheum.2014.164
2. Victoria G, Petrisor B, Drew B, Dick D. Bone stimulation for fracture healing: what's all the fuss? *Indian J Orthop*. 2009;43(2):117–120. doi:10.4103/0019-5413.50844
3. Clark D, Nakamura M, Miclau T, Marcucio R. Effects of aging on fracture healing. *Curr Osteoporos Rep*. 2017;15(6):601–608. doi:10.1007/s11914-017-0413-9
4. Nikolaou VS, Efstathopoulos N, Kontakis G, Kanakaris NK, Giannoudis PV. The influence of osteoporosis in femoral fracture healing time. *Injury*. 2009;40(6):663–668. doi:10.1016/j.injury.2008.10.035
5. Claes L, Grass R, Schmickal T, et al. Monitoring and healing analysis of 100 tibial shaft fractures. *Langenbecks Arch Surg*. 2002;387(3–4):146–152. doi:10.1007/s00423-002-0306-x
6. Cauley JA, Thompson DE, Ensrud KC, Scott JC, Black D. Risk of mortality following clinical fractures. *Osteoporos Int*. 2000;11(7):556–561. doi:10.1007/s001980070075
7. Gruber R, Koch H, Doll BA, Tegtmeier F, Einhorn TA, Hollinger JO. Fracture healing in the elderly patient. *Exp Gerontol*. 2006;41(11):1080–1093. doi:10.1016/j.exger.2006.09.008
8. Robinson CM, Court-Brown CM, McQueen MM, Wakefield AE. Estimating the risk of nonunion following nonoperative treatment of a clavicular fracture. *J Bone Joint Surg Am*. 2004;86(7):1359–1365. doi:10.2106/00004623-200407000-00002
9. Parker MJ, Raghavan R, Gurusamy K. Incidence of fracture-healing complications after femoral neck fractures. *Clin Orthop Relat Res*. 2007;458:175–179. doi:10.1097/BLO.0b013e3180325a42
10. Bergman RJ, Gazit D, Kahn AJ, Gruber H, McDougall S, Hahn TJ. Age-related changes in osteogenic stem cells in mice. *J Bone Miner Res*. 1996;11(5):568–577. doi:10.1002/jbmr.5650110504
11. Lu C, Miclau T, Hu D, et al. Cellular basis for age-related changes in fracture repair. *J Orthop Res*. 2005;23(6):1300–1307. doi:10.1016/j.orthres.2005.04.003.1100230610
12. Choi P, Ogilvie C, Thompson Z, Miclau T, Helms JA. Cellular and molecular characterization of a murine non-union model. *J Orthop Res*. 2004;22(5):1100–1107. doi:10.1016/j.orthres.2004.03.008
13. Oetgen ME, Merrell GA, Troiano NW, Horowitz MC, Kacena MA. Development of a femoral non-union model in the mouse. *Injury*. 2008;39(10):1119–1126. doi:10.1016/j.injury.2008.04.008
14. Garcia P, Herwerth S, Matthys R, et al. The LockingMouseNail—a new implant for standardized stable osteosynthesis in mice. *J Surg Res*. 2011;169(2):220–226. doi:10.1016/j.jss.2009.11.713
15. Homburger F, Russfield AB, Weisburger JH, Lim S, Chak SP, Weisburger EK. Aging changes in CD-1 HaM/ICR mice reared under standard laboratory conditions. *J Natl Cancer Inst*. 1975;55(1):37–45. doi:10.1093/jnci/55.1.37
16. Garcia P, Holstein JH, Maier S, et al. Development of a reliable non-union model in mice. *J Surg Res*. 2008;147(1):84–91. doi:10.1016/j.jss.2007.09.013
17. Goldberg VM, Powell A, Shaffer JW, Zika J, Bos GD, Heiple KG. Bone grafting: role of histocompatibility in transplantation. *J Orthop Res*. 1985;3(4):389–404. doi:10.1002/jor.1100030401
18. Histing T, Holstein JH, Garcia P, et al. Ex vivo analysis of rotational stiffness of different osteosynthesis techniques in mouse femur fracture. *J Orthop Res*. 2009;27(9):1152–1156. doi:10.1002/jor.20849
19. Bosemark P, Isaksson H, McDonald MM, Little DG, Tägil M. Augmentation of autologous bone graft by a combination of bone morphogenic protein and bisphosphonate increased both callus volume and strength. *Acta Orthop*. 2013;84(1):106–111. doi:10.3109/17453674.2013.773123

20. Morgan EF, Mason ZD, Chien KB, et al. Micro-computed tomography assessment of fracture healing: relationships among callus structure, composition, and mechanical function. *Bone*. 2009;44(2):335–344. doi:10.1016/j.bone.2008.10.039
21. Gerstenfeld LC, Wronski TJ, Hollinger JO, Einhorn TA. Application of histomorphometric methods to the study of bone repair. *J Bone Miner Res*. 2005;20(10):1715–1722. doi:10.1359/JBMR.050702
22. dos Santos Neto FL, Volpon JB. Experimental nonunion in dogs. *Clin Orthop Relat Res*. 1984;187:260–71.
23. Hietaniemi K, Peltonen J, Paavolainen P. An experimental model for non-union in rats. *Injury*. 1995;26(10):681–686. doi:10.1016/0020-1383(95)00135-2
24. Reed AA, Joyner CJ, Isefuku S, Brownlow HC, Simpson AH. Vascularity in a new model of atrophic nonunion. *J Bone Joint Surg Br*. 2003;85(4):604–610. doi:10.1302/0301-620x.85b4.12944
25. Nieminen S, Nurmi M, Satokari K. Healing of femoral neck fractures; influence of fracture reduction and age. *Ann Chir Gynaecol*. 1981;70(1):26–31.
26. Clark D, Brazina S, Yang F, et al. Age-related changes to macrophages are detrimental to fracture healing in mice. *Aging Cell*. 2020;19(3):e13112. doi:10.1111/acel.13112
27. Xie C, Ming X, Wang Q, et al. COX-2 from the injury milieu is critical for the initiation of periosteal progenitor cell mediated bone healing. *Bone*. 2008;43(6):1075–1083. doi:10.1016/j.bone.2008.08.109
28. Marsell R, Einhorn TA. The role of endogenous bone morphogenetic proteins in normal skeletal repair. *Injury*. 2009;40(suppl. 3):S4–S7. doi:10.1016/S0020-1383(09)70003-8
29. Bahney CS, Zondervan RL, Allison P, et al. Cellular biology of fracture healing. *J Orthop Res*. 2019;37(1):35–50. doi:10.1002/jor.24170
30. Boyle WJ, Simonet WS, Lacey DL. Osteoclast differentiation and activation. *Nature*. 2003;423(6937):337–342. doi:10.1038/nature01658
31. Komori T. Regulation of proliferation, differentiation and functions of osteoblasts by Runx2. *Int J Mol Sci*. 2019;20:1694. doi:10.3390/ijms20071694
32. Teitelbaum SL. Osteoclasts: what do they do and how do they do it? *Am J Pathol*. 2007;170(2):427–435. doi:10.2353/ajpath.2007.060834
33. Kanczler JM, Oreffo RO. Osteogenesis and angiogenesis: the potential for engineering bone. *Eur Cell Mater*. 2008;15:100–114. doi:10.22203/ecm.v015a08
34. Eckardt H, Ding M, Lind M, Hansen ES, Christensen KS, Hvid I. Recombinant human vascular endothelial growth factor enhances bone healing in an experimental nonunion model. *J Bone Joint Surg Br*. 2005;87(10):1434–1438. doi:10.1302/0301-620X.87B10.16226
35. Li R, Stewart DJ, von Schroeder HP, Mackinnon ES, Schemitsch EH. Effect of cell-based VEGF gene therapy on healing of a segmental bone defect. *J Orthop Res*. 2009;27(1):8–14. doi:10.1002/jor.20658
36. Fang TD, Salim A, Xia W, et al. Angiogenesis is required for successful bone induction during distraction osteogenesis. *J Bone Miner Res*. 2005;20(7):1114–1124. doi:10.1359/JBMR.050301
37. Fassbender M, Strobel C, Rauhe JS, Bergmann C, Schmidmaier G, Wildemann B. Local inhibition of angiogenesis results in an atrophic non-union in a rat osteotomy model. *Eur Cell Mater*. 2011;22:1–11. doi:10.22203/ecm.v022a01
38. Paley D, Catagni MA, Argnani F, et al. Ilizarov treatment of tibial nonunions with bone loss. *Clin Orthop Relat Res*. 1989;241:146–165.
39. Weber BG, Brunner C. The treatment of nonunions without electrical stimulation. *Clin Orthop Relat Res*. 1981;161:24–32.
40. Hu CT, Offley SC, Yaseen Z, O'Keefe RJ, Humphrey CA. Murine model of oligotrophic tibial nonunion. *J Orthop Trauma*. 2011;25(8):500–505. doi:10.1097/BOT.0b013e3182249fad
41. Brownlow HC, Reed A, Simpson AH. The vascularity of atrophic nonunions. *Injury*. 2002;33(2):145–150. doi:10.1016/s0020-1383(01)00153-x
42. Fleming I, Busse R. NO: the primary EDRF. *J Mol Cell Cardiol*. 1999;31(1):5–14. doi:10.1006/jmcc.1998.0839
43. Taddei S, Virdis A, Ghiadoni L, et al. Age-related reduction of NO availability and oxidative stress in humans. *Hypertension*. 2001;38(2):274–279. doi:10.1161/01.hyp.38.2.274
44. Diwan AD, Wang MX, Jang D, Zhu W, Murrell GA. Nitric oxide modulates fracture healing. *J Bone Miner Res*. 2000;15(2):342–351. doi:10.1359/jbmr.2000.15.2.342
45. Medhat D, Rodriguez CI, Infante A. Immunomodulatory effects of MSCs in bone healing. *Int J Mol Sci*. 2019;20:5467. doi:10.3390/ijms20215467
46. Hankenson KD, Zimmerman G, Marcucio R. Biological perspectives of delayed fracture healing. *Injury*. 2014;45(suppl. 2):S8–S15. doi:10.1016/j.injury.2014.04.003
47. Franceschi C, Bonafè M, Valensin S, et al. Inflamm-aging. An evolutionary perspective on immunosenescence. *Ann NY Acad Sci*. 2000;908:244–254. doi:10.1111/j.1749-6632.2000.tb06651.x
48. Wynn TA, Chawla A, Pollard JW. Macrophage biology in development, homeostasis and disease. *Nature*. 2013;496(7446):445–455. doi:10.1038/nature12034
49. Waza AA, Hamid Z, Ali S, Bhat SA, Bhat MA. A review on heme oxygenase-1 induction: is it a necessary evil. *Inflamm Res*. 2018;67(7):579–588. doi:10.1007/s00011-018-1151-x
50. Rochette L, Cottin Y, Zeller M, Vergely C. Carbon monoxide: mechanisms of action and potential clinical implications. *Pharmacol Ther*. 2013;137(2):133–152. doi:10.1016/j.pharmthera.2012.09.007
51. Tu TH, Joe Y, Choi HS, Chung HT, Yu R. Induction of heme oxygenase-1 with hemin reduces obesity-induced adipose tissue inflammation via adipose macrophage phenotype switching. *Mediators Inflamm*. 2014;2014:290708. doi:10.1155/2014/290708

Menger *et al.*
Journal of Translational Medicine (2023) 21:844
https://doi.org/10.1186/s12967-023-04661-y

Journal of
Translational Medicine

RESEARCH

Open Access

Parathyroid hormone stimulates bone regeneration in an atrophic non-union model in aged mice

Maximilian M. Menger[1,2*], Anne L. Tobias[2], David Bauer[2], Michelle Bleimehl[2], Claudia Scheuer[2], Michael D. Menger[2], Tina Histing[1] and Matthias W. Laschke[2]

Abstract

Background Non-union formation still represents a major burden in trauma and orthopedic surgery. Moreover, aged patients are at an increased risk for bone healing failure. Parathyroid hormone (PTH) has been shown to accelerate fracture healing in young adult animals. However, there is no information whether PTH also stimulates bone regeneration in atrophic non-unions in the aged. Therefore, the aim of the present study was to analyze the effect of PTH on bone regeneration in an atrophic non-union model in aged CD-1 mice.

Methods After creation of a 1.8 mm segmental defect, mice femora were stabilized by pin-clip fixation. The animals were treated daily with either 200 µg/kg body weight PTH 1–34 (n = 17) or saline (control; n = 17) subcutaneously. Bone regeneration was analyzed by means of X-ray, biomechanics, micro-computed tomography (µCT) imaging as well as histological, immunohistochemical and Western blot analyses.

Results In PTH-treated animals bone formation was markedly improved when compared to controls. This was associated with an increased bending stiffness as well as a higher number of tartrate-resistant acid phosphatase (TRAP)-positive osteoclasts and CD31-positive microvessels within the callus tissue. Furthermore, PTH-treated aged animals showed a decreased inflammatory response, characterized by a lower number of MPO-positive granulocytes and CD68-positive macrophages within the bone defects when compared to controls. Additional Western blot analyses demonstrated a significantly higher expression of cyclooxygenase (COX)-2 and phosphoinositide 3-kinase (PI3K) in PTH-treated mice.

Conclusion Taken together, these findings indicate that PTH is an effective pharmacological compound for the treatment of non-union formation in aged animals.

Keywords Non-union, Parathyroid hormone, Segmental defect, Bone regeneration, Fracture healing, Angiogenesis, Mice, Aging, Inflammation

Introduction

Despite increasing insights into the molecular and cellular mechanisms of fracture repair, non-union formation remains a major complication in orthopedic and trauma surgery [1]. In clinical practice, the treatment of non-unions is highly challenging and requires extensive revision surgery. Thus, non-union formation is not only associated with significant pain, loss of function

*Correspondence:
Maximilian M. Menger
maximilian.menger@uks.eu
[1] Department of Trauma and Reconstructive Surgery, Eberhard Karls University Tuebingen, BG Trauma Center Tuebingen, 72076 Tuebingen, Germany
[2] Institute for Clinical and Experimental Surgery, Saarland University, 66421 Homburg/Saar, Germany

and prolonged rehabilitation, but causes also a substantial economic burden for the health care system [2].

Due to the fact that the aged population is steadily increasing worldwide, the treatment of geriatric patients has become one of the major challenges in clinical practice [3]. The process of bone repair in the elderly is subject to physiological alterations, including decreased differentiation and proliferation of stem cells [4, 5] as well as delayed chondrogenesis and osteochondral ossification [6]. Accordingly, numerous clinical studies have reported that the aged population is at an increased risk for delayed fracture healing and non-union formation [7, 8]. To overcome this problem, there is a substantial need for the development of effective treatment strategies.

Parathyroid hormone (PTH), a peptide hormone secreted by the parathyroid glands, is a key regulator of calcium hemostasis in the body [9]. PTH raises the serum calcium levels by stimulating the reabsorption of calcium in the kidney and by stimulating osteoclast differentiation and proliferation, leading to osteoclastic bone resorption and calcium release from bone [10]. Moreover, PTH is the only clinically approved drug for the treatment of osteoporosis in the elderly. Of interest, several experimental studies demonstrated that PTH accelerates fracture healing [11–13] and stimulates bone regeneration in bone defects [14]. However, it is not known whether PTH also promotes the healing of atrophic non-unions in the aged.

To clarify this we analyzed in the present study, the effects of PTH treatment on atrophic non-unions using a well-established and reliable non-union model in aged CD-1 mice [15]. Bone regeneration was analyzed by means of X-ray, biomechanics, micro-computed tomography (μCT) imaging as well as histological, immunohistochemical and Western blot analyses.

Materials and methods

Animals

A total number of 34 male and female CD-1 mice with a body weight of 35–45 g and an age of 18–20 months were used. The age of 18–20 months was chosen according to reports of others, demonstrating age-associated physiological alterations and tumor development after 16–18 months in male and 18 months in female CD-1 mice [16]. The animals were bred at the Institute for Clinical and Experimental Surgery, Saarland University, Germany, and housed at a regular light and dark cycle with free access to tap water and standard pellet food (Altromin, Lage, Germany).

All experiments were performed according to the German legislation on the protection of animals and the National Institutes of Health (NIH) Guide for the Care and Use of Laboratory Animals (Institute of Laboratory Animal Resources, National Research Council, Washington DC, USA). The experiments were approved by the local governmental animal protection committee (permit number: 04/2019).

Surgical procedure

Mice were anesthetized by intraperitoneal (i.p.) injection of ketamine (75 mg/kg body weight, Ursotamin®, Serumwerke Bernburg, Bernburg, Germany) and xylazine (15 mg/kg body weight, Rompun®, Bayer, Leverkusen, Germany). The pin-clip model using a segmental defect served as control and was performed as described previously [15]. Under aseptic conditions, a ~4 mm medial parapatellar incision was created at the right knee and the patella was dislocated laterally. After drilling a hole (diameter of 0.50 mm) into the intracondylar notch, a distally flattened pressfit 24 Gauge needle (diameter of 0.55 mm) was implanted intramedullary and the wound was closed. The pin was flattened at the distal end to avoid secondary dislocation. After insertion of the pin, the diaphysis of the femur was exposed by a lateral approach. Subsequently, a custom-made clip of 6 mm length was implanted ventrodorsally into the femur and lateral of the already implanted pin. A gap size of 1.8 mm was created by means of a spherical trephine under permanent saline solution cooling. Moreover, the periosteum was stripped 2 mm proximally and distally of the gap along the longitudinal axis of the femoral bone. The implant position was confirmed by radiography (MX-20, Faxitron X-ray Corporation, Wheelin, IL, USA). All procedures were done under an operating microscope, guaranteeing a high level of precision. For analgesia the mice received tramadol-hydrochloride (Grünenthal, Aachen, Germany) in the drinking water (1 mg/mL) 1 day prior to surgery until 3 days after surgery.

Experimental protocol

Seventeen mice were daily treated with 200 μg/kg body weight PTH 1–34 (Bachem AG, Budendorf, Switzerland) dissolved in 100 μL saline, subcutaneously (PTH group). Control animals (n = 17) received an equal amount of saline (control group), subcutaneously. The used PTH dosage corresponds to other experimental studies investigating the effects of PTH on fracture healing in mice [13]. At 2 weeks [n = 5 each group (3 male; 2 female)] and 10 weeks [n = 9 each group (5 male; 4 female)] the animals were euthanized by an overdose of anesthetics and the femora were excised for further μCT and histological analyses. Additional animals were euthanized accordingly at 2 weeks [n = 3 each group (2 male; 1 female)] and tissue was harvested for Western blot analyses.

X-ray analysis

At 2 and 10 weeks after surgery the animals were anesthetized and lateral radiographs of the osteotomized femora were performed. Bone healing was analyzed according to the Goldberg score with stage 0 indicating radiological non-union, stage 1 indicating possible union and stage 2 indicating radiological union [17].

µCT analysis

The specimens were scanned (Skyscan 1176, Bruker, Billerica, MA) at a spatial resolution of 9 µm with a standardized setup (tube voltage: 50 kV; current: 200 µA; intervals: 0.4°; exposure time: 3500 ms; filter: 0.5 mm aluminum). Images were stored in three-dimensional arrays. To express gray values as mineral content (bone mineral density; BMD), calcium hydroxyapatite (CaHA) phantom rods with known BMD values (0.250 and 0.750 g CaHA/cm^3) were employed for calibration. The region of interest (ROI) defining the novel bone was contoured manually excluding any original cortical bone. The thresholding allowed the differentiation between poorly and highly mineralized bone. The threshold to distinguish between poorly and highly mineralized bone was based upon visual inspection of the images, qualitative comparison with histological sections and other studies investigating bone repair and callus tissue by µCT [18, 19]. A BMD with more than 0.642 g/cm^3, resulting in gray values of 98–255, was defined as highly mineralized bone. Poorly mineralized bone was assumed to have a BMD value between 0.410 g/cm^3 and 0.642 g/cm^3, resulting in gray values of 68–97.

The following parameters were calculated from the callus region of interest for each specimen: poorly mineralized bone volume (PM), highly mineralized bone volume (HM), bone volume fraction of tissue volume (BV/TV), bone surface (BS) density (BS/TV), trabecular thickness, trabecular separation and trabecular number.

Biomechanical analysis

After removal of the soft tissue and the implants, the bending stiffness of the isolated femora was measured by a 3-point-bending device using a non-destructive approach. This allowed the subsequent use of the specimens for µCT as well as histological and immunohistochemical analyses and, thus, a reduction of the number of laboratory animals. Due to the different stages of healing, the loads, which had to be applied, markedly varied between individual animals. Loading was stopped individually in every case when the actual load-displacement curve deviated more than 1% from linearity. Bending stiffness (N/mm) was calculated from the linear elastic part of the load-displacement diagram [20].

Histology and histomorphometry

After biomechanical testing and µCT analysis, bones were fixed in paraformaldehyde for 24 h. Subsequently, the specimens were embedded in a 30% sucrose solution for another 24 h and then frozen at −80° C. Longitudinal sections through the femoral axis with a thickness of 4 µm were cut by the Kawamotos film method [21, 22] for histomorphometric analyses and stained with Safranin-O. At a magnification of 12.5× (Olympus BX60 Microscope, Olympus, Shinjuku, Japan; Zeiss Axio Cam and Axio Vision 3.1, Zeiss) structural indices were calculated according to the recommendations of Gerstenfeld et al. [23]. The following histomorphometric parameters of the bone defects were evaluated: (i) total callus area, (ii) bone callus area, (iii) cartilaginous callus area and (iv) fibrous callus area. The total callus area was defined as the entire osseous, cartilaginous and fibrous callus tissue between the two drilling holes of the clip outside of the cortices. Pre-existing cortical bone of the proximal and distal fragment, however, was excluded. Each area was marked and calculated using the ImageJ analysis system (NIH, Bethesda, USA).

In addition, tartrate-resistant acid phosphate (TRAP) activity was analyzed in the callus tissue at 2 and 10 weeks after surgery. For this purpose, longitudinal sections of 4 µm were incubated in a mixture of 5 mg naphotol AS-MX phosphate and 11 mg fast red TR salt in 10 mL 0.2 M sodium acetate buffer (pH 5.0) for 1 h at 37 °C. Sections were counterstained with methyl green and covered with glycerin gelatin. TRAP-positive multinucleated cells (three or more nuclei each cell) were counted. In the specimens, one high-power field (HPF, 400× magnification) was placed in a standardized manner in the central region of the callus, while three additional HPFs were placed on each site of the periosteal callus.

Immunohistochemistry

To analyze the cellular composition within the callus tissue of atrophic non-unions at 2 and 10 weeks after surgery, longitudinal sections with a thickness of 4 µm were cut. For the immunohistochemical detection of microvessels, sections were stained with a monoclonal rat anti-mouse antibody against the endothelial cell marker CD31 (1:100; Abcam, Cambridge, UK). A goat anti-rat IgG-Alexa555 antibody served as secondary antibody (1:100; Life Technology, Eugene, USA). Cell nuclei were stained with Hoechst 33342 (2 µg/mL; Sigma-Aldrich, Taufkirchen Germany). To detect the neutrophilic granulocyte marker myeloperoxidase (MPO) and the macrophage marker CD68, sections were stained

with a polyclonal rabbit anti-mouse antibody against MPO (1:100; Abcam) and a polyclonal rabbit anti-mouse antibody against CD68 (1:100; Abcam). A goat anti-rabbit IgG-antibody (1:200; Dianova, Hamburg, Germany) served as corresponding secondary antibody.

In the specimens, the number of CD31-positive microvessels as well as MPO- and CD68-positive cells was counted. For this purpose, one HPF was placed in a standardized manner in the central region of the callus, while three additional HPFs were placed on each site of the periosteal callus.

Western blot analysis

Protein expression within the callus tissue was determined by Western blot analysis, including the expression of vascular endothelial growth factor (VEGF), cyclooxygenase (COX)-2 and phosphoinositide 3-kinase (PI3K). The callus tissue was frozen and stored at −80 °C until required. Analyses were performed from callus tissue at 2 weeks after surgery (n = 3 each group). After saving the whole protein fraction, analysis was performed using the following antibodies: rabbit anti-mouse VEGF (1:300, Abcam, Cambridge, UK), COX-2 (1:30, Abcam) and mouse anti-mouse PI3K (1:100, Santa Cruz Biotechnology, Heidelberg, Germany). Primary antibodies were followed by corresponding horseradish peroxidase-conjugated secondary antibodies (1:1000, R&D Systems). Protein expression was visualized by means of luminol-enhanced chemiluminescence after exposure of the membrane to the Intas ECL Chemocam Imager (Intas Science Imaging Instrument GmbH, Göttingen, Germany) and normalized to β-actin signals (1:1000, mouse anti-mouse β-actin, Santa Cruz Biotechnology) to correct for unequal loading.

Statistical analysis

All data are given as means ± SEM. After testing the data for normal distribution (Kolmogorov–Smirnov test) and equal variance (*F*-test), comparisons between the two groups were performed by an unpaired Student's *t*-test. For non-parametrical data, a Mann–Whitney *U*-test was used. All statistics were performed using the SigmaPlot 13.0 software (Jandel Corporation, San Rafael, CA, USA). A p-value of < 0.05 was considered to indicate significant differences.

Results

X-ray analysis

The radiographic analysis demonstrated a complete lack of osseous bridging in the control group throughout the entire observation period (Fig. 1A, B). X-rays showed a reliable non-union formation in all control mice with a large persisting gap between the adjoining rounded bone fragments (Fig. 1B). However, in PTH-treated animals the X-rays already indicated first signs of callus formation at 2 weeks after surgery (Fig. 1C) and even osseous bridging in 6 out of 9 (67.7%) animals at 10 weeks after surgery (Fig. 1D). Accordingly, the radiographic analysis revealed a significantly higher Goldberg score in PTH-treated animals at 10 weeks after surgery when compared to controls (0.0 ± 0.0 vs. 1.1 ± 0.3; $^*p < 0.05$ vs. control).

μCT analysis

In line with our X-ray analysis, μCT imaging showed a lack of osseous bridging in control animals throughout the entire 10-weeks observation period (Fig. 1E–H). In contrast, in the PTH group we observed signs of callus formation already at 2 weeks after surgery (Fig. 1I, J) and successful osseous bridging at 10 weeks after surgery (Fig. 1K, L), indicating an improved bone regeneration. Accordingly, the μCT analysis demonstrated a significantly higher amount of poorly and highly mineralized bone tissue in PTH-treated animals at 2 and 10 weeks after surgery (Fig. 1M, N).

In addition, we found a significantly higher BV/TV and bone surface density in PTH-treated mice at 2 and 10 weeks after surgery when compared to controls (Fig. 2A, B). Further analyses of the trabecular architecture demonstrated a significantly higher trabecular thickness in the PTH group at 2 and 10 weeks after surgery (Fig. 2C). This was associated with a significantly lower trabecular separation and, accordingly, a significantly higher trabecular number in PTH-treated animals when compared to controls throughout the 10-weeks observation period (Fig. 2D, E).

Biomechanical analysis

Femora of PTH-treated mice exhibited a significantly higher bending stiffness at 2 and 10 weeks after surgery when compared to controls (Fig. 2F). Notably, the bending stiffness of femora of control animals remained < 1 N/mm, indicating a complete failure of fracture healing (Fig. 2F).

Histomorphometric and immunohistochemical analysis

Histomorphometric analysis demonstrated a complete lack of osseous bridging in the control group at 2 and 10 weeks after surgery with abundant fibrous tissue between the bone fragments (Fig. 3A, B). In PTH-treated animals, distinct signs of endochondral ossification could be detected at 2 weeks after surgery (Fig. 3C), resulting in osseous bridging at 10 weeks (Fig. 3D). This indicates successful bone regeneration. Quantitative analyses revealed a significantly higher fraction of bone and cartilaginous tissue at 2 weeks after surgery in the PTH group when compared to controls, whereas the fraction

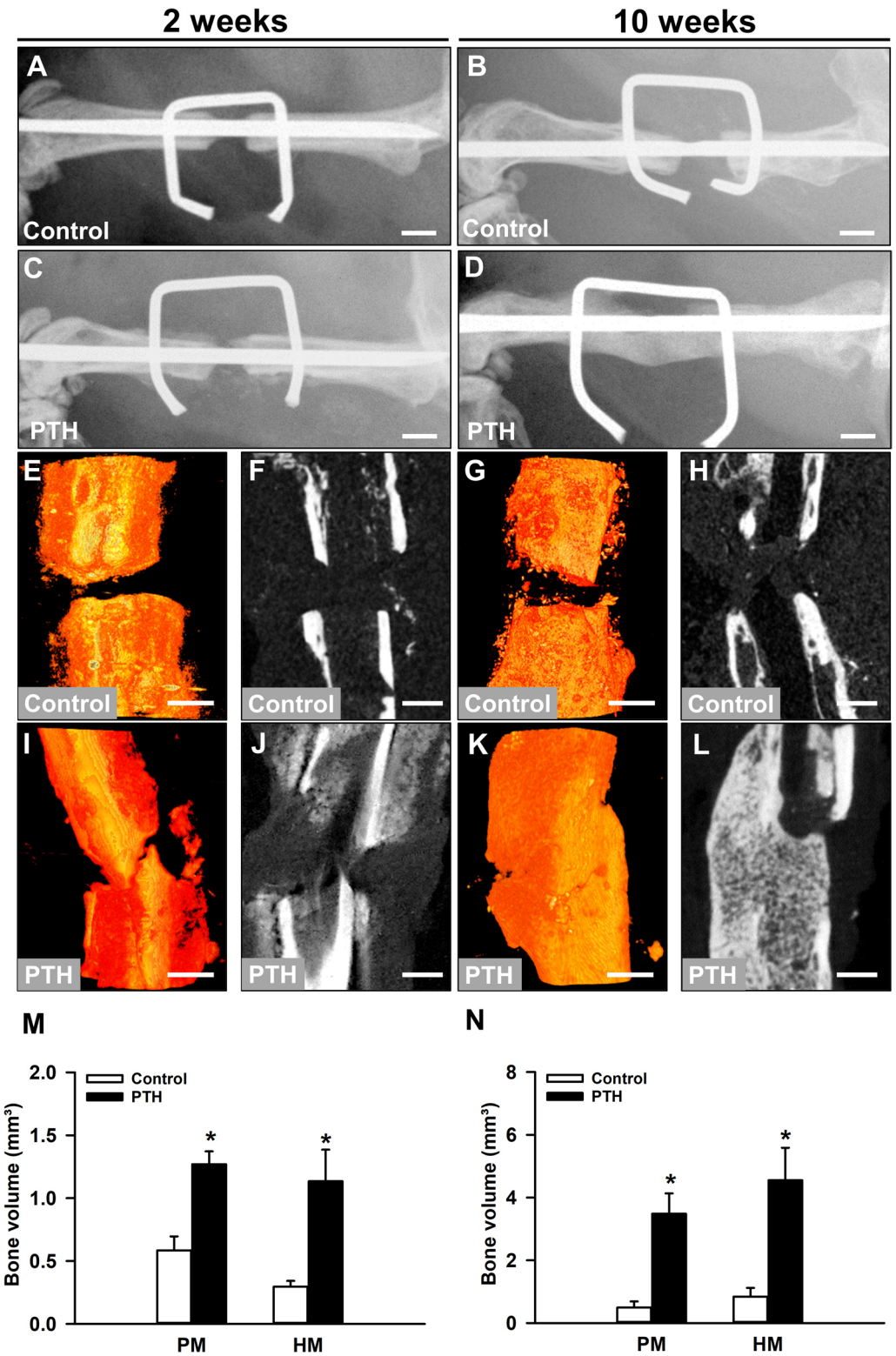

Fig. 1 **A**–**D** Representative X-rays of femora of controls (**A**, **B**) and PTH-treated mice (**C**, **D**) at 2 (**A**, **C**) and 10 weeks (**B**, **D**) after surgery. Scale bars: 1 mm. Representative µCT-3D reconstructions (**E**, **G**, **I**, **K**) and transversal µCT images (**F**, **H**, **J**, **L**) of controls (**E**–**H**) and PTH-treated animals (**I**–**L**) at 2 (**E**, **F**, **I**, **J**) and 10 weeks (**G**, **H**, **K**, **L**) after surgery. Scale bars: 0.5 mm. **M**, **N** Poorly (PM) and highly mineralized (HM) bone volume of the callus tissue of controls (white bars, n = 5 at 2 weeks after surgery, n = 9 at 10 weeks after surgery) and PTH-treated mice (black bars, n = 5 at 2 weeks after surgery, n = 9 at 10 weeks after surgery) at 2 (**M**) and 10 weeks (**N**) after surgery, as assessed by µCT analyses. Mean ± SEM; *p < 0.05 vs. control

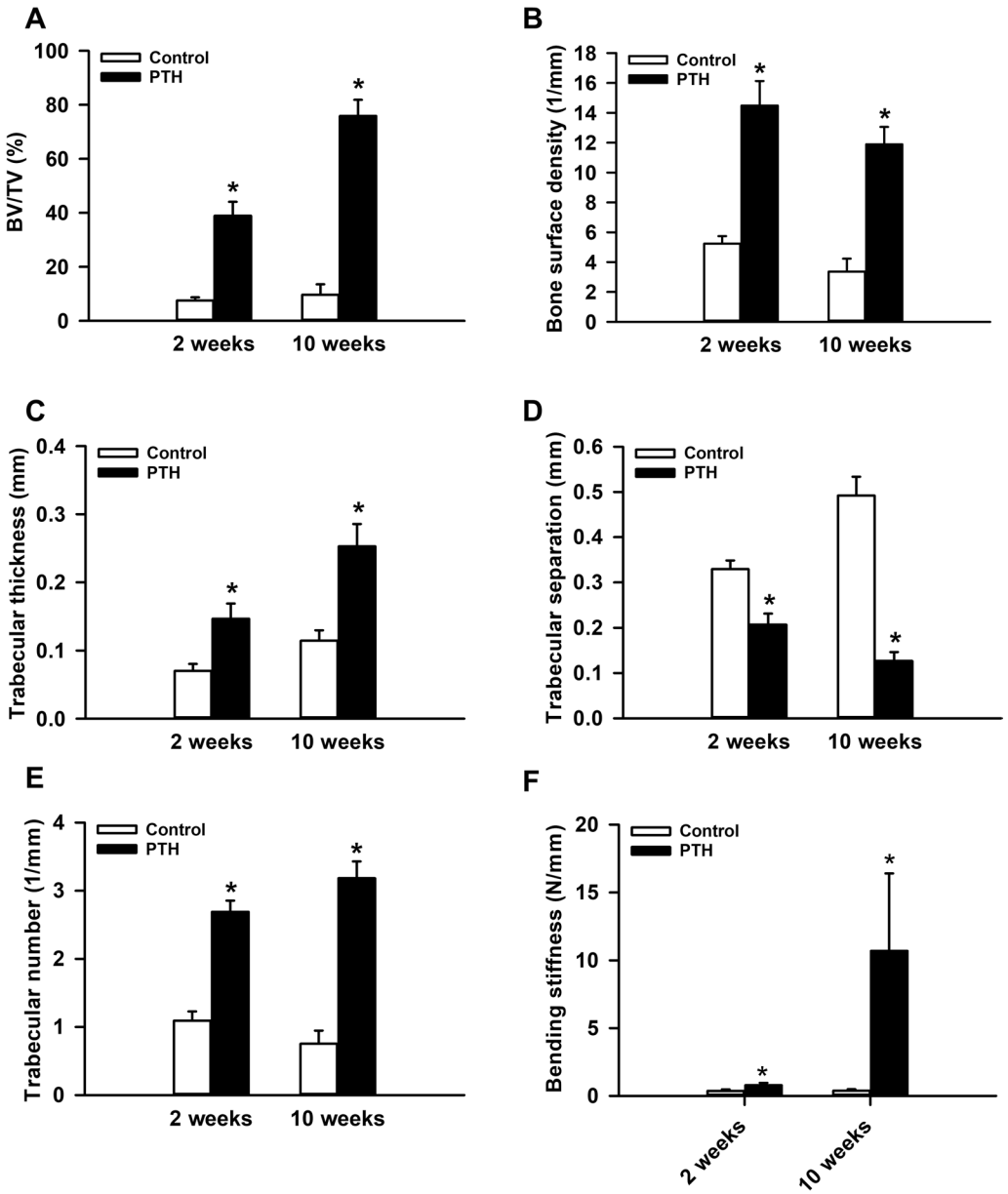

Fig. 2 **A**–**E** BV/TV (%) (**A**), bone surface density (1/mm) (**B**), trabecular thickness (mm) (**C**), trabecular separation (mm) (**D**) and trabecular number (1/mm) (**E**) of the callus tissue of controls (white bars, n = 5 at 2 weeks after surgery, n = 9 at 10 weeks after surgery) and PTH-treated mice (black bars, n = 5 at 2 weeks after surgery, n = 9 at 10 weeks after surgery) at 2 and 10 weeks after surgery, as assessed by µCT analyses. **F** Bending stiffness (N/mm) of femora of controls (white bars, n = 5 at 2 weeks after surgery, n = 9 at 10 weeks after surgery) and PTH-treated mice (black bars, n = 5 at 2 weeks after surgery, n = 9 at 10 weeks after surgery) at 2 and 10 weeks after surgery, as assessed by biomechanical analysis. Mean ± SEM; *p < 0.05 vs. control

of fibrous tissue was significantly lower (Fig. 3E). At 10 weeks, the callus tissue in the control group still consisted mainly of fibrous tissue, whereas in PTH-treated animals it mainly consisted of newly formed bone tissue. Notably, the amount of cartilaginous tissue did not significantly differ between the two study groups at 10 weeks after surgery (Fig. 3F).

In addition, the analysis of the number of TRAP-positive osteoclasts within the callus tissue, demonstrated a significantly higher number of positive cells in PTH-treated animals at 2 and 10 weeks when compared to controls (Fig. 3G, H). Moreover, the analysis of the vascularization of the callus tissue by immunohistochemical staining of CD31-positive microvessels, demonstrated a

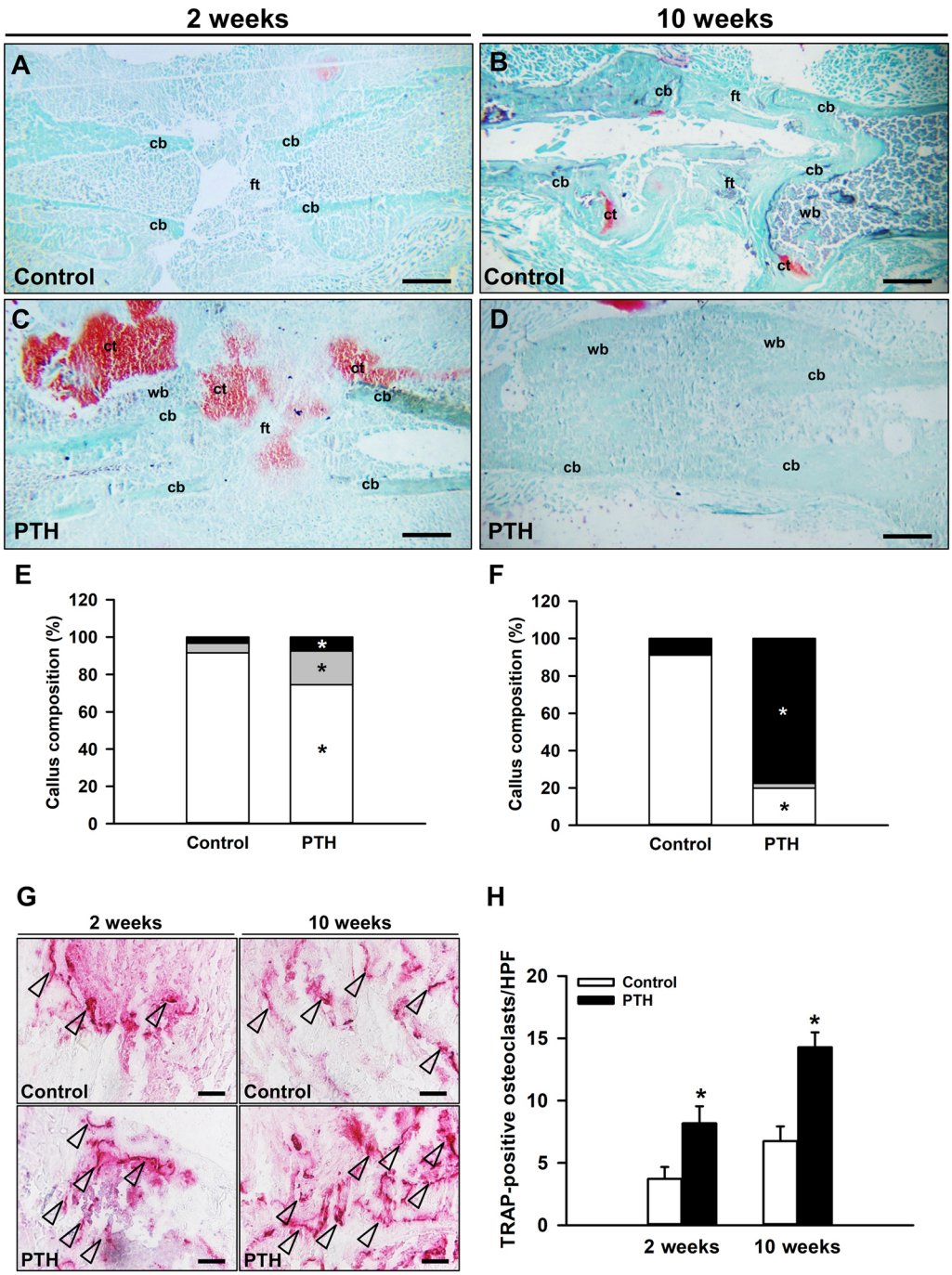

Fig. 3 **A**–**D** Representative histological images of Safranin-O-stained femora of controls (**A**, **B**) and PTH-treated mice (**C**, **D**) at 2 (**A**, **C**) and 10 weeks (**B**, **D**) after surgery. Fibrous tissue (ft), cartilaginous tissue (ct), woven bone (wb) and cortical bone (cb) are indicated. Scale bars: 0.5 mm. **E**, **F** Callus composition (%), including fibrous tissue (white), cartilaginous tissue (gray) and osseous tissue (black), of the callus of controls (n = 5 at 2 weeks after surgery, n = 9 at 10 weeks after surgery) and PTH-treated mice (n = 5 at 2 weeks after surgery, n = 9 at 10 weeks after surgery) at 2 (**E**) and 10 (**F**) weeks after surgery, as assessed by histomorphometric analysis. **G** Representative histological images of TRAP-positive osteoclasts (arrowheads) within the callus tissue of controls and PTH-treated mice at 2 and 10 weeks after surgery. Scale bars: 25 µm. **H** TRAP-positive osteoclasts/HPF within the callus tissue of controls (white bars, n = 5 at 2 weeks after surgery, n = 9 at 10 weeks after surgery) and PTH-treated mice (black bars, n = 5 at 2 weeks after surgery, n = 9 at 10 weeks after surgery) at 2 and 10 weeks after surgery, as assessed by histological analysis. Mean ± SEM; *p < 0.05 vs. control

slightly higher number of microvessels at 2 weeks after surgery, and a significantly higher number at 10 weeks in the PTH-group when compared to controls (Fig. 4A, B). Furthermore, the analysis of the inflammatory response in the callus tissue by staining MPO-positive granulocytes and CD68-positive macrophages revealed in PTH-treated animals a significantly lower number of MPO-positive granulocytes and CD68-positive macrophages at 2 and 10 weeks after surgery (Fig. 4C–F).

Western blot analysis

Western blot analyses of the callus tissue at 2 weeks after surgery revealed an over twofold higher expression of VEGF in the PTH group when compared to controls. However, this difference did not prove to be statistically significant (Fig. 5A, B). In contrast, the expression of COX2 and PI3K was significantly higher within the callus tissue of PTH-treated mice when compared to controls (Fig. 5A, C, D).

Discussion

Non-union formation still represents a major complication in trauma and orthopedic surgery, especially in geriatric patients. Therefore, the aim of the present study was to clarify, whether this problem may be overcome by stimulating bone regeneration with PTH. The major findings of the study are that in a murine atrophic non-union model, PTH treatment improves bone formation, resulting in successful osseous bridging at 10 weeks after surgery. This was associated with a higher bending stiffness and an increased vascularization within the callus tissue of femora of PTH-treated animals when compared to controls.

In clinical practice there are variabilities on the definition of delayed healing and non-union formation [24]. Non-unions are defined by the U.S. Federal Drug Administration council as 'failure to achieve union by 9 months since the injury, and for which there has been no signs of healing for 3 months' [25]. However, others define non-union formation in long bones after a period of 6 months without radiological signs of fracture healing [25]. In general, it should be considered that the diagnosis of non-union always includes both the radiological and clinical examination of the patient [26].

In the present study, we used the non-union model by Garcia et al. [27], which we recently established in geriatric CD-1 mice [15]. Notably, aging affects the process of bone regeneration by multiple factors, including (i) a decreased differentiation and proliferation of stem cells, (ii) a delay in chondrogenesis and osteochondral ossification as well as (iii) a dysfunction in the bone vascular system [15, 28]. In a recent study, we showed that aged CD-1 mice exhibit a delayed process of callus remodeling and, thus, a delayed fracture healing when compared to young adult animals. Interestingly, the overall healing capacity is not affected by aging, as indicated by the finding that both aged and young adult animals achieve complete femoral bone healing 4 to 5 weeks after fracture [29]. Non-union formation in these animals has been considered as lack of healing for at least 10 weeks [15, 27, 30]. This in line with human femoral fractures, which require around 12 weeks for normal healing and non-union is defined as lack of healing after 24 weeks, thus double of the normal healing period [27]. Our results demonstrate that PTH treatment leads to osseous bridging at 10 weeks after surgery and, therefore, overcomes failed fracture-healing and non-union formation.

As a species on the lower phylogenetic scale, mice possess a great potential for bone repair. Hence, the development of a reliable and reproducible non-union model is highly challenging. Garcia et al. [27] established such a model by creating a critical size femoral defect and performing additional periosteal stripping with subsequent fixation by a 'pin-clip' device. Interestingly, in this model a reliable non-union formation was only achieved with additional periosteal stripping after creation of the 1.8 mm femoral defect, whereas animals with intact periosteum demonstrated a partial healing at

(See figure on next page.)

Fig. 4 **A** Representative immunohistochemical images of CD31-positive microvessels (arrowheads) within the callus tissue of controls and PTH-treated mice at 2 and 10 weeks after surgery. Scale bars: 25 µm. **B** CD31-positive microvessels/HPF within the callus tissue of controls (white bars, n = 5 at 2 weeks after surgery, n = 9 at 10 weeks after surgery) and PTH-treated mice (black bars, n = 5 at 2 weeks after surgery, n = 9 at 10 weeks after surgery) at 2 and 10 weeks after surgery, as assessed by immunohistochemical analysis. Mean ± SEM; *p < 0.05 vs. control. **C** Representative immunohistochemical images of MPO-positive cells (arrowheads) within the callus tissue of controls and PTH-treated mice at 2 and 10 weeks after surgery. Scale bars: 25 µm. **D** MPO-positive cells/HPF within the callus tissue of controls (white bars, n = 5 at 2 weeks after surgery, n = 9 at 10 weeks after surgery) and PTH-treated mice (black bars, n = 5 at 2 weeks after surgery, n = 9 at 10 weeks after surgery) at 2 and 10 weeks after surgery, as assessed by immunohistochemical analysis. Mean ± SEM; *p < 0.05 vs. control. **E** Representative immunohistochemical images of CD68-positive cells (arrowheads) within the callus tissue of controls and PTH-treated mice at 2 and 10 weeks after surgery. Scale bars: 25 µm. **F** CD68-positive cells/HPF within the callus tissue of controls (white bars, n = 5 at 2 weeks after surgery, n = 9 at 10 weeks after surgery) and PTH-treated mice (black bars, n = 5 at 2 weeks after surgery, n = 9 at 10 weeks after surgery) at 2 and 10 weeks after surgery, as assessed by immunohistochemical analysis. Mean ± SEM; *p < 0.05 vs. control

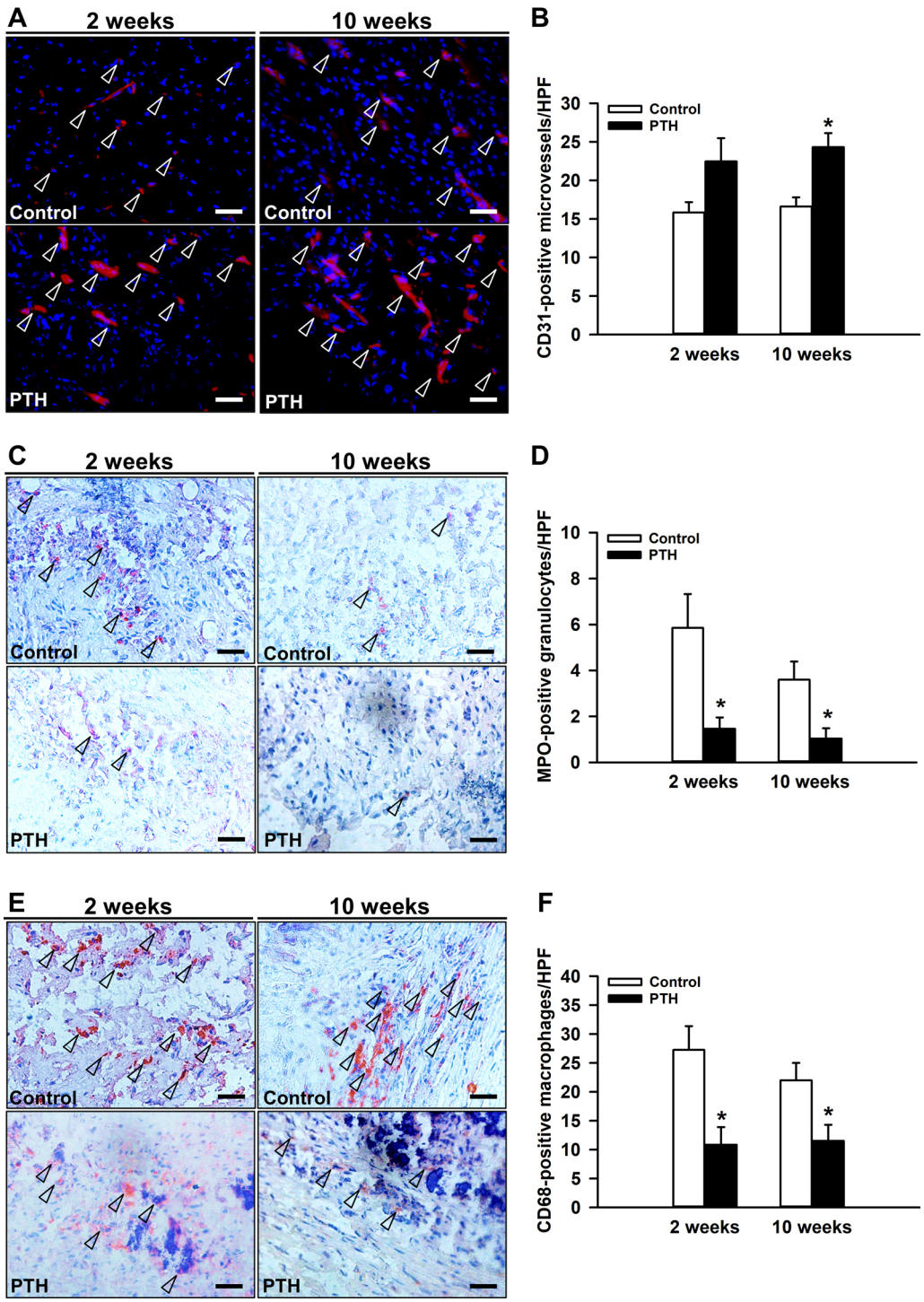

Fig. 4 (See legend on previous page.)

10 weeks after surgery [27]. The periosteum is a highly vascularized tissue, which plays a vital role in the process of physiological bone regeneration by providing the cortical blood supply [31] and serves as a reservoir for osteoprogenitor cells [32]. Moreover, it is well known that periosteal stripping impairs fracture healing [33, 34]. These findings may explain the additional deterioration of bone repair after periosteal stripping in the present non-union model.

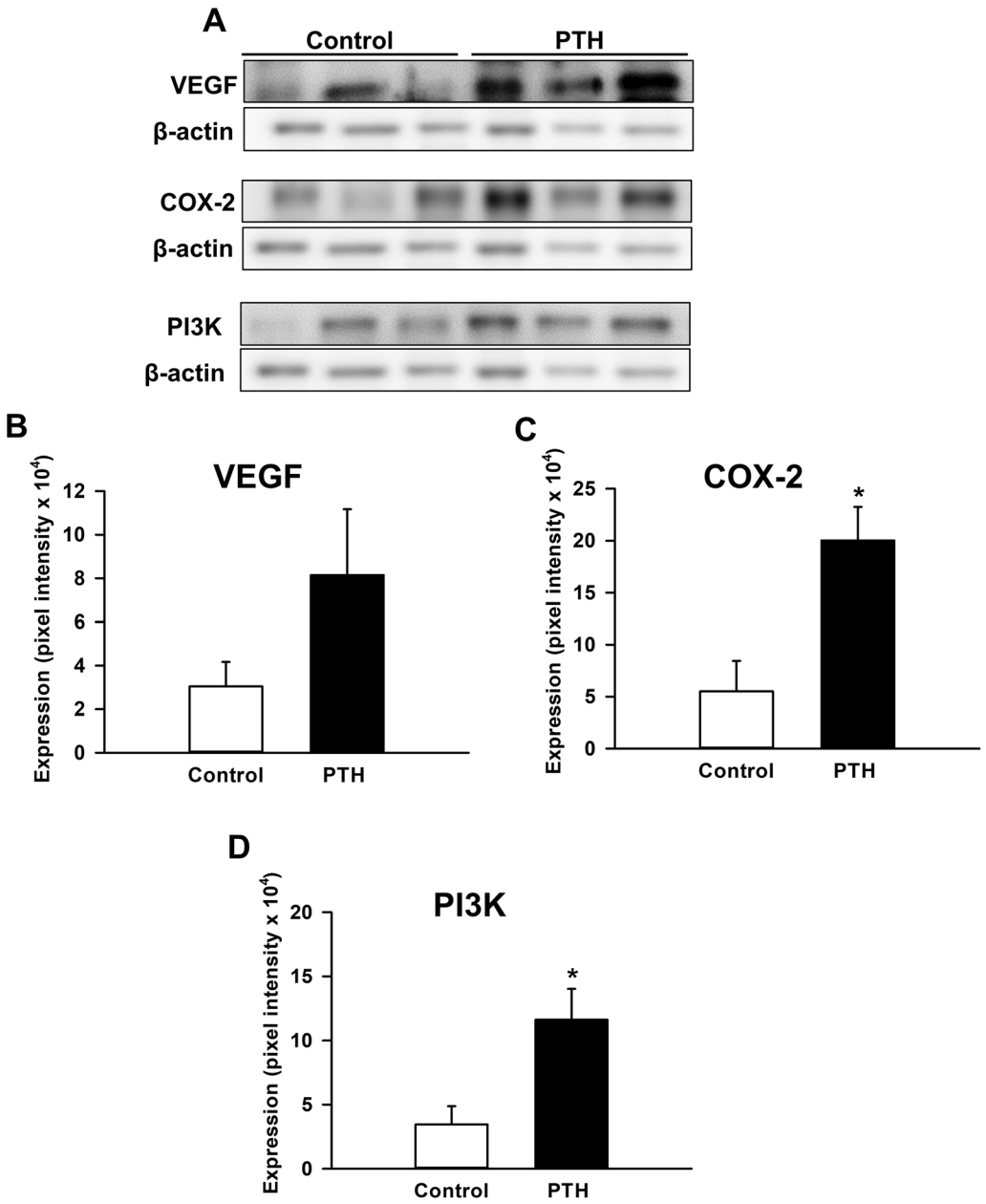

Fig. 5 **A** Representative Western blots of VEGF, COX-2, PI3K and β-actin expression within the callus tissue of controls and PTH-treated mice at 2 weeks after surgery. **B**–**D** Expression of VEGF (pixel intensity × 10^4) (**B**), COX-2 (pixel intensity × 10^4) (**C**) and PI3K (pixel intensity × 10^4) (**D**) within the callus tissue of controls (white bars, n = 3) and PTH-treated mice (black bars, n = 3) at 2 weeks after surgery, as assessed by Western blot analysis. Mean ± SEM; *p < 0.05 vs. control

Fracture healing is characterized by the formation of a soft callus tissue, which gradually transforms into bone by the resorption of calcified cartilage and the formation of novel bone tissue [35, 36]. Interestingly, our histomorphometric analysis showed a significantly higher fraction of cartilaginous tissue in PTH-treated aged animals at 2 weeks after surgery as a clear sign of endochondral ossification. This resulted in the formation of novel bone tissue and osseous bridging at 10 weeks after surgery. In contrast, no signs of endochondral ossification were evident in control animals throughout the 10-weeks observation period. Moreover, the callus tissue of PTH-treated animals showed a significantly higher number of TRAP-positive osteoclasts. Osteoclasts are vital for cartilage resorption and callus remodeling, promoting the

formation of mature novel bone tissue [37]. Therefore, it may be assumed that PTH treatment stimulates bone regeneration in aged mice by inducing endochondral ossification and osteoclast-mediated callus remodeling.

Angiogenesis plays a crucial role for fracture repair. In fact, newly formed blood vessels allow the delivery of nutrients to the fracture site and the infiltration of cells that are essential for callus remodeling [38]. The importance of vascularization is also highlighted by several experimental studies demonstrating that the pharmacological inhibition of angiogenesis by TNP-470, nonsteroidal anti-inflammatory drugs or fumagillin impairs fracture repair and eventually leads to non-union formation [39–41]. Interestingly, our immunohistochemical analysis showed an increased number of CD31-positive microvessels within the callus tissue of PTH-treated animals. This was associated with an over twofold higher expression of VEGF in the PTH group when compared to controls. VEGF is recognized as a main growth factor for the stimulation of angiogenesis [42]. Moreover, several studies indicated that VEGF is directly involved in the process of bone regeneration [43, 44]. Accordingly, inhibition of VEGF expression has been shown to impair fracture repair and to result in non-union formation [45], whereas stimulation of VEGF expression can accelerate fracture healing [46]. Notably, the effects of VEGF on fracture repair exceed the sole stimulation of angiogenesis, but also involve the direct stimulation of endochondral and intramembranous fracture healing as well as stem cell recruitment [43, 44]. Therefore, it may be speculated that PTH improves bone regeneration in aged mice not only by the stimulation of vascularization but also by directly inducing novel bone formation.

The inflammatory phase is a crucial part of successful bone regeneration, as neutrophilic granulocytes and macrophages remove injured and devitalized tissue within the callus and mesenchymal stem cells are directed to the fracture site [37, 47]. A dysregulated, perturbated or even chronic inflammation, however, can impair the process of bone regeneration and even lead to healing failure [48, 49]. Aged individuals exhibit higher levels of circulating pro-inflammatory cytokines, resulting in a chronic inflammatory status, referred to as "inflamm-aging" [50]. Accordingly, we previously detected an increased number of pro-inflammatory macrophages within the callus tissue of non-unions in aged mice when compared to young animals [51]. Moreover, in the present study our immunohistochemical analysis demonstrated that the improved bone regeneration in PTH-treated animals is associated with a significantly lowered number of neutrophilic granulocytes and macrophages within the callus tissue. In line with these findings, Clark et al. [28] recently showed that the inhibition of macrophage recruitment results in improved fracture healing with increased bone volume in aged mice. Thus, PTH treatment most likely inhibits the overshooting inflammatory response in non-unions of aged mice by reducing the number of granulocytes and macrophages within the callus, leading to the observed improved bone regeneration.

Cyclooxygenases (COXs) are necessary for the generation of prostaglandins, prostacyclins and thromboxanes during inflammation. Notably, COX-2 is highly expressed in chondrocytes and chondroprogenitors during the early stage of bone repair [52]. Moreover, Naik et al. [53] observed a delayed bone remodeling in aged mice with a decreased COX-2 expression during the early inflammatory phase of bone repair, highlighting the crucial role of COX-2 in bone healing. In the present study, Western blot analyses demonstrated during the early healing period of 2 weeks a significantly increased expression of COX-2 in PTH-treated mice. Hence, these findings indicate that PTH-treatment improves bone regeneration in aged mice by upregulating COX-2 expression within the callus tissue during the early stage of healing.

PI3K signaling is a pathway activated through receptor tyrosine kinases (RTKs) and G-protein coupled receptors, playing a vital role in cell metabolism and proliferation as well as the regulation of gene expression [54]. Moreover, there is evidence that PI3K signaling is directly involved in the regulation of osteoblastogenesis and skeletal remodeling by controlling osteoblast proliferation and differentiation [55]. Furthermore, Scanlon et al. [56] recently reported that knock-in mice with a global increase in PI3K signaling ($gCbl^{YF}$) exhibit an improved femoral bone healing, which is characterized by an enhanced proliferation of periosteal cells during the first days of fracture repair. In the present study, we found a significantly increased expression of PI3K within the callus tissue of aged PTH-treated mice. Therefore, it may be speculated that the improved bone healing observed in PTH-treated animals is mediated in part also by the activation of PI3K signaling.

In summary, our results demonstrate that PTH treatment significantly improves the regeneration of atrophic non-unions in aged mice. This was associated with an increased number of osteoclasts and CD31-positive microvessels as well as an enhanced expression of COX-2 and PI3K within the callus tissue of PTH-treated animals during the early healing phase. As PTH is a clinically approved drug [13], it may be a promising candidate for the future treatment of non-union formation in aged patients.

Acknowledgements
We are grateful for the excellent technical assistance of Sandra Hans and Caroline Bickelmann.

Author contributions
MMM: data analysis, figure preparation, data discussion and interpretation, manuscript writing. ALT: surgery, radiological, biomechanical and histological analysis. DB: surgery, radiological analysis. MB: surgery, radiological analysis. CS: Western blot analysis. MDM, TH: idea and study design, data interpretation, manuscript writing. MWL: idea and study design, data discussion and interpretation, critical manuscript revision. All authors reviewed and approved the final version of the manuscript.

Funding
Open Access funding enabled and organized by Projekt DEAL.

Availability of data and materials
The datasets during and/or analyzed during the current study available from the corresponding author on reasonable request.

Declarations

Ethics approval and consent to participate
Not applicable.

Consent for publication
Not applicable.

Competing interests
The authors declare that they have no competing interests.

Received: 21 August 2023 Accepted: 26 October 2023
Published: 23 November 2023

References

1. Einhorn TA, Gerstenfeld LC. Fracture healing: mechanisms and interventions. Nat Rev Rheumatol. 2015;11(1):45–54.
2. Victoria G, et al. Bone stimulation for fracture healing: what's all the fuss? Indian J Orthop. 2009;43(2):117–20.
3. Clark D, et al. Effects of aging on fracture healing. Curr Osteoporos Rep. 2017;15(6):601–8.
4. Gruber R, et al. Fracture healing in the elderly patient. Exp Gerontol. 2006;41(11):1080–93.
5. Bergman RJ, et al. Age-related changes in osteogenic stem cells in mice. J Bone Miner Res. 1996;11(5):568–77.
6. Lu C, et al. Cellular basis for age-related changes in fracture repair. J Orthop Res. 2005;23(6):1300–7.
7. Robinson CM, et al. Estimating the risk of nonunion following nonoperative treatment of a clavicular fracture. J Bone Joint Surg Am. 2004;86(7):1359–65.
8. Parker MJ, Raghavan R, Gurusamy K. Incidence of fracture-healing complications after femoral neck fractures. Clin Orthop Relat Res. 2007;458:175–9.
9. Wojda SJ, Donahue SW. Parathyroid hormone for bone regeneration. J Orthop Res. 2018;36(10):2586–94.
10. McSheehy PM, Chambers TJ. Osteoblastic cells mediate osteoclastic responsiveness to parathyroid hormone. Endocrinology. 1986;118(2):824–8.
11. Andreassen TT, Ejersted C, Oxlund H. Intermittent parathyroid hormone (1–34) treatment increases callus formation and mechanical strength of healing rat fractures. J Bone Miner Res. 1999;14(6):960–8.
12. Komatsubara S, et al. Human parathyroid hormone (1–34) accelerates the fracture healing process of woven to lamellar bone replacement and new cortical shell formation in rat femora. Bone. 2005;36(4):678–87.
13. Milstrey A, et al. Dose-dependent effect of parathyroid hormone on fracture healing and bone formation in mice. J Surg Res. 2017;220:327–35.
14. Andreassen TT, Cacciafesta V. Intermittent parathyroid hormone treatment enhances guided bone regeneration in rat calvarial bone defects. J Craniofac Surg. 2004;15(3):424–7.
15. Menger MM, et al. Establishment of a reliable model to study the failure of fracture healing in aged mice. J Gerontol A Biol Sci Med Sci. 2022;77(5):909–17.
16. Homburger F, et al. Aging changes in CD-1 HaM/ICR mice reared under standard laboratory conditions. J Natl Cancer Inst. 1975;55(1):37–45.
17. Goldberg VM, et al. Bone grafting: role of histocompatibility in transplantation. J Orthop Res. 1985;3(4):389–404.
18. Bosemark P, et al. Augmentation of autologous bone graft by a combination of bone morphogenic protein and bisphosphonate increased both callus volume and strength. Acta Orthop. 2013;84(1):106–11.
19. Morgan EF, et al. Micro-computed tomography assessment of fracture healing: relationships among callus structure, composition, and mechanical function. Bone. 2009;44(2):335–44.
20. Histing T, et al. Ex vivo analysis of rotational stiffness of different osteosynthesis techniques in mouse femur fracture. J Orthop Res. 2009;27(9):1152–6.
21. Kawamoto T, Kawamoto K. Preparation of thin frozen sections from nonfixed and undecalcified hard tissues using Kawamot's film method (2012). Methods Mol Biol. 2014;1130:149–64.
22. Morodomi Y, et al. Modified application of Kawamoto's film method for super-resolution imaging of megakaryocytes in undecalcified bone marrow. Res Pract Thromb Haemost. 2020;4(1):86–91.
23. Gerstenfeld LC, et al. Application of histomorphometric methods to the study of bone repair. J Bone Miner Res. 2005;20(10):1715–22.
24. Menger MM, et al. Vascularization strategies in the prevention of non-union formation. Tissue Eng Part B Rev. 2020;27:107–32.
25. Andrzejowski P, Giannoudis PV. The 'diamond concept' for long bone non-union management. J Orthop Traumatol. 2019;20(1):21.
26. Hak DJ, et al. Delayed union and nonunions: epidemiology, clinical issues, and financial aspects. Injury. 2014;45(Suppl 2):S3–7.
27. Garcia P, et al. Development of a reliable non-union model in mice. J Surg Res. 2008;147(1):84–91.
28. Clark D, et al. Age-related changes to macrophages are detrimental to fracture healing in mice. Aging Cell. 2020;19(3): e13112.
29. Menger MM, et al. Radiographic, biomechanical and histological characterization of femoral fracture healing in aged CD-1 mice. Bioengineering. 2023;10(2):275.
30. Garcia P, et al. Rodent animal models of delayed bone healing and non-union formation: a comprehensive review. Eur Cell Mater. 2013;26:1–12 (**discussion 12–4**).
31. Squier CA, Ghoneim S, Kremenak CR. Ultrastructure of the periosteum from membrane bone. J Anat. 1990;171:233–9.
32. Arnsdorf EJ, et al. The periosteum as a cellular source for functional tissue engineering. Tissue Eng Part A. 2009;15(9):2637–42.
33. Utvag SE, Grundnes O, Reikeraos O. Effects of periosteal stripping on healing of segmental fractures in rats. J Orthop Trauma. 1996;10(4):279–84.
34. Oni OO, Stafford H, Gregg PJ. An experimental study of the patterns of periosteal and endosteal damage in tibial shaft fractures using a rabbit trauma model. J Orthop Trauma. 1989;3(2):142–7.
35. Marsell R, Einhorn TA. The role of endogenous bone morphogenetic proteins in normal skeletal repair. Injury. 2009;40(Suppl 3):S4–7.
36. Histing T, et al. Pantoprazole, a proton pump inhibitor, delays fracture healing in mice. Calcif Tissue Int. 2012;90(6):507–14.
37. Bahney CS, et al. Cellular biology of fracture healing. J Orthop Res. 2019;37(1):35–50.
38. Schlundt C, et al. Clinical and Research approaches to treat non-union fracture. Curr Osteoporos Rep. 2018;16(2):155–68.
39. Fang TD, et al. Angiogenesis is required for successful bone induction during distraction osteogenesis. J Bone Miner Res. 2005;20(7):1114–24.
40. Murnaghan M, Li G, Marsh DR. Nonsteroidal anti-inflammatory drug-induced fracture nonunion: an inhibition of angiogenesis? J Bone Jt Surg Am. 2006;88(Suppl 3):140–7.
41. Fassbender M, et al. Local inhibition of angiogenesis results in an atrophic non-union in a rat osteotomy model. Eur Cell Mater. 2011;22:1–11.
42. Garcia P, et al. Temporal and spatial vascularization patterns of unions and nonunions: role of vascular endothelial growth factor and bone morphogenetic proteins. J Bone Joint Surg Am. 2012;94(1):49–58.

43. Beamer B, Hettrich C, Lane J. Vascular endothelial growth factor: an essential component of angiogenesis and fracture healing. HSS J. 2010;6(1):85–94.
44. Keramaris NC, et al. Fracture vascularity and bone healing: a systematic review of the role of VEGF. Injury. 2008;39(Suppl 2):S45–57.
45. Gaston MS, Simpson AH. Inhibition of fracture healing. J Bone Jt Surg Br. 2007;89(12):1553–60.
46. Peng H, et al. VEGF improves, whereas sFlt1 inhibits, BMP2-induced bone formation and bone healing through modulation of angiogenesis. J Bone Miner Res. 2005;20(11):2017–27.
47. Medhat D, Rodriguez CI, Infante A. Immunomodulatory effects of MSCs in bone healing. Int J Mol Sci. 2019;20(21):5467.
48. Loi F, et al. Inflammation, fracture and bone repair. Bone. 2016;86:119–30.
49. Hankenson KD, Zimmerman G, Marcucio R. Biological perspectives of delayed fracture healing. Injury. 2014;45(Suppl 2):S8–15.
50. Franceschi C, et al. Inflamm-aging. An evolutionary perspective on immunosenescence. Ann N Y Acad Sci. 2000;908:244–54.
51. Menger MM, et al. Establishment of a reliable model to study the failure of fracture healing in aged mice. J Gerontol A Biol Sci Med Sci. 2021;77:909–17.
52. Xie C, et al. COX-2 from the injury milieu is critical for the initiation of periosteal progenitor cell mediated bone healing. Bone. 2008;43(6):1075–83.
53. Naik AA, et al. Reduced COX-2 expression in aged mice is associated with impaired fracture healing. J Bone Miner Res. 2009;24(2):251–64.
54. Cantley LC. The phosphoinositide 3-kinase pathway. Science. 2002;296(5573):1655–7.
55. Guntur AR, Rosen CJ. The skeleton: a multi-functional complex organ: new insights into osteoblasts and their role in bone formation: the central role of PI3Kinase. J Endocrinol. 2011;211(2):123–30.
56. Scanlon V, et al. Loss of Cbl-PI3K interaction modulates the periosteal response to fracture by enhancing osteogenic commitment and differentiation. Bone. 2017;95:124–35.

Publisher's Note

6. Discussion

6.1 Discussion of material and methods

6.1.1. Non-union models in mice

Mice are a species on the lower physiological scale, therefore possessing a great potential for bone regeneration. In fact, even unstabilized fractures can heal in these animals [Colnot et al., 2003]. Accordingly, the development of a reliable non-union model is challenging and the number of available models is sparse [Garcia et al., 2013].

The first non-union model in mice was introduced by Choi et al. [2004]. The authors performed an osteotomy of mice tibia and stabilized the defect by an external fixator performing a distraction osteosynthesis. However, this model is lacking reliability, since only 60 % of all animals demonstrated a failure of fracture healing 27 days after surgery. Moreover, the observation period of only 27 days is too short to evaluate non-union formation. Since normal femoral fracture healing in mice takes around 4 weeks [Manigrasso and O'Connor, 2004; Holstein et al., 2007], a non-union in mice should be defined as healing failure 10 weeks after surgery. This also corresponds with human femoral fractures, which need approximately 12 weeks for the healing process, and non-union formation is considered 24 weeks after injury [Garcia et al., 2008]. Furthermore, the distraction osteosynthesis used in the model by Choi et al. [2004] represents another limitation of the model, as it does not mimic the pathophysiology of non-union formation after trauma and substantial bone tissue loss in humans.

In 2008, a different non-union model in mice was introduced by Oetgen et al. [2008]. The authors chose a lateral approach through the vastus muscle to expose the femur. Afterwards, a partial osteotomy covering 50 % of the diameter of the mid-diaphysis was performed and stabilized by a 25-gauge needle in a retrograde fashion. The fracture was completed at the site of the cortical osteotomy and, in addition, cauterization of the lateral periosteum was performed 2 mm distally and proximally. Of interest, the authors demonstrated that the model resulted in hypertrophic non-union formation 9 weeks after surgery, as indicated by a lack of osseous bridging and abundant formation of cartilaginous tissue at the fracture ends [Oetgen et al., 2008]. The cause for hypertrophic non-union formation may be the instable fixation by an intramedullary gauge needle, which did not achieve adequate rotational and axial stability. Hence, the model of Oetgen et al. [2008] is suitable for the preclinical analysis of hypertrophic non-union formation. However, most cases of hypertrophic non-union formation can be treated by a stable fixation and sufficient osteosynthesis. Thus, they do not represent a great clinical challenge and are, therefore, not of particular interest for further research.

Accordingly, a suitable non-union model for preclinical research should mimic atrophic non-union formation, as the pathophysiology is manifold and in many cases only poorly understood. Only with such a model, effective treatment approaches can be developed in a preclinical setting and translated into clinical practice. There are reports which describe the use of plates [Manassero et al., 2013; Kessler et al., 2024] and external fixators [Srouji et al., 2011; Zwingenberger et al., 2013] for the stabilization of critical size bone defects, resulting in healing failure. These implants are highly sophisticated, and the observed fracture healing failure also resembles atrophic non-union formation. However, disadvantages represent the very demanding surgical techniques as well as high costs of the corresponding implants, making these models less feasible in preclinical practice.

The periosteum is a highly vascularized tissue, which is of pivotal importance for successful bone regeneration due to providing an adequate blood supply and serving as a reservoir for the osteoblastic cell lineage [Squier et al., 1990; Arnsdorf et al., 2009]. Several experimental studies could already demonstrate the importance of a preserved periosteum for achieving fracture repair [Park et al., 1999; Probst et al., 1999; Landry et al., 2000]. Substantial bone defects caused by high-energy trauma are most likely associated with severe soft-tissue damage, including the periosteum. Therefore, damage to the periosteum by mechanical resection or cauterization is suitable for mimicking these injuries in a preclinical setting, which may provide a reliable development of fracture healing failure.

6.1.1.1 Segmental defect and pin-clip stabilization

In the present thesis, the non-union model of Garcia et al. [2008] was used in all three studies. In this model, axial and rotational stability was achieved by a ‘pin-clip device’: An intramedullary pin was inserted in a retrograde fashion after dislocation of the patella and inserting the pin through the intramedullary notch in the medullar cavity. Notably, the pin was fixed proximally in the area of the trochanter major to avoid dislocation. Moreover, a custom-made clip was implanted ventro-dorsally into the femur. Subsequently, a 1.8 mm wide segmental bone defect was created using a size-standardized spherical trephine by exposing the femur through a lateral approach. In addition, the periosteum was stripped 2 mm circumferentially distally and proximally of the segmental defect (Figure 2). All procedures were performed using an operation microscope to achieve an adequate level of accuracy during the procedure.

According to Garcia et al. [2008] the model leads to a reliable non-union formation of 100 % with no progression in bone repair 15 weeks after surgery. However, this is only achieved by means of additional resection of the periosteum 2 mm distally and proximally to the defect zone. Notably, an intact periosteum and smaller defect sizes lead to partial bridging of the bone

defect [Garcia et al., 2008]. Garcia et al. [2011a] also introduced another non-union model in mice with a femoral bone defect of 2.0 mm and stabilization by an intramedullary locking nail, resembling nail-osteosynthesis in humans. In this case, the periosteum was left intact [Garcia et al., 2011a]. Although this model also offers a reliable non-union formation and high standardization due to the sophisticated technique of osteosynthesis, the high costs of the implants are a major drawback. Moreover, the periosteal injury performed in the pin-clip model might more accurately mimic the severe soft-tissue injuries associated with non-union formation.

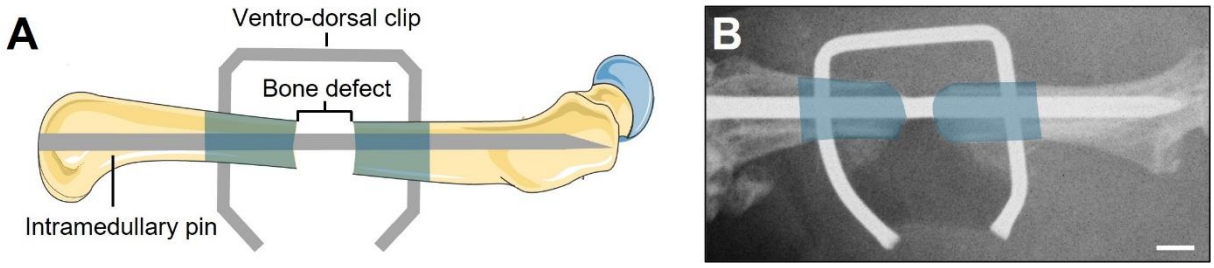

Figure 2**:** *(A) Schematic illustration of the pin-clip non-union model. The intramedullary pin, bone defect and ventro-dorsal clip are indicated. (B) Postoperative X-ray of the pin-clip non-union model. Scale bar: 1mm. The area of periosteal resection is indicated in (A) and (B) by blue background color. The figure was created using pictures from Servier Medical Art, provided by Servier, licensed under a Creative Commons Attribution 4.0 unported license (https://creativecommons.org/licenses/by/4.0/).*

Even though the surgical technique is easily applicable and standardized, the 'pin-clip' model may be associated with a few potential technical pitfalls, which need to be avoided:

- *Shortening of the intramedullary pin*. The intramedullary pin needs to be shortened after insertions to avoid substantial protrusion of the pin beyond the intercondylar notch. Thereby, limitations of knee movement and unnecessary pain for the animal can be prevented.
- *Proximal pin fixation.* The intramedullary pin must be fixated in the proximal part of the femur. When inserting the pin, a slight reduction of resistance is felt when penetrating the proximal femur around the area of the trochanter major. This is of pivotal importance to avoid implant dislocation. If in doubt, perioperative X-rays should be performed to confirm the correct implant positioning.
- *Defect drilling under saline cooling*. When creating the 1.8 mm defect with the spherical trephine, saline cooling of the situs is essential to avoid heat damage of the bone ends and the surrounding soft tissue.
- *Implantation of the ventro-dorsal clip.* From a surgical perspective, the implantation of the ventro-dorsal clip is the most demanding part of the procedure. Drilling of the holes for insertion of the clip in the correct ventro-dorsal angle without inflicting additional

damage to the cortex must be performed very carefully and only by using an operation microscope to guarantee an adequate precision.

- *Stripping of the periosteum.* To achieve a reliable non-union formation, the periosteal resection is of major importance in the present model. Hence, care should be taken to strip the periosteum along the complete circumference of the femur 2 mm distally and proximally to the defect zone.

6.1.1.2 Transverse fracture and K-wire stabilization

The second non-union model used in the first study of this thesis is an adaption of the non-union model in rats by Kokubu et al. [2003]. In the original model, the authors generated a stable closed femoral fracture with additional periosteal cauterization, which was stabilized by a 1.25 mm K-wire [Kokubu et al., 2003]. Notably, a non-union rate of 100 % was reported 8 weeks after surgery. In the present thesis, the model was modified and established in mice: A 0.6 mm K-wire was inserted through the intercondylar notch into the medullar cavity in a retrograde fashion using a motor-driven drill. Afterwards, the femur was fractured using a 3-point bending device and was exposed by a lateral approach. Subsequently, the periosteum was cauterized within a distance of 2 mm on each side of the fracture [Menger et al., 2022a] (Figure 3).

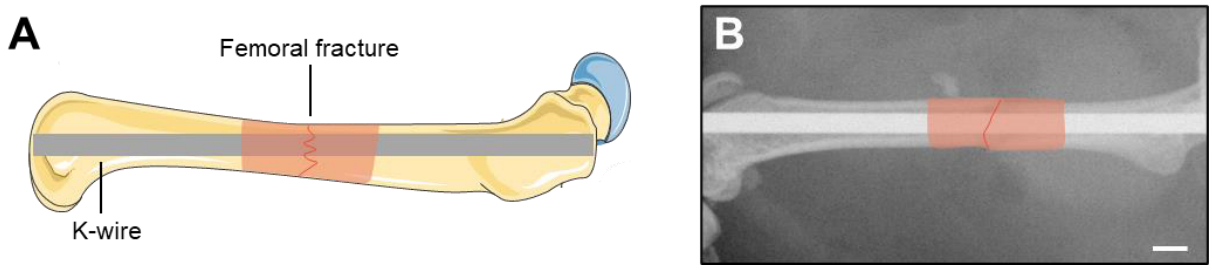

Figure 3: *(A) Schematic illustration of the K-wire non-union model. The K-wire and the femoral fracture are indicated. (B) Postoperative X-ray of the K-wire non-union model. Scale bar: 1mm. (B) The area of periosteal cauterization is indicated in (A) and (B) by red background color. The figure was created using pictures from Servier Medical Art, provided by Servier, licensed under a Creative Commons Attribution 4.0 unported license (https://creativecommons.org/licenses/by/4.0/).*

Notably, no implant dislocation or axial instability was observed indicating a press-fit stabilization of the fracture by the 0.6 mm K-wire. The K-wire non-union model is a versatile tool for the investigation of delayed fracture healing with damaged periosteum and impaired angiogenic capacity, resembling trauma-induced fracture with severe soft tissue injury. However, the model is also associated with potential pitfalls, which should be avoided:

- *Insertion of the K-wire.* The intramedullary canal of mice femora is relatively small with a diameter of 0.8-1.0 mm. Hence, the insertion of the 0.6 mm K-wire has to be performed with great care, especially when using a motor-driven drill. Otherwise,

severe damage of the bone and soft tissue including surrounding vessels and nerves (arteria, vena and nervus femoralis) can occur.

- *Shortening of the K-wire.* Similar to the intramedullary pin in the pin-clip model, the K-wire needs to be shortened at the distal end to avoid relevant protrusion of the implant beyond the intercondylar notch. A protruding implant into the knee joint may result in limitation of knee movement and additional pain for the animal.
- *Closed femoral fracture.* When performing the closed femoral fracture with the 3-point bending device, an exact positioning of the limb is of major importance. Otherwise, fractures may occur in the distal or proximal metaphysis, but not in the diaphysis. This must be avoided as there is evidence that metaphyseal and diaphyseal fracture healing exhibit significant differences.
- *Cauterization of the periosteum.* The cauterization of the periosteum must be performed with care in order to prevent thermal necrosis of the bone and additional thermal damage to the surrounding soft tissue.

6.1.2. µCT analysis

The use of µCT for the investigation of bone regeneration in preclinical research has gained increasing interest in recent years. Today, most experimental studies make use of this technique, as it allows the detailed analysis of the progression of fracture healing [O'Neill et al., 2012]. µCT analysis enables not only the assessment of tissue and bone volume, but also an in depth analysis of the trabecular architecture [Bouxsein et al., 2010]. This data is valuable, especially when evaluating the process of bone remodeling. To distinguish between soft tissue, poorly and highly mineralized bone, gray values need to be expressed as mineral content. Therefore, a calibration with calcium hydroxyapatite (CaHA) phantom rods with known bone mineral density (BMD) values (0.250 g and 0.750 g CaHA/cm^3) must be performed. Highly mineralized bone is defined as a BMD of more than 0.642 g/cm^3, resulting in gray values of 98-255 [Morgan et al., 2009; Bosemark et al., 2013]. Poorly mineralized bone is assumed to have a BMD value between 0.410 g/cm^3 and 0.642 g/cm^3 [Isaksson et al., 2009; Bosemark et al., 2013], resulting in gray values of 68-97 [Orth et al., 2017].

Of note, these thresholds are based on visual inspection of the images, qualitative comparison with histological sections as well as other studies investigating bone repair and callus tissue by µCT [Bosemark et al., 2013; Orth et al., 2017]. Notably, the µCT analysis enables the two- and three-dimensional visualization of the bone healing process (Figure 4). After creating the volume of interest (VOI), the newly formed callus tissue is countered manually excluding any

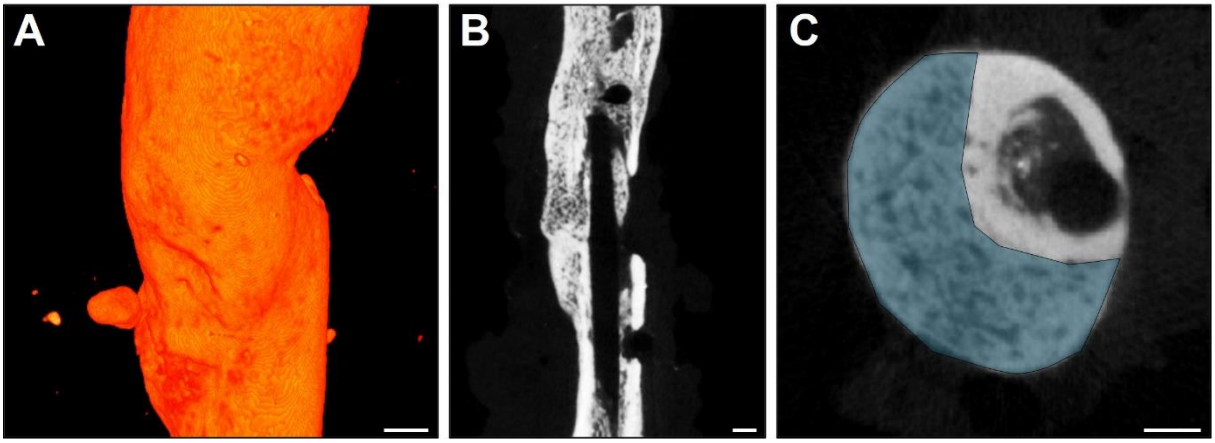

Figure 4. *(A-C) µCT imaging of a femur of a PTH-treated aged mouse 10 weeks after surgery. (A) 3D reconstruction, (B) transversal CT image, (C) Axial view. Newly formed bone tissue is indicated in (C) with blue background color. Scale bars: 0.5 mm.*

original cortical bone as region of interest (ROI). Subsequent analysis of the callus ROI includes the following parameters:

- Poorly mineralized bone volume (mm^3)
- Highly mineralized bone volume (mm^3)
- Bone volume fraction of tissue volume (BV/TV)
- Bone surface density ($1/mm^3$)

Parameters of trabecular architecture:

- Trabecular thickness (mm)
- Trabecular separation (mm)
- Trabecular number (1/mm)

Although the µCT analysis provides a detailed description of the bone architecture and the process of fracture repair, an additional histological analysis of the callus tissue should be performed to validate the radiological data. The calibration process for the interpretation of gray values as mineral content is based on visual comparison, and, thus, can represent a source of error. The histological analysis, on the other hand, is based on the measurement of the actual morphology of the callus tissue and does not rely on an optical calibration method. Hence, only a combination of histomorphometry and µCT imaging enables an adequate analysis of the callus tissue architecture.

6.2 Discussion of results

6.2.1 Comparison of two non-union models with damaged periosteum in mice

To gain further insights into the pathophysiological mechanisms of non-union formation in aged animals and, thus, to enable the development of novel treatment approaches, a reliable non-union model in mice is of crucial importance. Therefore, a non-union model in mice was established, which is characterized by a transverse femoral fracture, additional periosteal injury by cauterization and K-wire stabilization. Moreover, we compared its validity and reliability with the already established non-union model of Garcia et al. [2008].

The majority of preclinical models uses a large segmental defect to achieve bone healing failure [Choi et al., 2004; Zhang et al., 2010]. Accordingly, Garcia et al. [2008] induced a large segmental femoral defect and achieved 10 weeks after surgery a non-union rate of 100 %. The radiological and histological analyses demonstrated typical signs of atrophic non-union formation, including lack of fracture bridging, absence of bone formation and rounded bone ends. One major advantage of using segmental defects represents the fact that they mimic the resection of already established non-unions in clinical practice. On the other hand, the segmental resection of bone tissue is not comparable with a trauma-induced fracture injury. Atrophic non-unions in clinical practice also develop without significant loss of bone tissue [Kokubu et al., 2003]. Hence, a model using a transverse femoral fracture with additional periosteal injury and K-wire stabilization may overcome this problem [Menger et al., 2022a].

The data of the present thesis demonstrate that 10 out of 12 animals in the K-wire group exhibited non-union formation at 10 weeks after surgery with abundant fibrous tissue within the fracture gap. Two out of 12 mice, however, demonstrated osseous bridging, as indicated by radiological and histological analyses (Figure 5). These findings suggest that the periosteal cauterization performed in the K-wire model does not completely prevent the process of bone regeneration. Kokubu et al. [2003], however, demonstrated a non-union rate of 100 % when performing periosteal cauterization at a femoral shaft fracture site in rats. One possible explanation for these contradictory results may be the increased bone healing potential of mice when compared to rats [Garcia et al., 2013].

In line with these findings, the radiological and histological analysis revealed a significantly increased amount of bone tissue within the callus tissue of animals of the K-wire group when compared to the callus tissue of animals of the pin-clip group. This was associated with signs of endochondral ossification, as indicated by a higher amount of cartilaginous tissue at 2 weeks

after fracture and an increased bending stiffness throughout the observation period. Moreover, the Western blot analysis revealed a higher expression of the pro-osteogenic markers BMP-2, BMP-4 and cysteine-rich angiogenic inducer (CYR)61 as well as the cell proliferation marker PCNA within the callus tissue of femora in the K-wire group when compared to that of the pin-clip group. Notably, these proteins are expressed during endochondral ossification, reaching their maximum expression between 2 and 3 weeks after fracture [Histing et al., 2012b]. Hence,

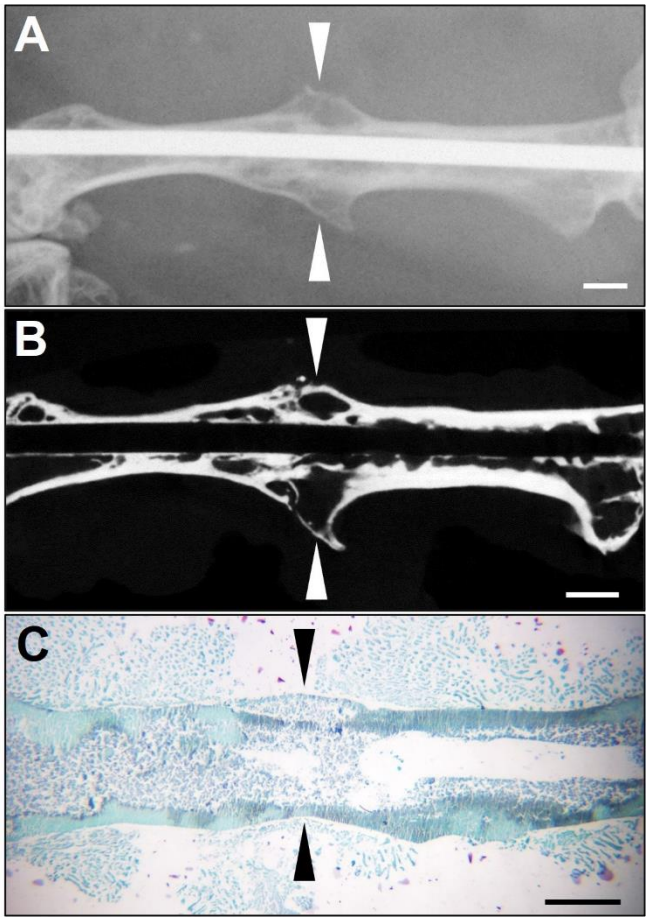

***Figure 5**. (A) X-ray, (B) transversal µCT image and (C) Safranin-O staining of a mouse femur in the K-wire group at 10 weeks after surgery. Arrows indicating osseous bridging of the fracture gap. Scale bars: 1 mm.*

the increased bone formation in the K-wire group was probably due to the enhanced expression of bone formation markers. Furthermore, the results showed significant differences in parameters of bone remodeling between the two study groups. The callus of femora of the K-wire group demonstrated a higher number of osteoclasts within the callus tissue as well as an increased expression of OPG and RANKL. It is well known that RANKL stimulates osteoclastogenesis by binding RANK on osteoclasts. OPG, however, acts as soluble decoy receptor by preventing RANKL-RANK binding, thereby inhibiting osteoclastogenesis [Simonet et al., 1997; Lacey et al., 1998; Menger et al., 2022a]. Interestingly, there is evidence that novel bone formation and subsequent cartilage resorption is associated with peaking RANKL and OPG levels. Several experimental studies could demonstrate that bone remodeling and fracture repair is compromised by systemic melatonin and pantoprazole treatment, resulting in

inhibition of RANKL expression [Histing et al., 2012a; Histing et al., 2012b]. Accordingly, the increased bone formation observed in the K-wire group may also be caused by an increased number of osteoclasts as well as an elevated expression of RANKL and OPG.

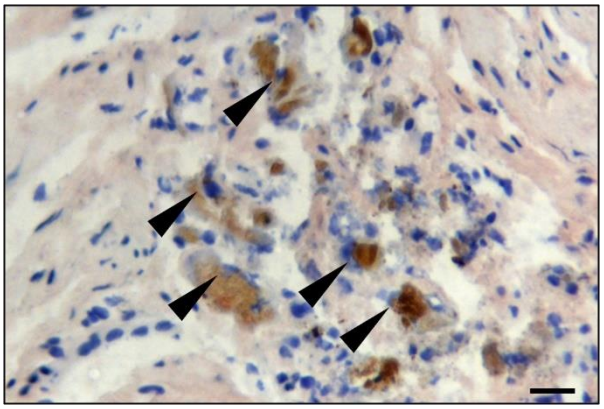

Figure 6. *PCNA-positive cells within the fibrous callus tissue in the K-wire group. Arrowheads indicate PCNA-positive cells. Scale bar: 50 µm.*

An adequate angiogenesis at the fracture site is of major importance for successful bone regeneration. Newly formed microvessels allow the transport of nutrients, oxygen and MSCs to the callus tissue and start the process of ossification [Kanczler and Oreffo, 2008]. In addition, stimulation of vascularization by pro-angiogenic markers and compounds, such as VEGF and erythropoietin (EPO), improve fracture repair in preclinical bone healing models [Eckardt et al., 2005; Garcia et al., 2011b]. In contrast, inhibition of angiogenesis hinders adequate bone formation and can result in failure of fracture healing [Fassbender et al., 2011]. Notably, in the present study a significantly lower number of microvessels was observed within the callus tissue of mice in the K-wire group at 2 and 5 weeks after surgery when compared to the pin-clip group. These findings are most likely caused by the periosteal cauterization performed during the intervention in the K-wire group. The periosteum is of pivotal importance for an adequate blood supply at the fracture site and represents an important source for the callus vasculature [Squier et al., 1990; Bahney et al., 2019]. Hence, it can be assumed that the cauterization causes a more severe damage to the periosteum than the mechanical stripping performed in the pin-clip model. The reduced angiogenesis at the fracture site may result in ischemic conditions, which, on the one hand, suppress osteogenic differentiation, and, on the other hand, induce proliferation of fibrous tissue [Lu et al., 2007; Menger et al., 2022d]. Accordingly, in most animals of the K-wire group fibrous tissue was abundant and novel bone formation was scarce, ultimately resulting in non-union formation. In line with this, the immunohistochemical analysis demonstrated that PCNA-positive cells were concentrated within the fibrous tissue of the callus (Figure 6).

In conclusion, the first study of this thesis demonstrated that compromised fracture healing in the K-wire model is most likely due to an impaired angiogenesis and vascularization at the fracture site caused by periosteal cauterization. The non-union model using a segmental defect and pin-clip device creates a failure of fracture healing by a diminished expression of pro-osteogenic factors and a decrease of the number and activity of osteoclasts. Notably, the pin-

clip model has proven a reliability of 100 % atrophic non-union formation at 10 weeks after surgery. Hence, this model is especially suitable for the analysis of pathophysiological mechanisms in atrophic non-union formation and the evaluation of novel treatment approaches. The K-wire model, on the other hand, can be applied in preclinical studies analyzing trauma-induced compromised and delayed fracture healing and appropriate treatment strategies due to severe soft tissue injuries with damaged periosteum and impaired angiogenesis.

6.2.2 Establishment and characterization of a reliable model to study non-union formation in aged mice

In the second study of this thesis, the more reliable pin-clip non-union model was used in aged CD-1 mice. Moreover, the biological response of fracture healing failure was characterized and compared between young adult and aged animals by radiological, histological, immunohistochemical and biochemical analyses.

Experimental non-union models remain the gold standard for analyzing the molecular and cellular basis of fracture healing in preclinical research. Due to an increasing older population, and the knowledge that healing in the elderly differs substantially from healing in young adults, it is of high clinical interest to establish and characterize such a non-union model in aged mice. The radiological and biomechanical analysis of the applied pin-clip model revealed a non-union rate of 100 % in aged animals [Menger et al., 2022c]. Moreover, the results showed a lower bending stiffness and a decreased bone formation in aged mice when compared to young adult animals. Furthermore, µCT analyses demonstrated a more fragile trabecular architecture in aged animals, characterized by an enhanced trabecular separation and a lower trabecular number when compared to young adult animals. These findings are in line with previous reports indicating a higher risk for non-union formation in geriatric patients [Nieminen et al., 1981; Parker et al., 2007]. Furthermore, several preclinical studies revealed a lower bone healing capacity in aged animals. Clark et al. [2020] demonstrated an inferior bone healing of geriatric mice when compared to young animals in an experimental tibia fracture model. Additionally, Lu et al. [2005] reported a delayed cell differentiation, a prolonged phase of endochondral ossification and compromised bone remodeling in aged mice, ultimately resulting in impaired fracture healing.

Interestingly, the reduced bone formation in non-unions of aged animals, observed in the present study, was associated with a lower expression of the pro-osteogenic markers BMP-2 and BMP-4 as well as COX-2, which is critical for the initiation of periosteal cortical bone healing [Xie et al., 2008]. Furthermore, Western blot analyses showed a significantly

decreased expression of CYR61, which also exhibits pro-osteogenic properties. In fact, CYR61 stimulates osteoblast proliferation, differentiation and cell adhesion [Si et al., 2006]. Additionally, the stimulation of fracture repair by phosphodiesterase-3 and -5 inhibitors is associated with an increase in CYR61 expression [Histing et al., 2011b; Herath et al., 2015]. Hence, the reduced bone formation observed in aged animals is most likely due to the lower expression of pro-osteogenic markers, such as CYR61.

The process of bone remodeling in non-union formation was investigated by measuring the number and activity of osteoclasts within the callus tissue. Notably, aged animals showed a lower number of TRAP-positive osteoclasts within their segmental defects. Moreover, the ratio of OPG, an inhibitor of osteoclastogenesis, to RANKL, a stimulator of osteoclastogenesis, was increased when compared to young adult mice. These findings indicate a reduced differentiation and lower activity of osteoclasts in non-unions of geriatric animals. Another important marker for bone remodeling and formation represents runt-related transcription factor (RUNX)-2. This protein plays a vital role in the coordination of signaling pathways involved in osteoblast differentiation, such as fibroblast growth factor (FGF), hedgehog and the wingless-type MMTV integration site family (WNT) [Komori, 2019]. Of interest, bone turnover and remodeling is characterized by bone resorption of osteoclasts and the formation of novel bone tissue by osteoblasts [Teitelbaum, 2007]. Therefore, the reduced osteoclast number and activity as well as the impaired osteoblast differentiation suggest a reduction in bone remodeling in aged mice.

It is well known that an adequate angiogenesis is essential for bone regeneration [Kanczler and Oreffo, 2008]. The role of vascularization in non-unions however, is controversially discussed [Menger et al., 2022b]. Some experimental studies demonstrate that the blockade of vascularization by pharmacological compounds, such as fumagillin, NSAIDs or TNP-470, can result in non-union formation [Hausman et al., 2001; Murnaghan et al., 2006; Fassbender et al., 2011]. Hence, non-unions are often considered to be the result of an avascular and biological inert environment at the fracture site. However, there is evidence that this view is oversimplified. In fact, some authors reported that the callus tissue of not only hypertrophic but also of atrophic non-unions is indeed richly vascularized [Santavirta et al., 1992; Brownlow et al., 2002; Reed et al., 2002]. The immunohistochemical analysis of CD31-positive endothelial cells in non-unions of aged and young adult mice confirms the latter findings. Both study groups showed a substantial number of microvessels within the segmental defects (Figure 7), which even increased from 2 to 10 weeks after surgery. Nevertheless, the results showed a significantly lower number of blood vessels in non-unions of aged animals when compared to young adult ones. These findings are in line with the results of previous reports, showing an

age-dependent dysfunction of the bone vascular system and a reduced potential to regenerate in healing [Clark et al., 2017; Orth et al., 2019].

The endothelial nitric oxide synthase (eNOS) is located in endothelial cells and is responsible for the production of the potent vasodilator NO [Fleming and Busse, 1999]. Of note, aging is associated with a reduction of endothelium-dependent vasodilatation, caused by an alteration of a L-arginine-NO pathway and a subsequent compromised NO availability in aged individuals [Taddei et al., 2001]. In addition, previous reports delineate that eNOS is directly involved in the process of bone regeneration and modulation of fracture repair [Diwan et al., 2000; Zhu et al., 2002]. Western blot analyses demonstrated a reduced expression of the activated phosphorylated eNOS (peNOS) in aged animals, resulting in a decrease in peNOS/eNOS ratio. These findings suggest a reduced activation of eNOS and, thus, a deterioration of the vascular function within the callus tissue of non-unions in geriatric mice. Overall, the reduced vascularization and vascular dysfunction observed in aged mice may have also inhibited the formation of novel bone tissue.

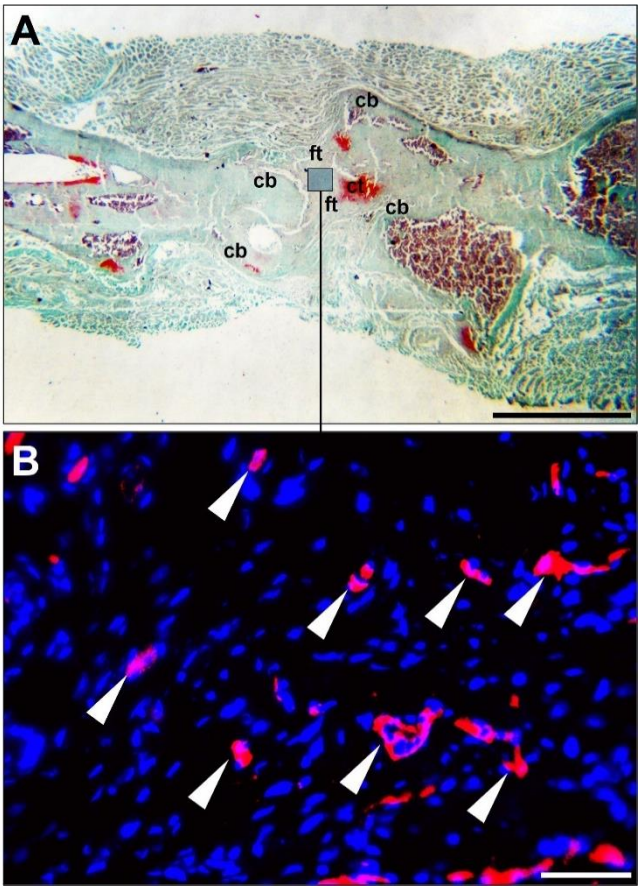

Figure 7. *(A) Safranin-O staining of a non-union in a young adult mouse 10 weeks after surgery. Cortical bone (cb), cartilaginous tissue (ct) and fibrous tissue (ft) are indicated. Scale bar: 2 mm. (B) Vasculature within the fibrous tissue of the callus. Arrowheads indicate CD31-positive endothelial cells. Scale bar: 50 µm.*

The inflammatory response after bone injury is mediated by granulocytes and macrophages and is an essential part of tissue regeneration and fracture healing. MSCs are redirected to the fracture site by macrophages secreting pro-inflammatory cytokines, such as IL-1β and TNF-α [Loi et al., 2016]. An overshooting or prolonged inflammatory phase, however, can impair the process of bone regeneration [Hankenson et al., 2014; Menger et al., 2023a]. Interestingly, aged individuals demonstrate a chronically elevated inflammatory status, also referred to as “inflamm-aging”, which is characterized by high levels of circulating pro-inflammatory cytokines [Franceschi et al., 2000]. The immunohistochemical analysis showed a significantly higher

number of macrophages within the callus of non-unions in aged mice when compared to young adult animals. In addition, heme oxygenase (HO)-1 expression was found decreased in aged mice. Of note, HO-1 is known to exert protective effects against oxidative injury. Moreover, HO-1 downregulates the inflammatory response in a variety of tissues [Rochette et al., 2013; Histing et al., 2016]. Interestingly, it has been reported that HO-1 stimulates macrophage polarization from the pro-inflammatory M1 phenotype towards the anti-inflammatory M2 phenotype [Tu et al., 2014]. Thus, it may be hypothesized that an overall increased number of macrophages and, in addition, an imbalance of macrophage polarization towards the pro-inflammatory M1-phenotype results in a prolonged inflammatory status within non-unions of aged mice. In the future, experimental studies using the pin-clip model need to fully elucidate the pathophysiological mechanisms of the overshooting inflammatory response during non-union formation in aged mice.

Taken together, in the second study of this thesis a reliable atrophic non-union model was established in aged CD-1 mice. The non-unions in aged animals exhibited a lower osteogenic and angiogenic capacity when compared to the ones of young adult mice. Moreover, aged mice showed a reduced bone remodeling, whereas the inflammatory response within the callus was elevated. In the future, the present model will be useful to further delineate the pathophysiology of non-union formation in aged individuals. In addition, novel treatment approaches, such as bone substitutes and tissue engineering constructs, can be evaluated in a preclinical setting. In addition, genetically altered knockout-mice may reveal the impact of specific molecular pathways on fracture healing failure in the aged.

6.2.3 PTH stimulates bone regeneration in atrophic non-unions in aged mice

In the third study of this thesis the effects of systemic PTH treatment on bone regeneration in atrophic non-unions in aged mice were analyzed. The results demonstrated that PTH treatment stimulates bone formation, leading to successful osseous bridging at 10 weeks after surgery and a higher bending stiffness of the injured femora. Notably, these findings were associated with a higher number of microvessels within the callus tissue of PTH-treated mice when compared to that of the control group [Menger et al., 2023b].

Milstrey et al. [2017] showed in an experimental study using a closed femoral fracture model in mice that the osteoanabolic effects of PTH are dose-dependent. Interestingly, the authors found that a dosage of 200 µg/kg induced the largest amount of novel bone formation and the highest trabecular number within the callus tissue. Hence, the dosage of 200 µg/kg was also used in the present study for the treatment of non-union formation.

Bone healing is characterized by the formation of a fracture callus with cartilaginous tissue, which gradually calcifies and transforms into novel bone tissue [Marsell and Einhorn, 2009]. Notably, the histomorphometric analysis revealed a higher fraction of cartilaginous tissue in PTH-treated aged mice at 2 weeks after surgery when compared to controls, indicating endochondral ossification. Ultimately, this ossification resulted in osseous bridging at 10 weeks after surgery. In the control group, however, endochondral ossification was absent throughout the entire observation period, leading to atrophic non-union formation with rounded bone ends and abundant fibrous tissue within the callus. Further histological analyses showed a significantly higher number of TRAP-positive osteoclasts within the callus tissue of PTH-treated aged mice. Osteoclasts are of crucial importance for cartilage resorption, callus remodeling and the subsequent formation of mature lamellar bone. Thus, systemic PTH treatment may improve bone regeneration by stimulating endochondral ossification as well as osteoclast-mediated bone remodeling.

Additional immunohistochemical analyses revealed a significantly higher number of CD31-positive endothelial cells within the callus tissue of PTH-treated animals. This was associated with a more than twofold higher expression of the pro-angiogenic marker VEGF when compared to controls. It is well known that VEGF induces the process of angiogenesis [Garcia et al., 2012]. Moreover, there is evidence that VEGF is capable of directly inducing bone regeneration by stimulating both endochondral and intramembranous fracture healing as well as the recruitment of stem cells [Keramaris et al., 2008; Beamer et al., 2010]. As a result, the stimulation of VEGF expression can accelerate fracture repair [Peng et al., 2005]. Furthermore, PTH treatment may also increase angiogenesis independent from VEGF by enhancing the migration of angiogenic $CD45^+/CD34^+$ progenitor cells [Zaruba et al., 2008]. Taken together, PTH stimulates the vascularization of the callus tissue in segmental bone defects and may directly induce bone formation by stimulating VEGF expression.

The inflammatory status within non-unions of aged mice is characterized by an increase of inflammatory cells as well as a downregulation of anti-inflammatory proteins [Menger et al., 2022c]. This prolonged and overshooting inflammatory response may impair the process of bone regeneration and even lead to bone healing failure [Hankenson et al., 2014; Loi et al., 2016]. Interestingly, the immunohistochemical analysis showed a significantly lower number of MPO-positive granulocytes and CD68-positive macrophages within the callus tissue of PTH-treated aged mice at 2 and 10 weeks after surgery when compared to controls. These findings indicate that PTH treatment attenuates the inflammatory response in aged animals and may, thereby, improve the process of bone repair. This assumption is supported by a study of Clark et al. [2020], reporting that the pharmacological targeting of macrophage recruitment in aged

mice by a macrophage-colony stimulating factor-1 receptor (M-CSF-1R) inhibitor improved bone regeneration. Therefore, novel treatment approaches targeting inflammatory cells may be a versatile approach to overcome fracture healing failure in the aged.

Several experimental studies could demonstrate that COX-2 is critically involved in the process of fracture healing. Zhang et al. [2002] showed that COX-2 regulates the differentiation of MSCs into the osteoblast lineage. The authors found impaired bone formation in COX-2-knockout mice, most likely caused by a deficit in osteoblastogenesis [Zhang et al., 2002]. Interestingly, Simon et al. [2002] reported that COX-2 is indeed vital for bone regeneration. However, COX-2-knockout mice are still capable of forming a normal skeleton. These findings indicate that fetal osteogenesis and fracture healing, although resembling each other in many ways, are in fact different and probably initiated and maintained by different molecular mechanisms [Simon et al., 2002]. Additionally, Xie et al. [2008] highlighted that COX-2 is required in the early milieu of a bone injury to initiate the process of chondrogenesis and osteoblastogenesis. The absence of COX-2, on the other hand, impairs the activation, proliferation and differentiation of donor periosteal progenitor cells, resulting in a high incidence of fibrotic non-union after bone graft transplantation [Xie et al., 2008]. Furthermore, Naik et al. [Naik et al., 2009] observed that a decreased COX-2 expression in aged mice during the early inflammatory period of bone healing is associated with a delay in bone remodeling. In the third study of this thesis, Western blot analyses revealed a significantly higher expression of COX-2 within the callus tissue of PTH-treated aged mice when compared to controls. As a result, it may be assumed that PTH treatment improves bone regeneration by the upregulation of COX-2 within the callus tissue.

PI3K-signaling is activated by receptor tyrosine kinases (RTKs) and G protein coupled receptors. The PI3K-pathway is crucial for cell metabolism and proliferation as well as for the regulation of gene expression [Cantley, 2002]. Interestingly, there is growing evidence that PI3K plays also a major role in controlling osteoblast proliferation and differentiation [Guntur and Rosen, 2011]. Moreover, inhibition of PI3K-signaling impaired osteoblast growth and survival [Grey et al., 2003; Dufour et al., 2008], indicating a stimulation of osteoblast precursors by PI3K. Additionally, the absence of PI3K regulation by the E3 ubiquitin ligase (Cbl) stimulates bone formation and modulates the osteogenic response of periosteal progenitor cells in fracture healing in mice [Scanlon et al., 2015; Scanlon et al., 2017]. Therefore, the increased bone formation observed in PTH-treated animals may also be due to an enhanced expression of PI3K within the callus tissue.

Taken together, PTH treatment improves bone regeneration in an atrophic non-union model in aged mice. The stimulation of bone formation was associated with an enhanced angiogenesis, a reduced inflammatory response and an increased COX-2 and PI3K expression (Figure 8). These findings demonstrate that PTH may be a promising compound for the future treatment of non-unions in aged patients [Menger et al., 2023b].

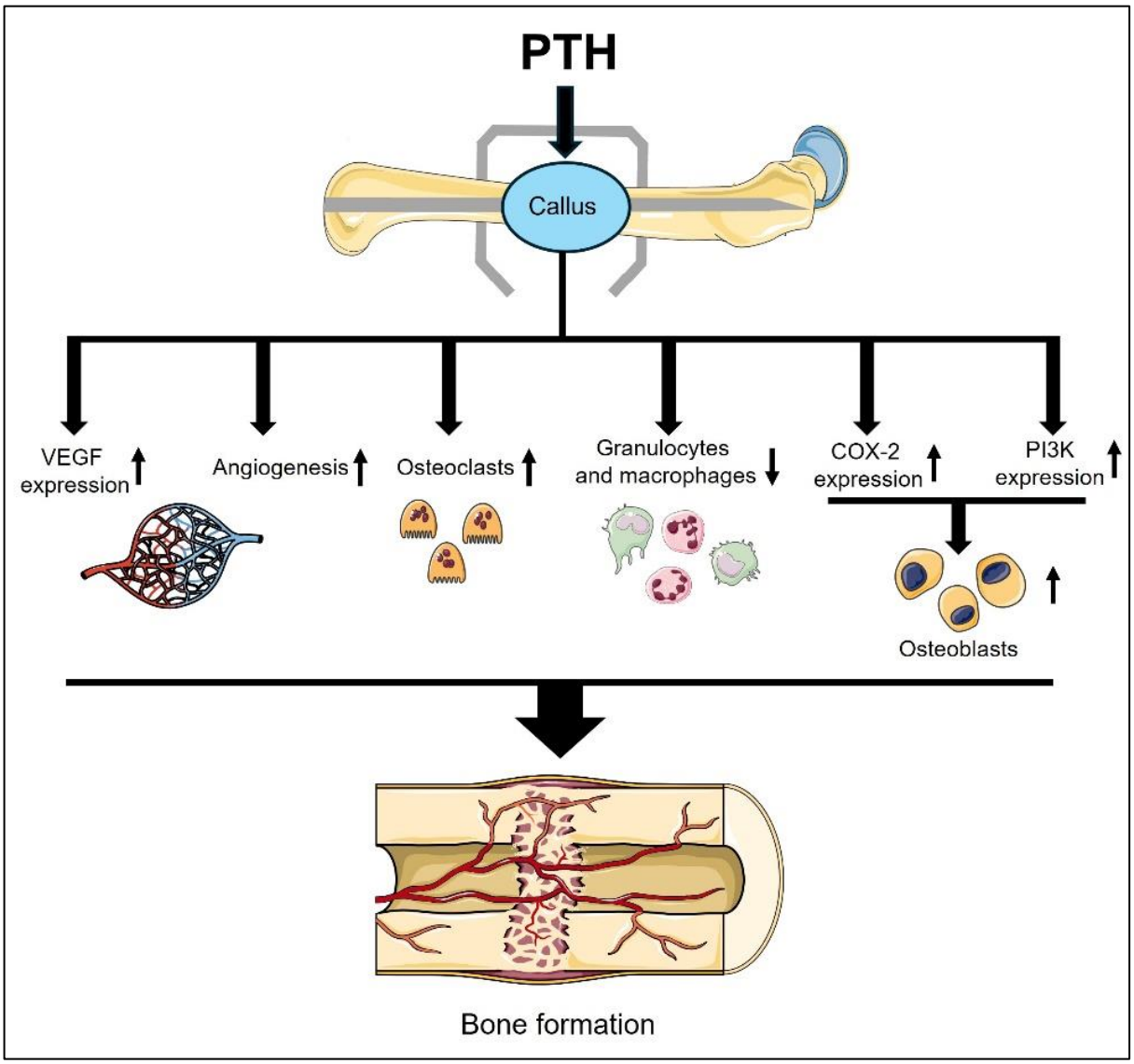

Figure 8. *Effects of PTH treatment on bone regeneration in aged mice. PTH increases VEGF expression and migration of endothelial progenitor cells, overall stimulating angiogenesis. Moreover, the number of osteoclasts is enhanced, whereas the inflammatory response is reduced by decreasing the number of granulocytes and macrophages. In addition, osteoblast differentiation is stimulated by an increase in COX-2 and PI3K expression, resulting in a stimulation of bone formation. The figure was created using pictures from Servier Medical Art, provided by Servier, licensed under a Creative Commons Attribution 4.0 unported license. (https://creativecommons.org/licenses/by/4.0/).*

6.2.4 Conclusion

The murine non-union model using a segmental defect and pin-clip fixation represents a reliable and feasible tool for the preclinical analysis of non-union formation in aged mice. Non-unions in geriatric animals demonstrate specific biological differences compared to failed fracture healing in young adult mice, including an impaired angiogenic capacity, a reduced pro-osteogenic growth factor expression as well as an overshooting inflammatory response within the callus tissue. PTH treatment in aged animals revealed promising results by inducing bone formation at an early healing time point within the segmental defects of aged mice, ultimately leading to osseous bridging at 10 weeks after surgery. Moreover, PTH treatment induced blood vessel formation and a reduction of the inflammatory response within the callus of aged animals, thereby, supporting the process of regeneration. Since PTH is an already clinically approved drug, these findings make PTH a promising compound for the treatment of non-union formation in geriatric patients. Future prospective clinical trials should evaluate the effectiveness of PTH treatment in cases of delayed healing and non-union formation in aged patients and screen for potential side effects. Thereby, this novel therapeutic approach may be successfully translated into a clinical setting and may help to overcome non-union formation in the aged population.

7. References

1. **Andreassen TT, Ejersted C, Oxlund H**. Intermittent parathyroid hormone (1-34) treatment increases callus formation and mechanical strength of healing rat fractures. *J Bone Miner Res* 14: 960-968, 1999.

2. **Andreassen TT, Cacciafesta V**. Intermittent parathyroid hormone treatment enhances guided bone regeneration in rat calvarial bone defects. *J Craniofac Surg* 15: 424-427; discussion 428-429, 2004.

3. **Andrzejowski P, Giannoudis PV**. The 'diamond concept' for long bone non-union management. *J Orthop Traumatol* 20: 21, 2019.

4. **Arnsdorf EJ, Jones LM, Carter DR, Jacobs CR**. The periosteum as a cellular source for functional tissue engineering. *Tissue Eng Part A* 15: 2637-2642, 2009.

5. **Bahney CS, Zondervan RL, Allison P, Theologis A, Ashley JW, Ahn J, Miclau T, Marcucio RS, Hankenson KD**. Cellular biology of fracture healing. *J Orthop Res* 37: 35-50, 2019.

6. **Beamer B, Hettrich C, Lane J**. Vascular endothelial growth factor: an essential component of angiogenesis and fracture healing. *HSS J* 6: 85-94, 2010.

7. **Bergman RJ, Gazit D, Kahn AJ, Gruber H, McDougall S, Hahn TJ**. Age-related changes in osteogenic stem cells in mice. *J Bone Miner Res* 11: 568-577, 1996.

8. **Black DM, Greenspan SL, Ensrud KE, Palermo L, McGowan JA, Lang TF, Garnero P, Bouxsein ML, Bilezikian JP, Rosen CJ, Pa THSI**. The effects of parathyroid hormone and alendronate alone or in combination in postmenopausal osteoporosis. *N Engl J Med* 349: 1207-1215, 2003.

9. **Bosemark P, Isaksson H, McDonald MM, Little DG, Tagil M**. Augmentation of autologous bone graft by a combination of bone morphogenic protein and bisphosphonate increased both callus volume and strength. *Acta Orthop* 84: 106-111, 2013.

10. **Bouxsein ML, Boyd SK, Christiansen BA, Guldberg RE, Jepsen KJ, Muller R**. Guidelines for assessment of bone microstructure in rodents using micro-computed tomography. *J Bone Miner Res* 25: 1468-1486, 2010.

11. **Brandi ML, Collin-Osdoby P**. Vascular biology and the skeleton. *J Bone Miner Res* 21: 183-192, 2006.

12. **Brownlow HC, Reed A, Simpson AH**. The vascularity of atrophic non-unions. *Injury* 33: 145-150, 2002.

13. **Buck DW, 2nd, Dumanian GA**. Bone biology and physiology: Part I. The fundamentals. *Plast Reconstr Surg* 129: 1314-1320, 2012.

14. **Cantley LC**. The phosphoinositide 3-kinase pathway. *Science* 296: 1655-1657, 2002.

15. **Choi P, Ogilvie C, Thompson Z, Miclau T, Helms JA**. Cellular and molecular characterization of a murine non-union model. *J Orthop Res* 22: 1100-1107, 2004.

16. **Clark D, Nakamura M, Miclau T, Marcucio R**. Effects of aging on fracture healing. *Curr Osteoporos Rep* 15: 601-608, 2017.

17. **Clark D, Brazina S, Yang F, Hu D, Hsieh CL, Niemi EC, Miclau T, Nakamura MC, Marcucio R**. Age-related changes to macrophages are detrimental to fracture healing in mice. *Aging Cell* 19: e13112, 2020.

18. **Clark HB, Jr., Hayes PA**. A study of the comparative effects of "rigid" and "semirigid" fixation on the healing of fractures of the mandible in dogs. *J Bone Joint Surg Am* 45-A: 731-741, 1963.

19. **Clarke B**. Normal bone anatomy and physiology. *Clin J Am Soc Nephrol* 3: 131-139, 2008.

20. **Colnot C, Thompson Z, Miclau T, Werb Z, Helms JA**. Altered fracture repair in the absence of MMP9. *Development* 130: 4123-4133, 2003.

21. **Dempster DW, Cosman F, Kurland ES, Zhou H, Nieves J, Woelfert L, Shane E, Plavetic K, Muller R, Bilezikian J, Lindsay R**. Effects of daily treatment with parathyroid hormone on bone microarchitecture and turnover in patients with osteoporosis: a paired biopsy study. *J Bone Miner Res* 16: 1846-1853, 2001.

22. **Dimitriou R, Jones E, McGonagle D, Giannoudis PV**. Bone regeneration: current concepts and future directions. *BMC Med* 9: 66, 2011.

23. **Diwan AD, Wang MX, Jang D, Zhu W, Murrell GA**. Nitric oxide modulates fracture healing. *J Bone Miner Res* 15: 342-351, 2000.

24. **Dufour C, Holy X, Marie PJ**. Transforming growth factor-beta prevents osteoblast apoptosis induced by skeletal unloading via PI3K/Akt, Bcl-2, and phospho-Bad signaling. *Am J Physiol Endocrinol Metab* 294: 794-801, 2008.

25. **Eckardt H, Ding M, Lind M, Hansen ES, Christensen KS, Hvid I**. Recombinant human vascular endothelial growth factor enhances bone healing in an experimental nonunion model. *J Bone Joint Surg Br* 87: 1434-1438, 2005.

26. **Einhorn TA, Gerstenfeld LC**. Fracture healing: mechanisms and interventions. *Nat Rev Rheumatol* 11: 45-54, 2015.

27. **Fang TD, Salim A, Xia W, Nacamuli RP, Guccione S, Song HM, Carano RA, Filvaroff EH, Bednarski MD, Giaccia AJ, Longaker MT**. Angiogenesis is required for successful bone induction during distraction osteogenesis. *J Bone Miner Res* 20: 1114-1124, 2005.

28. **Fassbender M, Strobel C, Rauhe JS, Bergmann C, Schmidmaier G, Wildemann B**. Local inhibition of angiogenesis results in an atrophic non-union in a rat osteotomy model. *Eur Cell Mater* 22: 1-11, 2011.

29. **Fayaz HC, Giannoudis PV, Vrahas MS, Smith RM, Moran C, Pape HC, Krettek C, Jupiter JB**. The role of stem cells in fracture healing and nonunion. *Int Orthop* 35: 1587-1597, 2011.

30. **Fleming I, Busse R**. NO: the primary EDRF. *J Mol Cell Cardiol* 31: 5-14, 1999.

31. **Franceschi C, Bonafe M, Valensin S, Olivieri F, De Luca M, Ottaviani E, De Benedictis G**. Inflamm-aging. An evolutionary perspective on immunosenescence. *Ann N Y Acad Sci* 908: 244-254, 2000.

32. **Garcia P, Holstein JH, Maier S, Schaumloffel H, Al-Marrawi F, Hannig M, Pohlemann T, Menger MD**. Development of a reliable non-union model in mice. *J Surg Res* 147: 84-91, 2008.

33. **Garcia P, Herwerth S, Matthys R, Holstein JH, Histing T, Menger MD, Pohlemann T**. The LockingMouseNail – a new implant for standardized stable osteosynthesis in mice. *J Surg Res* 169: 220-226, 2011a.

34. **Garcia P, Speidel V, Scheuer C, Laschke MW, Holstein JH, Histing T, Pohlemann T, Menger MD**. Low dose erythropoietin stimulates bone healing in mice. *J Orthop Res* 29: 165-172, 2011b.

35. **Garcia P, Pieruschka A, Klein M, Tami A, Histing T, Holstein JH, Scheuer C, Pohlemann T, Menger MD**. Temporal and spatial vascularization patterns of unions and nonunions: role of vascular endothelial growth factor and bone morphogenetic proteins. *J Bone Joint Surg Am* 94: 49-58, 2012.

36. **Garcia P, Histing T, Holstein JH, Klein M, Laschke MW, Matthys R, Ignatius A, Wildemann B, Lienau J, Peters A, Willie B, Duda G, Claes L, Pohlemann T, Menger MD**. Rodent animal models of delayed bone healing and non-union formation: a comprehensive review. *Eur Cell Mater* 26: 1-12; discussion 12-14, 2013.

37. **Grey A, Chen Q, Xu X, Callon K, Cornish J**. Parallel phosphatidylinositol-3 kinase and p42/44 mitogen-activated protein kinase signaling pathways subserve the mitogenic and antiapoptotic actions of insulin-like growth factor I in osteoblastic cells. *Endocrinology* 144: 4886-4893, 2003.

38. **Gruber R, Koch H, Doll BA, Tegtmeier F, Einhorn TA, Hollinger JO**. Fracture healing in the elderly patient. *Exp Gerontol* 41: 1080-1093, 2006.

39. **Guntur AR, Rosen CJ**. The skeleton: a multi-functional complex organ: new insights into osteoblasts and their role in bone formation: the central role of PI3Kinase. *J Endocrinol* 211: 123-130, 2011.

40. **Gustilo RB, Gruninger RP, Davis T**. Classification of type III (severe) open fractures relative to treatment and results. *Orthopedics* 10: 1781-1788, 1987.

41. **Hak DJ, Fitzpatrick D, Bishop JA, Marsh JL, Tilp S, Schnettler R, Simpson H, Alt V**. Delayed union and nonunions: epidemiology, clinical issues, and financial aspects. *Injury* 45: 3-7, 2014.

42. **Hankenson KD, Zimmerman G, Marcucio R**. Biological perspectives of delayed fracture healing. *Injury* 45: 8-15, 2014.

43. **Hausman MR, Schaffler MB, Majeska RJ**. Prevention of fracture healing in rats by an inhibitor of angiogenesis. *Bone* 29: 560-564, 2001.

44. **Heppenstall RB, Brighton CT, Esterhai JL, Jr., Katz M, Schumacher R**. Synovial pseudarthrosis: a clinical, roentgenographic-scintigraphic, and pathologic study. *J Trauma* 27: 463-470, 1987.

45. **Herath SC, Lion T, Klein M, Stenger D, Scheuer C, Holstein JH, Morsdorf P, Rollmann MF, Pohlemann T, Menger MD, Histing T**. Stimulation of angiogenesis by cilostazol accelerates fracture healing in mice. *J Orthop Res* 33: 1880-1887, 2015.

46. **Histing T, Garcia P, Holstein JH, Klein M, Matthys R, Nuetzi R, Steck R, Laschke MW, Wehner T, Bindl R, Recknagel S, Stuermer EK, Vollmar B, Wildemann B, Lienau J, Willie B, Peters A, Ignatius A, Pohlemann T, Claes L, Menger MD**. Small animal bone healing models: standards, tips, and pitfalls results of a consensus meeting. *Bone* 49: 591-599, 2011a.

47. **Histing T, Marciniak K, Scheuer C, Garcia P, Holstein JH, Klein M, Matthys R, Pohlemann T, Menger MD**. Sildenafil accelerates fracture healing in mice. *J Orthop Res* 29: 867-873, 2011b.

48. **Histing T, Anton C, Scheuer C, Garcia P, Holstein JH, Klein M, Matthys R, Pohlemann T, Menger MD**. Melatonin impairs fracture healing by suppressing RANKL-mediated bone remodeling. *J Surg Res* 173: 83-90, 2012a.

49. **Histing T, Stenger D, Scheuer C, Metzger W, Garcia P, Holstein JH, Klein M, Pohlemann T, Menger MD**. Pantoprazole, a proton pump inhibitor, delays fracture healing in mice. *Calcif Tissue Int* 90: 507-514, 2012b.

50. **Histing T, Andonyan A, Klein M, Scheuer C, Stenger D, Holstein JH, Veith NT, Pohlemann T, Menger MD**. Obesity does not affect the healing of femur fractures in mice. *Injury* 47: 1435-1444, 2016.

51. **Holstein JH, Menger MD, Culemann U, Meier C, Pohlemann T**. Development of a locking femur nail for mice. *J Biomech* 40: 215-219, 2007.

52. **Homburger F, Russfield AB, Weisburger JH, Lim S, Chak SP, Weisburger EK**. Aging changes in CD-1 HaM/ICR mice reared under standard laboratory conditions. *J Natl Cancer Inst* 55: 37-45, 1975.

53. **Isaksson H, Grongroft I, Wilson W, van Donkelaar CC, van Rietbergen B, Tami A, Huiskes R, Ito K**. Remodeling of fracture callus in mice is consistent with mechanical loading and bone remodeling theory. *J Orthop Res* 27: 664-672, 2009.

54. **Jiang Y, Zhao JJ, Mitlak BH, Wang O, Genant HK, Eriksen EF**. Recombinant human parathyroid hormone (1-34) [teriparatide] improves both cortical and cancellous bone structure. *J Bone Miner Res* 18: 1932-1941, 2003.

55. **Jilka RL**. Molecular and cellular mechanisms of the anabolic effect of intermittent PTH. *Bone* 40: 1434-1446, 2007.

56. **Kanczler JM, Oreffo RO**. Osteogenesis and angiogenesis: the potential for engineering bone. *Eur Cell Mater* 15: 100-114, 2008.

57. **Keramaris NC, Calori GM, Nikolaou VS, Schemitsch EH, Giannoudis PV**. Fracture vascularity and bone healing: a systematic review of the role of VEGF. *Injury* 39: 45-57, 2008.

58. **Kessler F, Arnke K, Eggerschwiler B, Neldner Y, Marsmann S, Groninger O, Casanova EA, Weber FA, Konig MA, Stark WJ, Pape HC, Cinelli P, Tiziani S**. Murine iPSC-loaded scaffold grafts improve bone regeneration in critical-size bone defects. *Int J Mol Sci* 25: 5555, 2024.

59. **Kokubu T, Hak DJ, Hazelwood SJ, Reddi AH**. Development of an atrophic nonunion model and comparison to a closed healing fracture in rat femur. *J Orthop Res* 21: 503-510, 2003.

60. **Komatsubara S, Mori S, Mashiba T, Nonaka K, Seki A, Akiyama T, Miyamoto K, Cao Y, Manabe T, Norimatsu H**. Human parathyroid hormone (1-34) accelerates the fracture healing process of woven to lamellar bone replacement and new cortical shell formation in rat femora. *Bone* 36: 678-687, 2005.

61. **Komori T**. Regulation of proliferation, differentiation and functions of osteoblasts by Runx2. *Int J Mol Sci* 20: 1684, 2019.

62. **Kon T, Cho TJ, Aizawa T, Yamazaki M, Nooh N, Graves D, Gerstenfeld LC, Einhorn TA**. Expression of osteoprotegerin, receptor activator of NF-kappaB ligand (osteoprotegerin ligand) and related proinflammatory cytokines during fracture healing. *J Bone Miner Res* 16: 1004-1014, 2001.

63. **Lacey DL, Timms E, Tan HL, Kelley MJ, Dunstan CR, Burgess T, Elliott R, Colombero A, Elliott G, Scully S, Hsu H, Sullivan J, Hawkins N, Davy E, Capparelli C, Eli A, Qian YX, Kaufman S, Sarosi I, Shalhoub V, Senaldi G, Guo J, Delaney J, Boyle WJ**. Osteoprotegerin ligand is a cytokine that regulates osteoclast differentiation and activation. *Cell* 93: 165-176, 1998.

64. **Landry PS, Marino AA, Sadasivan KK, Albright JA**. Effect of soft-tissue trauma on the early periosteal response of bone to injury. *J Trauma* 48: 479-483, 2000.

65. **Lettin AW**. The effects of axial compression on the healing of experimental fractures of the rabbit tibia. *Proc R Soc Med* 58: 882-886, 1965.

66. **Lin TH, Gibon E, Loi F, Pajarinen J, Cordova LA, Nabeshima A, Lu L, Yao Z, Goodman SB**. Decreased osteogenesis in mesenchymal stem cells derived from the aged mouse is associated with enhanced NF-kappaB activity. *J Orthop Res* 35: 281-288, 2017.

67. **Loi F, Cordova LA, Pajarinen J, Lin TH, Yao Z, Goodman SB**. Inflammation, fracture and bone repair. *Bone* 86: 119-130, 2016.

68. **Lu C, Miclau T, Hu D, Hansen E, Tsui K, Puttlitz C, Marcucio RS**. Cellular basis for age-related changes in fracture repair. *J Orthop Res* 23: 1300-1307, 2005.

69. **Lu C, Miclau T, Hu D, Marcucio RS**. Ischemia leads to delayed union during fracture healing: a mouse model. *J Orthop Res* 25: 51-61, 2007.

70. **Lu C, Hansen E, Sapozhnikova A, Hu D, Miclau T, Marcucio RS**. Effect of age on vascularization during fracture repair. *J Orthop Res* 26: 1384-1389, 2008.

71. **Manassero M, Viateau V, Matthys R, Deschepper M, Vallefuoco R, Bensidhoum M, Petite H**. A novel murine femoral segmental critical-sized defect model stabilized by plate osteosynthesis for bone tissue engineering purposes. *Tissue Eng Part C Methods* 19: 271-280, 2013.

72. **Manigrasso MB, O'Connor JP**. Characterization of a closed femur fracture model in mice. *J Orthop Trauma* 18: 687-695, 2004.

73. **Marsell R, Einhorn TA**. The role of endogenous bone morphogenetic proteins in normal skeletal repair. *Injury* 40: 4-7, 2009.

74. **Marsell R, Einhorn TA**. The biology of fracture healing. *Injury* 42: 551-555, 2011.

75. **Mathieu M, Rigutto S, Ingels A, Spruyt D, Stricwant N, Kharroubi I, Albarani V, Jayankura M, Rasschaert J, Bastianelli E, Gangji V**. Decreased pool of mesenchymal stem cells is associated with altered chemokines serum levels in atrophic nonunion fractures. *Bone* 53: 391-398, 2013.

76. **McSheehy PM, Chambers TJ**. Osteoblastic cells mediate osteoclastic responsiveness to parathyroid hormone. *Endocrinology* 118: 824-828, 1986.

77. **Menger MM, Laschke MW, Orth M, Pohlemann T, Menger MD, Histing T**. Vascularization strategies in the prevention of nonunion formation. *Tissue Eng Part B Rev* 27: 107-132, 2021.

78. **Menger MM, Bauer D, Bleimehl M, Scheuer C, Ehnert S, Menger MD, Histing T, Laschke MW**. Comparison of two non-union models with damaged periosteum in mice: segmental defect and pin-clip fixation versus transverse fracture and K-wire stabilization. *Bone* 162: 116475, 2022a.

79. **Menger MM, Laschke MW, Nussler AK, Menger MD, Histing T**. The vascularization paradox of non-union formation. *Angiogenesis* 25: 279-290, 2022b.

80. **Menger MM, Laschke MW, Scheuer C, Bauer D, Bleimehl M, Spater T, Rollmann MF, Braun BJ, Herath SC, Raza A, Menger MD, Histing T**. Establishment of a reliable model to study the failure of fracture healing in aged mice. *J Gerontol A Biol Sci Med Sci* 77: 909-917, 2022c.

81. **Menger MM, Stutz J, Ehnert S, Nussler AK, Rollmann MF, Herath SC, Braun BJ, Pohlemann T, Menger MD, Histing T**. Development of an ischemic fracture healing model in mice. *Acta Orthop* 93: 466-471, 2022d.

82. **Menger MM, Manuschewski R, Ehnert S, Rollmann MF, Maisenbacher TC, Tobias AL, Menger MD, Laschke MW, Histing T**. Radiographic, biomechanical and histological characterization of femoral fracture healing in aged CD-1 mice. *Bioengineering (Basel)* 10: 2023a.

83. **Menger MM, Tobias AL, Bauer D, Bleimehl M, Scheuer C, Menger MD, Histing T, Laschke MW**. Parathyroid hormone stimulates bone regeneration in an atrophic non-union model in aged mice. *J Transl Med* 21: 844, 2023b.

84. **Milstrey A, Wieskoetter B, Hinze D, Grueneweller N, Stange R, Pap T, Raschke M, Garcia P**. Dose-dependent effect of parathyroid hormone on fracture healing and bone formation in mice. *J Surg Res* 220: 327-335, 2017.

85. **Morgan EF, Mason ZD, Chien KB, Pfeiffer AJ, Barnes GL, Einhorn TA, Gerstenfeld LC**. Micro-computed tomography assessment of fracture healing: relationships among callus structure, composition, and mechanical function. *Bone* 44: 335-344, 2009.

86. **Murnaghan M, Li G, Marsh DR**. Nonsteroidal anti-inflammatory drug-induced fracture nonunion: an inhibition of angiogenesis? *J Bone Joint Surg Am* 88: 140-147, 2006.

87. **Naik AA, Xie C, Zuscik MJ, Kingsley P, Schwarz EM, Awad H, Guldberg R, Drissi H, Puzas JE, Boyce B, Zhang X, O'Keefe RJ**. Reduced COX-2 expression in aged mice is associated with impaired fracture healing. *J Bone Miner Res* 24: 251-264, 2009.

88. **Neer RM, Arnaud CD, Zanchetta JR, Prince R, Gaich GA, Reginster JY, Hodsman AB, Eriksen EF, Ish-Shalom S, Genant HK, Wang O, Mitlak BH**. Effect of parathyroid hormone (1-34) on fractures and bone mineral density in postmenopausal women with osteoporosis. *N Engl J Med* 344: 1434-1441, 2001.

89. **Nieminen S, Nurmi M, Satokari K**. Healing of femoral neck fractures; influence of fracture reduction and age. *Ann Chir Gynaecol* 70: 26-31, 1981.

90. **Nunamaker DM, Perren SM**. A radiological and histological analysis of fracture healing using prebending of compression plates. *Clin Orthop Relat Res* 138: 167-174, 1979.

91. **O'Neill KR, Stutz CM, Mignemi NA, Burns MC, Murry MR, Nyman JS, Schoenecker JG**. Micro-computed tomography assessment of the progression of fracture healing in mice. *Bone* 50: 1357-1367, 2012.

92. **Oetgen ME, Merrell GA, Troiano NW, Horowitz MC, Kacena MA**. Development of a femoral non-union model in the mouse. *Injury* 39: 1119-1126, 2008.

93. **Olerud S, Danckwardt-Lilliestrom G**. Fracture healing in compression osteosynthesis in the dog. *J Bone Joint Surg Br* 50: 844-851, 1968.

94. **Orth M, Kruse NJ, Braun BJ, Scheuer C, Holstein JH, Khalil A, Yu X, Murphy WL, Pohlemann T, Laschke MW, Menger MD**. BMP-2-coated mineral coated microparticles improve bone repair in atrophic non-unions. *Eur Cell Mater* 33: 1-12, 2017.

95. **Orth M, Baudach J, Scheuer C, Osche D, Veith NT, Braun BJ, Rollmann MF, Herath SC, Pohlemann T, Menger MD, Histing T**. Erythropoietin does not improve fracture healing in aged mice. *Exp Gerontol* 122: 1-9, 2019.

96. **Park SH, O'Connor K, Sung R, McKellop H, Sarmiento A**. Comparison of healing process in open osteotomy model and closed fracture model. *J Orthop Trauma* 13: 114-120, 1999.

97. **Parker MJ, Raghavan R, Gurusamy K**. Incidence of fracture-healing complications after femoral neck fractures. *Clin Orthop Relat Res* 458: 175-179, 2007.

98. **Peng H, Usas A, Olshanski A, Ho AM, Gearhart B, Cooper GM, Huard J**. VEGF improves, whereas sFlt1 inhibits, BMP2-induced bone formation and bone healing through modulation of angiogenesis. *J Bone Miner Res* 20: 2017-2027, 2005.

99. **Perren SM, Rahn BA**. Biomechanics of fracture healing. *Can J Surg* 23: 228-232, 1980.

100. **Prisby RD, Ramsey MW, Behnke BJ, Dominguez JM, 2nd, Donato AJ, Allen MR, Delp MD**. Aging reduces skeletal blood flow, endothelium-dependent vasodilation, and NO bioavailability in rats. *J Bone Miner Res* 22: 1280-1288, 2007.

101. **Probst A, Jansen H, Ladas A, Spiegel HU**. Callus formation and fixation rigidity: a fracture model in rats. *J Orthop Res* 17: 256-260, 1999.

102. **Reed AA, Joyner CJ, Brownlow HC, Simpson AH**. Human atrophic fracture non-unions are not avascular. *J Orthop Res* 20: 593-599, 2002.

103. **Reed AA, Joyner CJ, Isefuku S, Brownlow HC, Simpson AH**. Vascularity in a new model of atrophic nonunion. *J Bone Joint Surg Br* 85: 604-610, 2003.

104. **Robinson CM, Court-Brown CM, McQueen MM, Wakefield AE**. Estimating the risk of nonunion following nonoperative treatment of a clavicular fracture. *J Bone Joint Surg Am* 86: 1359-1365, 2004.

105. **Rochette L, Cottin Y, Zeller M, Vergely C**. Carbon monoxide: mechanisms of action and potential clinical implications. *Pharmacol Ther* 137: 133-152, 2013.

106. **Rollmann MF, Herath SC, Braun BJ, Holstein JH, Pohlemann T, Menger MD, Histing T**. In-hospital mortality of pelvic ring fractures in older adults now and then: a pelvic registry study. *Geriatr Gerontol Int* 19: 24-29, 2019.

107. **Santavirta S, Konttinen YT, Nordstrom D, Makela A, Sorsa T, Hukkanen M, Rokkanen P**. Immunologic studies of nonunited fractures. *Acta Orthop Scand* 63: 579-586, 1992.

108. **Saul D, Khosla S**. Fracture healing in the setting of endocrine diseases, aging, and cellular senescence. *Endocr Rev* 43: 984-1002, 2022.

109. **Saul D, Menger MM, Ehnert S, Nussler AK, Histing T, Laschke MW**. Bone healing gone wrong: pathological fracture healing and non-unions-overview of basic and clinical aspects and systematic review of risk factors. *Bioengineering (Basel)* 10: 85, 2023.

110. **Scanlon V, Soung do Y, Adapala NS, Morgan E, Hansen MF, Drissi H, Sanjay A**. Role of Cbl-PI3K interaction during skeletal remodeling in a murine model of bone repair. *PLoS One* 10: e0138194, 2015.

111. **Scanlon V, Walia B, Yu J, Hansen M, Drissi H, Maye P, Sanjay A**. Loss of Cbl-PI3K interaction modulates the periosteal response to fracture by enhancing osteogenic commitment and differentiation. *Bone* 95: 124-135, 2017.

112. **Schell H, Duda GN, Peters A, Tsitsilonis S, Johnson KA, Schmidt-Bleek K**. The haematoma and its role in bone healing. *J Exp Orthop* 4: 5, 2017.

113. **Schlundt C, Bucher CH, Tsitsilonis S, Schell H, Duda GN, Schmidt-Bleek K**. Clinical and research approaches to treat non-union fracture. *Curr Osteoporos Rep* 16: 155-168, 2018.

114. **Schmidmaier G, Capanna R, Wildemann B, Beque T, Lowenberg D**. Bone morphogenetic proteins in critical-size bone defects: what are the options? *Injury* 40: 39-43, 2009.

115. **Si W, Kang Q, Luu HH, Park JK, Luo Q, Song WX, Jiang W, Luo X, Li X, Yin H, Montag AG, Haydon RC, He TC**. CCN1/Cyr61 is regulated by the canonical Wnt signal and plays an important role in Wnt3A-induced osteoblast differentiation of mesenchymal stem cells. *Mol Cell Biol* 26: 2955-2964, 2006.

116. **Simon AM, Manigrasso MB, O'Connor JP**. Cyclo-oxygenase 2 function is essential for bone fracture healing. *J Bone Miner Res* 17: 963-976, 2002.

117. **Simonet WS, Lacey DL, Dunstan CR, Kelley M, Chang MS, Luthy R, Nguyen HQ, Wooden S, Bennett L, Boone T, Shimamoto G, DeRose M, Elliott R, Colombero A, Tan HL, Trail G, Sullivan J, Davy E, Bucay N, Renshaw-Gegg L, Hughes TM, Hill D, Pattison W, Campbell P, Sander S, Van G, Tarpley J, Derby P, Lee R, Boyle WJ**. Osteoprotegerin: a novel secreted protein involved in the regulation of bone density. *Cell* 89: 309-319, 1997.

118. **Squier CA, Ghoneim S, Kremenak CR**. Ultrastructure of the periosteum from membrane bone. *J Anat* 171: 233-239, 1990.

119. **Srouji S, Ben-David D, Kohler T, Muller R, Zussman E, Livne E**. A model for tissue engineering applications: femoral critical size defect in immunodeficient mice. *Tissue Eng Part C Methods* 17: 597-606, 2011.

120. **Taddei S, Virdis A, Ghiadoni L, Salvetti G, Bernini G, Magagna A, Salvetti A**. Age-related reduction of NO availability and oxidative stress in humans. *Hypertension* 38: 274-279, 2001.

121. **Taichman RS**. Blood and bone: two tissues whose fates are intertwined to create the hematopoietic stem-cell niche. *Blood* 105: 2631-2639, 2005.

122. **Teitelbaum SL**. Osteoclasts: what do they do and how do they do it? *Am J Pathol* 170: 427-435, 2007.

123. **Tu TH, Joe Y, Choi HS, Chung HT, Yu R**. Induction of heme oxygenase-1 with hemin reduces obesity-induced adipose tissue inflammation via adipose macrophage phenotype switching. *Mediators Inflamm* 2014: 290708, 2014.

124. **Veneroni G, Boccadoro B, Pluchino F**. Fixation of P-32 in the focus of a fracture and in osseous callus in the long bones in rabbits. *Arch Ortop* 75: 1338-1341, 1962.

125. **Victoria G, Petrisor B, Drew B, Dick D**. Bone stimulation for fracture healing: What's all the fuss? *Indian J Orthop* 43: 117-120, 2009.

126. **Whiteside LA, Lesker PA**. The effects of extraperiosteal and subperiosteal dissection. II. On fracture healing. *J Bone Joint Surg Am* 60: 26-30, 1978.

127. **Wojda SJ, Donahue SW**. Parathyroid hormone for bone regeneration. *J Orthop Res* 36: 2586-2594, 2018.

128. **Xie C, Ming X, Wang Q, Schwarz EM, Guldberg RE, O'Keefe RJ, Zhang X**. COX-2 from the injury milieu is critical for the initiation of periosteal progenitor cell mediated bone healing. *Bone* 43: 1075-1083, 2008.

129. **Yu B, Zhao X, Yang C, Crane J, Xian L, Lu W, Wan M, Cao X**. Parathyroid hormone induces differentiation of mesenchymal stromal/stem cells by enhancing bone morphogenetic protein signaling. *J Bone Miner Res* 27: 2001-2014, 2012.

130. **Zaruba MM, Huber BC, Brunner S, Deindl E, David R, Fischer R, Assmann G, Herbach N, Grundmann S, Wanke R, Mueller-Hoecker J, Franz WM**. Parathyroid hormone treatment after myocardial infarction promotes cardiac repair by enhanced neovascularization and cell survival. *Cardiovasc Res* 77: 722-731, 2008.

131. **Zhang X, Schwarz EM, Young DA, Puzas JE, Rosier RN, O'Keefe RJ**. Cyclooxygenase-2 regulates mesenchymal cell differentiation into the osteoblast lineage and is critically involved in bone repair. *J Clin Invest* 109: 1405-1415, 2002.

132. **Zhang ZY, Teoh SH, Chong MS, Lee ES, Tan LG, Mattar CN, Fisk NM, Choolani M, Chan J**. Neo-vascularization and bone formation mediated by fetal mesenchymal stem cell tissue-engineered bone grafts in critical-size femoral defects. *Biomaterials* 31: 608-620, 2010.

133. **Zhu W, Murrell GA, Lin J, Gardiner EM, Diwan AD**. Localization of nitric oxide synthases during fracture healing. *J Bone Miner Res* 17: 1470-1477, 2002.

134. **Zwingenberger S, Niederlohmann E, Vater C, Rammelt S, Matthys R, Bernhardt R, Valladares RD, Goodman SB, Stiehler M**. Establishment of a femoral critical-size bone defect model in immunodeficient mice. *J Surg Res* 181: e7-e14, 2013.

8. Acknowledgements

I would like to take this opportunity and thank everyone, who contributed to this work.

First, Prof. Dr. Matthias Laschke for the unique opportunity to join his research group and the possibility to work on this exciting project. His constant advice, input and guidance made my MD-PhD thesis an outstanding experience with a significant impact on both my professional and personal development. Moreover, I would like to thank him for the ongoing collaboration and support in the future, which inspired me for many other research projects.

Prof. Dr. Tina Histing for her continuous support in my endeavor to achieve a MD-PhD thesis during my residency in trauma and reconstructive surgery. She always advised, assisted and encouraged me all along the way.

Furthermore, Anne Tobias, David Bauer and Michelle Bleimehl for their assistance and friendship. Their support in µCT and histological analyses as well as taking care of the animals was excellent.

I would also like to thank Dr. Claudia Scheuer and Julia Parakenings for their support in the Western blot analyses, Ashan Raza for the introduction to the µCT investigation, Sandra Hans, Caroline Bickelmann and Janine Becker for the preparation of the histological samples as well as all the co-workers of the animal facility for taking great care of my animals.

Special thanks go to Dr. Thomas Später, PD Dr. Mika Rollmann, Prof. Dr. Benedikt Braun, PD Dr. Steven Herath and Prof. Dr. Sabrina Ehnert for supporting me during the project.

Finally, I would like to thank my parents, Michael and Christine Menger for their great support in achieving a MD-PhD.

9. Publications

9.1 Original articles from the present thesis

1. **Menger MM**, Bauer D, Bleimehl M, Scheuer C, Ehnert S, Menger MD, Histing T, Laschke MW. Comparison of two non-union models with damaged periosteum in mice: segmental defect and pin-clip fixation versus transverse fracture and K-wire stabilization. *Bone* 162: 116475, 2022. (IF: 4.1)

2. **Menger MM**, Laschke MW, Scheuer C, Bauer D, Bleimehl M, Später T, Rollmann MF, Braun BJ, Herath SC, Raza A, Menger MD, Histing T. Establishment of a reliable model to study the failure of fracture healing in aged mice. *J Gerontol A Biol Sci Med Sci* 77: 909-917, 2022. (IF: 5.1)

3. **Menger MM**, Tobias AL, Bauer D, Bleimehl M, Scheuer C, Menger MD, Histing T, Laschke MW. Parathyroid hormone stimulates bone regeneration in an atrophic non-union model in aged mice. *J Transl Med* 21: 844, 2023. (IF: 6.1)

9.2 Congress contributions from the present thesis

1. **Menger MM**, Bauer D, Bleimehl M, Scheur C, Braun BJ, Herath SC, Rollmann MF, Menger MD, Histing T, Laschke MW. Comparison of two compromised fracture healing models in mice: segmental defect versus periosteal cauterization. *21. Chirurgischen Forschungstage,* Leipzig (Onlineformat), 2021.

2. **Menger MM**, Laschke MW, Scheuer C, Bauer D, Bleimehl M, Menger MD, Histing T. Comparison of wo compromised fracture healing models in mice: segmental defect versus periosteal cauterization. *Deutscher Kongress für Orthopädie und Unfallchirurgie*, Berlin, 2021.

3. **Menger MM**, Bauer D, Scheuer C, Bauer D, Braun BJ, Herath SC, Rollmann MF, Bleimehl M, Menger MD, Histing T, Laschke MW. Vergleich zweier Pseudarthrose-Modelle in der Maus: segmentaler Defekt mit Pin-Clip Fixierung versus Querfraktur und K-Draht Stabilisierung. 7*0. Jahrestagung der Vereinigung Süddeutscher Orthopäden und Unfallchirurgen*, Baden Baden, 2022.

9.3 Further original articles

1. **Menger MM**, Nalbach L, Roma LP, Körbel C, Wrubleswky S, Glanemann M, Laschke MW, Menger MD, Ampofo E. Erythropoietin accelerates the revascularization of transplanted pancreatic islets. *Br J Pharmacol* 177: 1651-1665, 2020. (IF: 8.740)

2. Später T, Tobias AL, **Menger MM**, Nickels RM, Menger MD, Laschke MW. Biological coating with platelet-rich plasma and adipose-tissue derived microvascular fragments improves the vascularization, biocompatibility and tissue incorporation of porous polyethylene. Acta Biomater 108: 194-206, 2020. (IF: 8.947)

3. **Menger MM**, Nalbach L, Roma LP, Wrubleswky S, Glanemann M, Gu Y, Laschke MW, Menger MD, Ampofo E. Darbepoetin-α increases the blood volume flow in transplanted pancreatic islets in mice. *Acta Diabetol* 57: 1009-1018, 2020. (IF: 4.280)

4. Später T, **Menger MM**, Nickels RM, Menger MD, Laschke MW. Macrophages promote network formation and maturation of transplanted adipose tissue-derived microvascular fragments. *J Tissue Eng* 11: 2041731420911816, 2020. (IF: 7.813)

5. Nalbach L, Roma LP, Schmitt BM, Becker V, Körbel C, Wrublewsky S, Pack M, Später T, Metzger W, **Menger MM**, Frueh FS, Götz C, Lin H, Manning Fox JE, MacDonald PE, Menger MD, Laschke MW, Ampofo E. Improvement of islet transplantation by the fusion of islet cells with functional blood vessels. *EMBO Mol Med* 13: e12616, 2020. (IF: 12.137)

6. **Menger MM**, Bremer P, Scheuer C, Rollmann MF, Braun BJ, Herath SC, Orth M, Später T, Pohlemann T, Menger MD, Histing T. Pantoprazole impairs fracture healing in aged mice. *Sci Rep* 10: 22376, 2020. (IF: 4.380)

7. Später T, Worringer DM, **Menger MM**, Menger MD, Laschke MW. Systemic low-dose erythropoietin administration improves the vascularization of collagen-glycosaminoglycan matrices seeded with adipose tissue-derived microvascular fragments. *J Tissue Eng* 12: 20417314211000304, 2021. (IF: 7.940)

8. Unger EW, Histing T, Rollmann MF, Orth M, Herath E, **Menger M**, Herath SC, Grimm B, Pohlemann T, Braun BJ. Development of a dynamic fall risk profile in elderly nursing home residents: A free field gait analysis based study. *Arch Gerontol Geriatr* 93: 104294, 2021. (IF: 4.163)

9. Häussling V, Aspera-Werz RH, Rinderknecht H, Springer F, Arnscheidt C, **Menger MM**, Histing T, Nussler AK, Ehnert S. 3D environment is required in vitro to demonstrate altered bone metabolism characteristic for type 2 diabetics. *Int J Mol Sci* 22: 2925, 2021. (IF: 6.208)

10. Chen Y, Aspera-Werz RH, **Menger MM**, Falldorf K, Ronniger M, Stacke C, Histing T, Nussler AK, Ehnert S. Exposure to 16 Hz pulsed electromagnetic fields protect the structural integrity of primary cilia and associated TGF-β signaling in osteoprogenitor cells harmed by cigarette smoke. *Int J Mol Sci* 22: 7036, 2021. (IF: 6.208)

11. **Menger MM**, Merscher B, Scheuer C, Braun BJ, Herath SC, Rollmann MF, Stenger D, Später T, Pohlemann T, Menger MD, Histing T. Amlodipine accelerates bone healing in a stable closed fracture healing model in mice. *Eur Cell Mater* 41: 592-602, 2021. (IF: 4.325)

12. **Menger MM**, Nalbach L, Roma LP, Laschke MW, Menger MD, Ampofo E. Erythropoietin exposure of isolated pancreatic islets accelerates their revascularization after transplantation. *Acta Diabetol* 58: 1637-1647, 2021. (IF: 4.087)

13. Chen Y, **Menger MM**, Braun BJ, Schweizer S, Linnemann C, Falldorf K, Ronniger M, Wang H, Histing T, Nussler AK, Ehnert S. Modulation of macrophage activity by pulsed electromagnetic fields in the context of fracture healing. *Bioengineering* 8: 167, 2021. (IF: 5.046)

14. **Menger MM,** Stutz J, Ehnert S, Nussler AK, Rollmann MF, Herath SC, Braun BJ, Pohlemann T, Menger MD, Histing T. Development of an ischemic fracture healing model in mice. *Acta Orthop* 93: 466-471, 2022. (IF: 3.7)

15. Braun BJ, Histing T, Rollmann MFR, **Menger MM**, Osche D, Orth M, Pohlemann T, Herath SC. Weight-bearing restrictions after acetabular fracture, necessity or false hope? A brief observational study. *Acta Chir Orthop Traumatol Cech* 89: 146-149, 2022. (IF: 0.4)

16. Braun BJ, Histing T, Herath SC, Rollmann MFR, Reumann M, **Menger MM**, Springer F, Andres A, Diebels S, Roland M. Movement analysis and musculoskeletal simulation in non-union treatment-experiences and first clinical results. *Unfallchirurgie (Heidelb)* 125: 619-627, 2022. (IF: 0.8)

17. Huang X, Nussler AK, Reumann MK, Augat P, **Menger MM**, Ghallab A, Hengstler JG, Histing T, Ehnert S. Contribution to the 3R principle: description of a specimen-specific finite element model simulating 3-point-bending tests in mouse tibiae. *Bioengineering* 9: 337, 2022. (IF: 4.6)

18. **Menger MM**, Körbel C, Bauer D, Bleimehl M, Tobias AL, Braun BJ, Herath SC, Rollmann MF, Laschke MW, Menger MD, Histing T. Photoacoustic imaging for the study of oxygen saturation and total hemoglobin in bone healing and non-union formation. *Photoacoustics* 28: 100409, 2022. (IF: 7.9)

19. Stachel N, Braun BJ, Orth M, Herath SC, Rollmann MFR, **Menger MM**, Histing T, Pohlemann T. Locking nail versus plate fixation in calcaneal fractures: brief report on a retrospective analysis of treatment characteristics and radiographic correction potential. *Acta Chir Orthop Traumatol Cech* 89: 349-352, 2022. (IF: 0.4)

20. **Menger MM**, Manuschewski R, Ehnert S, Rollmann MF, Maisenbacher TC, Tobias AL, Menger MD, Laschke MW, Histing T. Radiographic, biomechanical and histological characterization of femoral fracture healing in aged CD-1 mice. *Bioengineering (Basel)* 10: 275, 2023. (IF: 3.8)

21. Braun BJ, Histing T, **Menger MM**, Platte J, Grimm B, Hanflik AM, Richter PH, Sivananthan S, Yarboro SR, Gueorguiev B, Pokhvashchev D, Marmor MT. "Bring your own device"-a new approach to wearable outcome assessment in trauma. *Medicina (Kausus)* 59: 403, 2023. (IF: 2.4)

22. Chen Y, Braun BJ, **Menger MM**, Ronniger M, Falldorf K, Histing T, Nussler AK, Ehnert S. Intermittent exposure to a 16 Hz extremely low frequency pulsed electromagnetic field promotes osteogenesis in vitro through activating piezo 1-Induced Ca2+ influx in osteoprogenitor cells. *J Funct Biomater* 14: 165, 2023. (IF: 5.0)

23. **Menger MM**, Stief M, Scheuer C, Rollmann MF, Herath SC, Braun BJ, Ehnert S, Nussler AK, Menger MD, Laschke MW, Histing T. Diclofenac, a NSAID, delays fracture healing in aged mice. *Exp Gerontol* 178: 112201, 2023. (IF: 3.3)

24. **Menger MM**, Bauer D, Bleimehl M, Scheuer C, Braun BJ, Herath SC, Rollmann MF, Menger MD, Laschke MW, Histing T. Sildenafil, a phosphodiesterase-5 inhibitor, stimulates angiogenesis and bone regeneration in an atrophic non-union model in mice. *J Transl Med* 21: 607, 2023. (IF: 6.1)

25. Unger EW, Pohlemann T, Orth M, Rollmann MFR, **Menger MM**, Herath SC, Histing T, Braun BJ. "Fall risk scoring" in outpatient gait analysis: validation of a new fall risk assessment for nursing home residents. *Z Orthop Unfall* 162: 474-478, 2023. (IF: 1.0)

26. **Menger MM**, Bleimehl M, Bauer D, Scheuer C, Hans S, Saul D, Ehnert S, Menger MD, Histing T, Laschke MW. Cilostazol promotes blood vessel formation and bone regeneration in a murine non-union model. *Biomed Pharmacother* 168: 115697, 2023. (IF: 6.9)

27. Braun BJ, Histing T, **Menger MM**, Herath SC, Mueller-Franzes GA, Grimm B, Marmor MT, Truhn D; AO Smart Digital Solutions Task Force (Andrew M Hanflik, Peter H Richter, Sureshan Sivananthan, Seth R Yarboro). Wearable activity data can predict functional recovery after musculoskeletal injury: feasibility of a machine learning approach. *Injury* 55: 111254, 2024. (IF: 2.2)

28. Reumann MK, Hillrichs H, **Menger MM**, Herath SC, Rollmann MFR, Stuby F, Histing T, Braun BJ. Nonunions after intertrochanteric and subtrochanteric femoral fractures. *Unfallchirurgie (Heidelb)* 127: 356-363, 2024. (IF: 0.6)

29. **Menger MM**, Emmerich M, Scheuer C, Hans S, Ehnert S, Nüssler AK, Herath SC, Steinestel K, Menger MD, Histing T, Laschke MW. Cilostazol stimulates angiogenesis and accelerates fracture healing in aged male and female mice by increasing the expression of PI3K and RUNX2. *Int J Mol Sci* 25: 755, 2024. (IF: 4.9)

30. **Menger MM**, Wenz H, Bamberg M, Krauß S, Lauer H, Viergutz T, Fontana J. Severe burn injuries – the day the sodium starts rising. *In vivo* 38: 747-753, 2024. (IF: 1.8)

31. **Menger MM**, Emmerich M, Scheuer C, Hans S, Braun BJ, Herath SC, Rollmann MF, Menger MD, Laschke MW, Histing T. Sildenafil delays bone remodeling of fractured femora in aged mice by reducing the number and activity of osteoclasts within the callus tissue. *Biomed Pharmacother* 173: 116291, 2024. (IF: 6.9)

32. Bamberg M, **Menger MM**, Thiel JT, Lauer H, Viergutz T, Fontana J. Antibiotics in patients with severe burn injury-a modifiable variable in hypernatremia etiology. *Injury* 111573, 2024. (IF: 2.2)

33. **Menger MM**, Herath SC, Ellmerer AE, Trulson A, Hoßfeld M, Leis A, Ollig A, Histing T, Küper MA, Audretsch CK. Different coupling mechanisms for a novel modular plate in acetabular fractures-a comparison using a laparoscopic model. *Front Surg* 11: 1357581, 2024. *(*IF: 1.6)

34. Maisenbacher TC, Libicher S, Erne F, **Menger MM**, Reumann MK, Schindler Y, Niemeyer F, Engelhardt L, Histing T, Braun BJ. Case studies of a simulation workflow to improve bone healing assessment in impending non-unions. *J Clin Med* 13: 3922, 2024. (IF: 3.0)

35. Tümen L, Pollmann-Schweckhorst L, Breinbauer R, Hammour MM, Aspera-Werz RH, Blumenstock G, Histing T, **Menger MM**, Ehnert S, Nüssler AK. Smoking increases risk of complication after musculoskeletal surgery: analysis of single immune parameter to predict complication risk. *EXCLI J* 23: 967-990, 2024. (IF: 3.8)

36. Chen G, Xin Y, Hammour MM, Braun B, Ehnert S, Springer F, Vosough M, **Menger MM**, Kumar A, Nüssler AK, Aspera-Werz RH. Establishment of a human 3D in vitro liver-bone model as a potential system for drug toxicity screening. *Arch Toxicol* doi: 10.1007/s00204-024-03899-9, 2024. (IF: 4.8)

37. **Menger MM**, Speicher R, Hans S, Histing T, El Kayali MKD, Ehnert S, Menger MD, Ampofo E, Wrublewsky S, Laschke MW. *Nlrp3* deficiency does not substantially affect femoral fracture healing in mice. *Int J Mol Sci* 25: 11788, 2024. (IF: 4.9)

9.4 Review articles

1. **Menger MM**, Laschke MW, Orth M, Pohlemann T, Menger MD, Histing T. Vascularization strategies in the prevention of non-union formation. *Tissue Eng Part B Rev* 27: 107-132, 2021. (IF: 7.376)

2. **Menger MM,** Braun BJ, Herath SC, Küper MA, Rollmann MF, Histing T. Fractures of the femoral head: a narrative review. *EFORT Open Rev* 6: 1122-1131, 2021. (IF: 4.775)

3. **Menger MM**, Laschke MW, Nussler AK, Menger MD, Histing T. The vascularization paradox of non-union formation. *Angiogenesis* 25: 279-290, 2022. (IF: 9.8)

4. Reumann MK, Braun BJ, **Menger MM**, Springer F, Jazewitsch J, Schwarz T, Nüssler A, Histing T, Rollmann MFR. Artificial intelligence and novel approaches for treatment of non-union in bone: from established standard methods in medicine up to novel fields of research. *Unfallchirurgie (Heidelb)* 125: 611-618, 2022. (IF: 0.8)

5. Saul D, **Menger MM**, Ehnert S, Nüssler AK, Histing T, Laschke MW. Bone healing gone wrong: pathological fracture healing and non-unions-overview of basic and clinical aspects and systematic review of risk factors. *Bioengineering (Basel)* 10: 85, 2023. IF: (3.8)

6. Ritter J, **Menger M**, Herath SC, Histing T, Kolbenschlag J, Daigeler A, Heinzel JC, Prahm C. Translational evaluation of gait behavior in rodent models of arthritic disorders with the CatWalk device - a narrative review. *Frond Med (Lausanne)* 10: 1255215, 2023. (IF: 3.1)

7. Braun BJ, Hofmann K, Rollmann MF, **Menger MM**, Ahrend MD, Ihle C, Histing T, Herath SC. Weight-bearing restrictions after distal femur fractures - review of current literature. *Z Orthop Unfall* 161: 610-618, 2023. (IF: 1.0)

8. Maisenbacher TC, Ehnert S, Histing T, Nüssler AK, **Menger MM**. Advantages and limitations of diabetic bone healing in mouse models: a narrative review. *Biomedicines* 11: 3302, 2023. (IF: 3.9)

9. Vogel C, Reumann MK, **Menger MM**, Herath SC, Rollmann MFR, Lauer H, Histing T, Braun BJ. Non-unions of the upper extremities. *Chirurgie (Heidelb)* 95: 671-682, 2024. (IF: 0.6)

10. Braun BJ, Herath SC, **Menger MM**, Rollmann MFR, Histing T, Braun EM. Surgeon well-being and mindfulness-A narrative review on how come, for what reason, why in times of surgeon shortage. *Chirurgie (Heidelb)* doi: 10.1007/s00104-024-02177-9, 2024. (IF: 0.6)

9.5 Case reports

1. Braun BJ, Herath SC, Rollmann MFR, **Menger MM**, Baumgartner H, Reumann M, Histing T. Atrophic sternum nonunion-case report based on the nonunion scoring system. *Unfallchirurg* 125: 628-633, 2022. (IF: 0.8)

9.6 Awards

2021 **Eduard-Martin Preis der Universität des Saarlandes**
for the thesis “Die Auswirkungen von Erythropoese-stimulierenden Substanzen auf die Revaskularisierung transplantierter Langerhans’scher Inseln“

2023 **Nachwuchsförderpreis 2023 der Sektion für Chirurgische Forschung der Deutschen Gesellschaft für Chirurgie**
for the paper “Photoacoustic imaging for the study of oxygen saturation and total hemoglobin in bone healing and non-union formation”

10. Curriculum vitae

Aus datenschutzrechtlichen Gründen wird der Lebenslauf in der elektronischen Fassung der Dissertation nicht veröffentlicht.